

POLITECNICO DI TORINO

CORSO DI LAUREA MAGISTRALE IN INGEGNERIA CIVILE

Tesi di Laurea Magistrale

**Global stability analysis and soil-structure
interaction. Application to EPR**



Relatore:

Rosario Ceravolo

Candidato:

Tiziano Iacovelli

Ottobre 2019

Abstract

During the design process of a building, several aspects have to be taken into consideration: static and variable loads, environmental conditions, accidental situations and the evolution of these along the time. An aspect that often is underestimated is the relation between the structure and the ground beneath it, the so-called soil-structure interaction (SSI).

The objective of this study is to understand the theory behind the problem and find a methodology to simulate it numerically on a finite element software in order to evaluate the sliding and the uplift of a structure.

The core of the study is the modelling of the interface between the soil and the structure. In computational mechanics, this is realized by means of a particular family of finite elements called contact elements. They allow transferring loads, heat or electricity between two bodies that come into contact.

Then, the evaluation of the before mentioned quantities has to be done along the time. This means the use of transient dynamic analysis in order to obtain a complete displacements history of the body.

All the models and analysis will be realized with ANSYS, a powerful finite element software capable to manage both contact element and transient analysis. Then, the results so obtained, will be compared with those evaluated with the Newmark-Elms methodology, a simplified numerical procedure used to calculate the displacement history of punctual mass on an infinitive rigid ground.

Contents

ABSTRACT	I
1. INTRODUCTION	5
1.1 GENERAL DESCRIPTION OF THE PROBLEM	5
1.2 THE ETC CODE.....	6
1.3 STABILITY VERIFICATIONS	7
1.3.1 <i>Static bearing capacity of the soil</i>	8
1.3.2 <i>Overturning</i>	8
1.3.3 <i>Sliding</i>	9
1.4 STATE OF THE ART IN EGIS.....	10
1.4.1 <i>Sliding evaluation: Newmark – Elms method</i>	10
1.4.2 <i>Uplift evaluation</i>	15
1.5 SOFTWARE UTILIZED	16
1.6 THE COMPANY	17
2. CONTACT MECHANICS.....	19
2.1 INTRODUCTION.....	19
2.2 NUMERICAL PROCEDURE FOR CONTACT PROBLEMS.....	20
2.2.1 <i>Contact detection</i>	21
2.2.2 <i>Contact discretization</i>	22
2.2.3 <i>Contact resolution</i>	23
3 STUDY CASES PRESENTATION	27
3.1 THE TEST CASES	27
3.2 MODELS	33
3.2.1 <i>Model 1</i>	33
3.2.2 <i>Model 2</i>	36
3.2.3 <i>Model 3</i>	40
3.3 MATERIALS.....	42
3.3.1 <i>Concrete</i>	42
3.3.2 <i>Friction model</i>	42
3.4 LOAD DESCRIPTION	43
3.4.1 <i>Dead load</i>	43
3.4.2 <i>Static lateral pressure due to earth</i>	44
3.4.3 <i>Permanent level of the groundwater table</i>	44
3.4.4 <i>Dynamic lateral earth pressure due to earthquake</i>	45
3.4.5 <i>Hydrodynamic pressure of the groundwater</i>	46

3.5	LOADS APPLICATION	47
3.5.1	<i>Inertia loads</i>	47
3.5.2	<i>Lateral static and dynamic earth/water action</i>	48
3.6	BOUNDARY CONDITION.....	51
4	CASE STUDY 1	52
4.1	AUGMENTED LAGRANGE CONTACT ALGORITHM	52
4.1.1	<i>Absolute displacements</i>	52
4.1.2	<i>FKN – Sub step interaction</i>	55
4.2	PURE LAGRANGE CONTACT ALGORITHM	60
4.2.1	<i>Absolute displacements</i>	60
5	CASE STUDY 2	68
5.1	AUGMENTED LAGRANGE CONTACT ALGORITHM	68
5.1.1	<i>Absolute displacements</i>	68
6	CASE STUDY 3	77
6.1	AUGMENTED LAGRANGE CONTACT ALGORITHM	77
6.2	PURE LAGRANGE CONTACT ALGORITHM	86
6.3	UPLIFT EVALUATION	90
7	CONCLUSIONS AND FUTURE DEVELOPMENTS.....	97
	BIBLIOGRAFY	100

1. Introduction

This chapter contains a general overview of the study that has been conducted, before explaining the issues and normative references, and then showing what is the actual state of the art with which the company actually face the problem of the global stability verifications. Next, a brief description of the software used will be presented.

1.1 General description of the problem

This study born in the frame of EPR UK project, a third-generation nuclear power plant under planning by Egis and other partners and commissioned by EDF (Electricité de France).

The nuclear power plant is composed by several parts: the core, which contains the real reactor, is placed at the centre with other auxiliary buildings on a common raft, called nuclear island (NI). Then there are several support buildings adjacent to NI or far from it, which are completely independent. The image below shows the typical layout for this model of power plant:

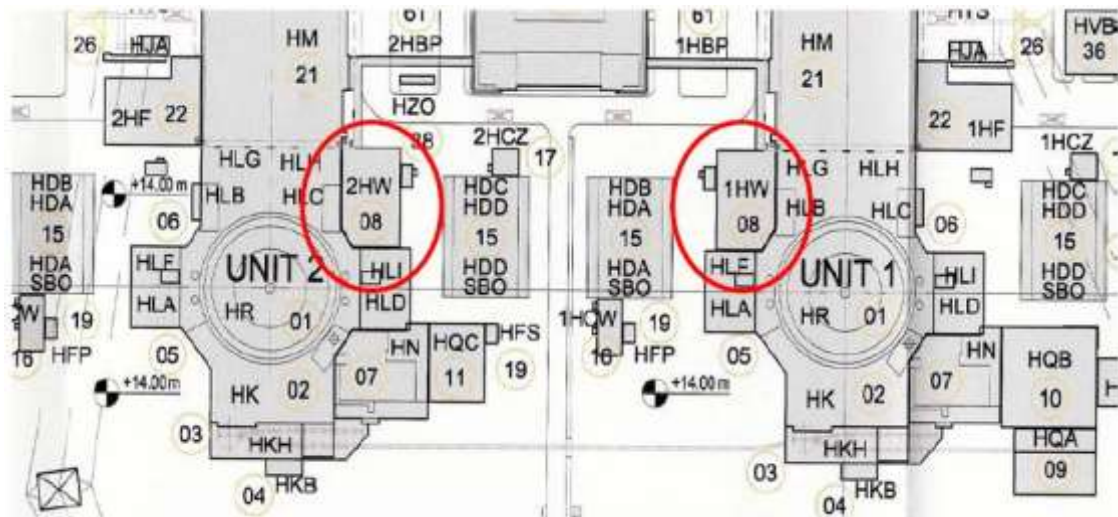


Figure 1.1 Layout of the EPR facility

The NI includes the following structures:

- APC Shell: airplane crash shell which protects the reactor
- Reactor building (HR): where the nuclear process takes place
- Fuel building (HK)

- The safeguard and electrical auxiliary buildings (HL)

The independent buildings are:

- Diesel buildings
- Access buildings
- Others for storing, wastes or office

The independent buildings are separated from NI from their foundations. Being separated, all the verifications are done separately. The NI buildings have an important mass and they share the foundation raft with a large surface. For these aspects, the global stability verifications (sliding, uplift, rocking and bearing capacity) are often satisfied in the linear and elastic analysis.

For the independent buildings, it is not always the same. Several difficulties can come out during the global stability verifications. In particular:

- The non-sliding criterion is not satisfied for some seismic combinations;
- The uplift of the building exceeds the limit of the validity for linear soil-structure interaction.

The evaluation of these quantities is usually performed in linear elastic field: modal and spectral analysis followed by one among many combination criteria known in civil engineering. Nevertheless, even if these methods are easier and faster, they are more conservative.

When the analysis performed in the linear-elastic field are not satisfied there are several ways to intervene in the project, the most valid are the following:

- 1) To modify the pre-design (change geometry, materials etc.)
- 2) To provide calculations more pushed (change analysis type)

The first one is not always permitted, especially in so important and strategic project. Therefore, the solution can be to perform specific studies to evaluate the effective sliding and uplift of the structure. The scope of this work is to show the approach, the hypotheses and the implementation of this type of problems. Non-Linear (NL) and transient analysis have been performed to try to reproduce the structure real response during an earthquake. Soil-Structure Interaction (SSI) is taken into account too. Finally, a real case study is reported.

1.2 The ETC code

The standards for the design of EPR power plants are developed by AFCEN, a French association founded in 1980 with the goal to guarantee a high level of quality and safety required for a nuclear reactor.

They are collected in a series of code where each of them covers a specific aspect or part of the system:

- RCC – M: Mechanical components
- RCC – E: Electrical and I&C systems
- RCC – C: Fuel assemblies
- ETC – C: Civil works
- ETC – F: Fire protection

For structural design and verification, the reference part is the ETC – C: it contains rules for the design, construction and testing of the EPR civil engineering structures. It describes the principles and requirements for safety, serviceability and durability conditions for concrete and steelwork structures on the basis of Eurocode design principles (European standards for structures) together with specific provisions for safety-class buildings.

The code consists of four parts:

- PART 0 defines the structure and the scope of the code;
- PART1 defines:
 - The action and combination to be taken into account;
 - The rules and criteria needed to design concrete structures, metal parts, pool and tank liners, structural steelwork and geotechnical structures.
- PART2 provides construction criteria;
- PART3 provides the main principles for containment testing, covering the initial acceptance test and subsequent periodic tests.

1.3 Stability verifications

Stability conditions fall inside the geotechnical verification; for them, the ETC-C code (Par.1.9.2.4) assert to use the same rules contained in the Eurocode 7 part 6. They cover the verification at ULS and SLS of spread foundations and between these, we can found:

- Loss of overall stability
- Bearing resistance failure
- Failure by sliding
- Combined failure inside ground and structure
- Structural failure due to ground movement
- Excessive settlements
- Excessive heave due to swelling frost heave and other causes

- Inacceptable vibrations

Between them, will be examined only those which fall in the field of application of the problem under examination.

1.3.1 Static bearing capacity of the soil

The bearing capacity verification concerns the capacity of the soil under the foundation to supports the pressure exerted by the overlying structure. At the ULS the bearing capacity, represent the maximum pressure that can be supported without causing failure for shear in the ground. When failure condition is reached, a sliding surface inside the ground is generated, making the soil unstable and causing large displacement in the structure. The image below shows the failure process:

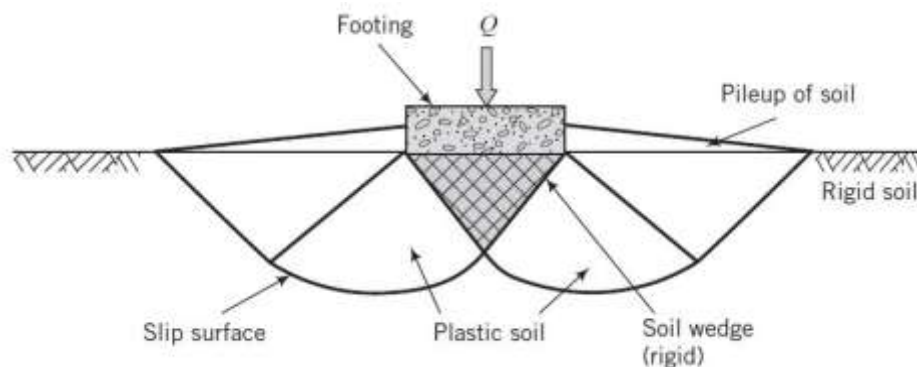


Figure 1.2 Ground failure mechanism

The final value of q_{LIM} depends on several characteristics of the soil such as density, water content angle of internal friction and by the way the loads are applied on the soil. It can be calculated by several empiric formulations; it is important to remember that these are approximate theory because when a failure condition is reached, the ground enters in the plastic field and here the principle of superposition of effects is not valid. So, the solution is approximated but cautionary.

1.3.2 Overturning

The overturning is represented by a rotation of the structure respect to the toe of the foundation. If this is too big, an overturn of the entire structure may occur. The actions that cause this phenomenon are the horizontal component of the earth and water thrust against the structure, while the actions that stabilize the structure are given by all the vertical loads acting on the body. Analytically, to ensure the stability of the structure, the stabilizing moment M_S must be bigger of the overturning moment M_R , both calculated with respect to the rotation centre located on the toe of the foundation.

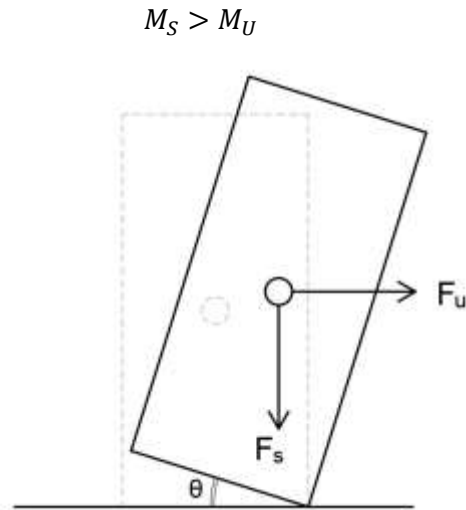


Figure 1.3 Forces position for overturning verification

$$M_S = F_S \cdot b_v$$

$$M_U = F_U \cdot b_h$$

When the inequality is not respected the body is overturning. With this methodology, the structure is considered as a rigid body and it is not possible to obtain further information like the percentage of uplifted area. To do that, it has to be taken into consideration the deformability of the soil under the foundation, and so more complex and refined models.

1.3.3 Sliding

Sliding occurs when the horizontal forces acting on a body are higher than those given by the friction which opposes to the motion direction. The forces that cause sliding are given by earth and water thrust acting against the structure or by the inertial forces induced by an acceleration of the structures, while the force that opposes the sliding is given by the resultant of the normal force multiplied by the friction coefficient.

$$F_H < F_N \cdot \mu$$

This inequality, known as Coulomb's law, when is not respected, states the begin of the sliding. On the other hand, this model does not allow to calculate the sliding distance. Sometimes this is not so big to cause problems to the structure, so another methodology to analyze this phenomenon is necessary.

1.4 State of the art in EGIS

In the previous paragraph have been showed the limitations relative to the usual verification technique. To overcome these limits, EGIS developed some numerical procedure that allowed to calculate both sliding distance and uplifted area. In this paragraph, both the methodology are presented, explaining the theory behind them, the input data needed and the output information that is possible to obtain.

1.4.1 Sliding evaluation: Newmark – Elms method

Originally, Newmark developed this model to study the behaviour of dams and embankments during an earthquake. It was composed by a sliding rigid block on a horizontal surface able to slide only along one direction. This is obviously a limit of the model because an earthquake acts along three directions, so Elms modified the original model in order to overcome this limitation and study more realistic cases (Elms 00).

The methodology presented is based on the following assumptions:

- The system is composed of a solid block sliding on a rigid surface. The interaction between the solid block and the rigid surface is driven by a friction coefficient. All other actions or effects except seismic inertial forces (static and dynamic pressures of surrounding soils) are considered as static forces (unchanged in functions of the time) applied to the solid block. However, dynamic pressures are dependent on time even if they are applied as static (but values are updated at each time-step). This whole system will be loaded in X, Y and Z directions with accelerations coming from seismic accelerograms. The velocity and displacement of the solid block is calculated as a function of time;
- Dynamic SSI is not considered: the building is a solid block. The method cannot capture the realistic dynamic response of the building;
- The embedment effect is not fully considered. Indeed, the presence of lateral soil is taken into account as a static force. No dynamic effect (functions of the time) of lateral soil is captured (passive resistance of soil is not taken into account. Favourable effect discarded).
- In this seismic time history analysis, there is no damping in the system (neither damping of soil nor that of the building nor interaction of soil and building). The only parameter to dissipate “seismic energy” is the friction between soil and building.
- Only the displacement due to the sliding of the solid block is captured.

The image below shows the model and the forces acting on it:

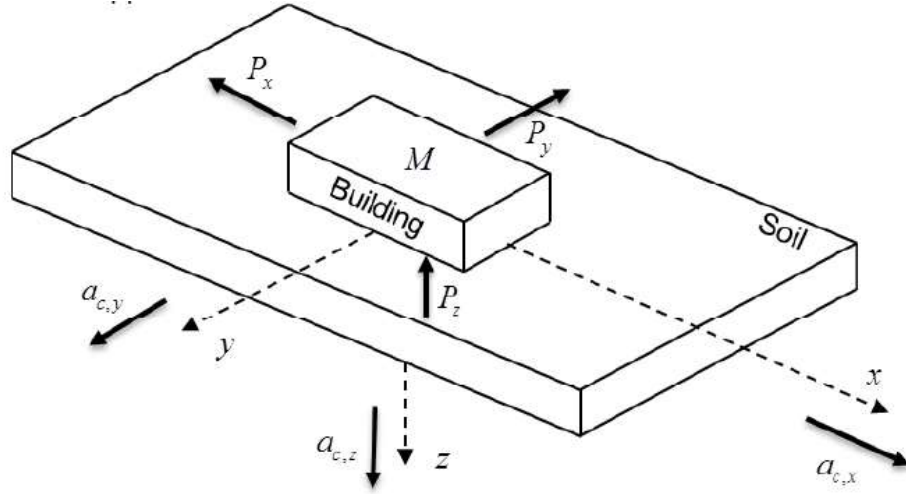


Figure 1.4 Newmark - Elms model

$$P_x = (\Delta P_{d,x} + E_{wd,x} + R_{st,x}) / Mg \quad (1)$$

$$P_y = (\Delta P_{d,y} + E_{wd,y} + R_{st,y}) / Mg \quad (2)$$

$$P_z = F_{v,w} / Mg \quad (3)$$

Where:

$a_{c,x}; a_{c,y}; a_{c,z}$ Soil accelerations (time-histories/accelerograms values) in X/Y/Z direction for a time step t;

$\Delta P_{d,x}; \Delta P_{d,y}$ Dynamic pressure resultant in X/Y direction;

$E_{wd,x}; E_{wd,y}$ Hydrodynamic pressure resultant in X/Y direction;

$R_{st,x}; R_{st,y}$ Earth and water static pressure resultant in X/Y direction

$F_{v,w}$ Resultant of the static pressure under the raft

Figure 1.4 gives the equilibrium equation as follows (see derivation in (Elms 00)):

$$(1 - k_z - P_z)^2 \mu^2 > (P_x - k_x)^2 + (P_y - k_y)^2 \quad (4)$$

Until the sliding does not begin, the acceleration of the block and of the soil will be equal, which means that as long as (Equat. 4) is satisfied $C_x; C_y; C_z = k_x; k_y; k_z$; in this condition the previous equation can be rewritten as follows:

$$(M(g - a_{c,z}) - F_{v,w}) \frac{\tan \phi}{\gamma_{R,H}} > \sqrt{(Ma_{c,x} + \Delta P_{d,x} + E_{wd,x} + R_{st,x})^2 + (Ma_{c,y} + \Delta P_{d,y} + E_{wd,y} + R_{st,y})^2} \quad (5)$$

When sliding continues, the frictional force will act in the opposite direction to the relative velocity between the building and the soil:

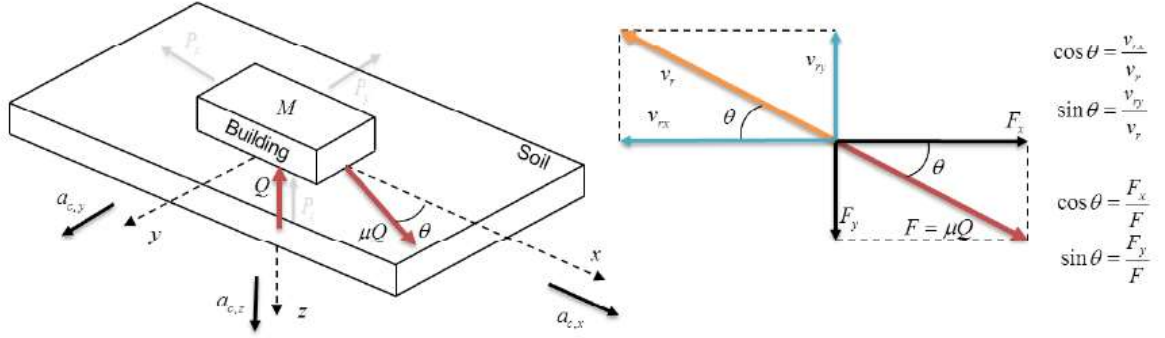


Figure 1.5: Velocity directions

Where:

v_{rx} Relative velocity in X direction

v_{ry} Relative velocity in Y direction

$$v_r = \sqrt{v_{rx}^2 + v_{ry}^2} \quad \text{Total quadratic relative velocity}$$

Therefore, the accelerations of the building in X and Y directions (k_x and k_y), which are different from the accelerations of the soil (C_x and C_y), are:

$$k_x = -\frac{v_{rx}}{v_r} \mu(1 - k_z - P_z) - P_x \quad (6a)$$

$$k_y = -\frac{v_{ry}}{v_r} \mu(1 - k_z - P_z) - P_y \quad (6b)$$

In Z direction, the acceleration of the building is assumed to be the same as the acceleration of the soil: $k_z = C_z$. Thus, no detachment between the block and the foundation soil is considered.

When the block initially begins to slide the relative velocity (v_r) will be zero and therefore the equations will be indeterminate. This is addressed by considering Newton's second law in X and Y directions:

$$F_x = Mg(C_x + P_x) \quad (7a)$$

$$F_y = Mg(C_y + P_y) \quad (7b)$$

The proportions of frictional forces are:

$$\frac{F_x}{\sqrt{F_x^2 + F_y^2}} = \frac{(C_x + P_x)}{\sqrt{(C_x + P_x)^2 + (C_y + P_y)^2}} \quad (8a)$$

$$\frac{F_y}{\sqrt{F_x^2 + F_y^2}} = \frac{(C_y + P_y)}{\sqrt{(C_x + P_x)^2 + (C_y + P_y)^2}} \quad (8b)$$

It is assumed that for the initial sliding (when it starts sliding and $v_r = 0$) the direction of the relative velocity is opposite of the frictional force (see Figure 1.5). It gives:

$$\left. \frac{v_{rx}}{v_r} \right|_{ini} = \frac{-(C_x + P_x)}{\sqrt{(C_x + P_x)^2 + (C_y + P_y)^2}} \quad (9a)$$

$$\left. \frac{v_{ry}}{v_r} \right|_{ini} = \frac{-(C_y + P_y)}{\sqrt{(C_x + P_x)^2 + (C_y + P_y)^2}} \quad (9b)$$

When the building slides and is governed by (Equation 6a) and (Equation 6b), computationally (implementation in a code/software), it can be written:

$$k_x(t) = \frac{v_{rx}(t-1)}{v_r(t-1)} \cdot \mu[(1 - C_z(t) - P_z(t))] \quad (10)$$

$$v_x(t) = v_x(t-1) + \int_{t-1}^t k_x \cdot dt = v_x(t-1) + \Delta t \frac{k_x(t) + k_x(t-1)}{2} \quad (11)$$

$$d_x(t) = d_x(t-1) + \int_{t-1}^t v_x \cdot dt = d_x(t-1) + \Delta t \frac{v_x(t) + v_x(t-1)}{2} \quad (12)$$

The relative velocities and displacements are calculated by subtracting the soil velocities and displacements:

$$v_{x,soil}(t) = v_{x,soil}(t-1) + \int_{t-1}^t C_x \cdot dt = v_{x,soil}(t-1) + \Delta t \frac{C_x(t) + C_x(t-1)}{2} \quad (13)$$

$$d_{x,soil}(t) = d_{x,soil}(t-1) + \int_{t-1}^t v_{x,soil} \cdot dt = d_{x,soil}(t-1) + \Delta t \frac{v_{x,soil}(t) + v_{x,soil}(t-1)}{2} \quad (13)$$

Equivalent equations can be derived for the Y direction.

The process to assess the displacement in time is the following one (see Figure 1.8):

1. Determination of accelerations at time step t, in x, y and z directions ($a_{c,x}$; $a_{c,y}$; $a_{c,z}$): read on the accelerograms.
2. Verification of the equilibrium at time step t:
 - a) If (Equation 5) is satisfied: No sliding. Iterate to next time step t + 1.
 - b) If (Equation 5) is not satisfied: Sliding occurs. Assess the displacement in x and y directions separately (see 1.4)
3. If equilibrium is not satisfied, the building is considered as sliding at time step t:
 - a) Determine the accelerations of the building with (Equation 6a) and (Equation 6b).
 - b) Calculate the relative speed by integrating the accelerations values given by (Equation 6a) and (Equation 6b).
 - c) Calculate the displacement by integrating two times the accelerations values.

4. Verification of relative movement at time step t : the building “slides” until the relative speeds comes back to zero:

a) The speed curve is integrated between t_{ini} and t_{end} to get the relative displacement:

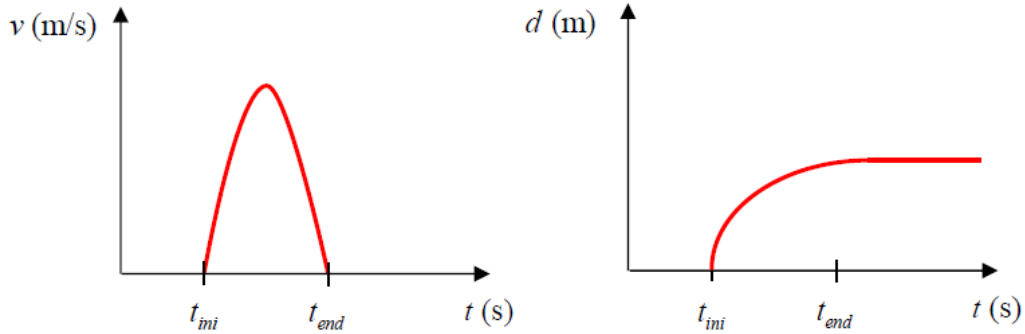


Figure 1.6 Velocity and displacement curve

b) When sliding occurs, the speed curve is calculated separately in x and y directions. For this reason, there are two different times t_{end} at which it stops sliding.

c) The hypothesis of calculation is that the greater one is kept:

$$t_{end} = \text{Max}(t_{end,x}; t_{end,y})$$

Until t_{end} , sliding is considered to be on-going and displacements along X and Y directions are calculated. The eventual negative relative velocity until t_{end} is not considered for the displacement calculation for the sake of simplifying the calculations.

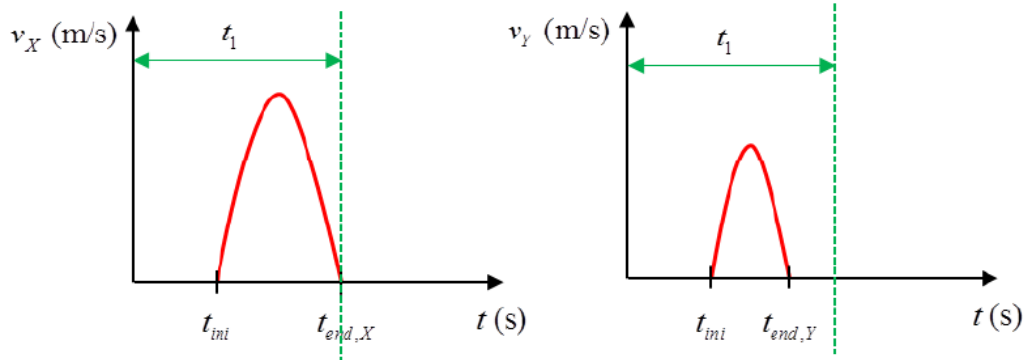


Figure 1.7 Simplification on the velocity

The computational process is summarized in the Figure below:

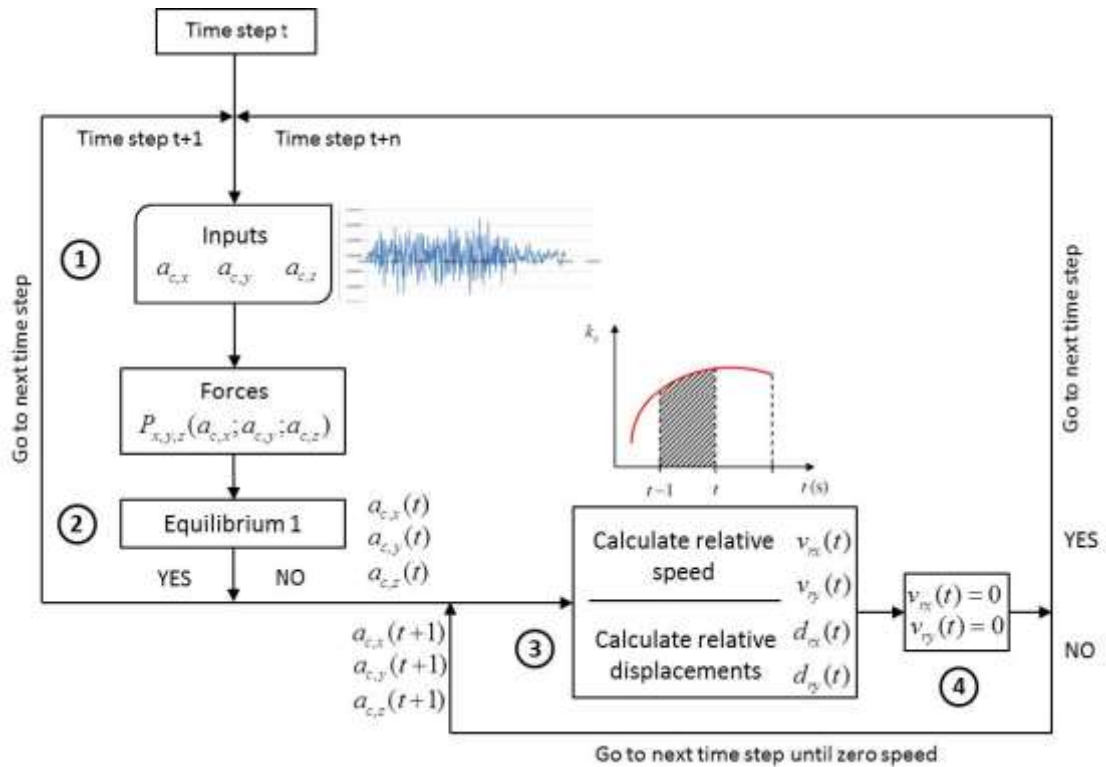


Figure 1.8 Sliding calculation procedure

The result is a complete time-history of the displacements of the structure along x and y directions, which allow determining if the peak displacement respect the limit imposed by the norm or not.

1.4.2 Uplift evaluation

This procedure allows determining the percentage of the uplifted area of a rigid foundation under a compressive and bending stress resting on a deformable ground represented by a bed of springs. It calculates also the position of the neutral axis, the maximum compressive stress of the soil and the stress under the geometric centre of gravity.

All these variables are calculated with two methods:

- **Moments equivalence**

For a given stress distribution, the program integrates the stresses on the compressed part of the soil and compares the values obtained from the resulting torsor calculated at the CDG of the slab (N_c, M_{xc}, M_{yc}) with the torsor of the external forces (N, M_x, M_y). Then, the distribution of the constraints is corrected iteratively until the cancellation of the gaps ($\Delta N, \Delta M_x, \Delta M_y$)

- **Energetic equivalence**

From a given constraint distribution, the program calculates the work of the switching moment W_{n1} (taking into account the detachment of the slab) and it compares it to the work of the moment of changeover W_1 which one finds if one supposes that there is no detachment of the raft (the springs also work in tension). Then, the distribution of the stresses is iteratively corrected according to the differences (ΔN , ΔW) while keeping a ratio M_{yc} / M_{xc} (or M_{xc} / M_{yc} if $M_x = 0$) constant equal to the data of the problem M_y / M_x (or M_x / M_y if $M_x = 0$).

Unlike the other methodology, the previous algorithms do not give a time-history result. Indeed, the input torsors are calculated with a response spectrum analysis, combined with a CQC or SRSS rule and then combined again with the Newmark combination in order to take into account different directions of the earthquake.

1.5 Software utilized

Among the different software utilized at Egis Industries, all the study has been conducted with ANSYS, a multipurpose finite element analysis software. It allows executing accurate numerical simulations in several fields: from the design of semiconductors to structural, fluid dynamics and electromagnetic field analysis.

Since its creation, in 1970, the program has been continuously developed and innovated so that today it is widely used to determine how a product will respond under its working condition without the necessity to build the product or conducting a crash test. The reliability of the software is proved by many experiments conducted by researchers and companies all over the world.

Between the various products offered by the software house, for structural analysis is present ANSYS Mechanical: it offers a solution for linear /nonlinear analysis both in a static and dynamic field, a complete set of material model, element behaviour and coupled-physics capabilities.

The design process with ANSYS is articulated in three well-separated phases, where each one corresponds to a set of commands. They are the following:

- **PRE-PROCESSOR:** it is composed of several indispensable sub-phases:
 - **Geometry definition:** it can be imported from an external application or defined and parametrized directly by an APDL script;

- Material definition: the setup of all the parameters that compose the constitutive law that is intended to simulate. The number of parameters depends on the complexity of the behaviour;
- Element definition: they differ by shape, number of nodes, DOF, etc. The default library is very wide and its definition depends on the physical problem that is going to be studied.
- Mesh generation: it consists of an overlap of the numerical element on the geometric model, then, different options can be adjusted like mesh size, regularity,
- Constraints definition: the imposition of all the external condition that constrains the structure;
- Load application: definition of the load (concentrated, distributed, temperature, etc.) and its intensity and position.
- SOLUTION: inside this phase, it has to be defined the type of analysis to be performed on the numerical model and their setting.
- POSTPROCESSOR: once the analysis is performed is possible to analyse all the data that the software calculated; it is possible to create a contour map, vector plot or graph directly inside the Mechanical environment, or export the results in order to analyse them with another software.

The entire project has been developed with ANSYS Parametric Design Language (APDL), a built-in coding language useful to parametrize the model, automate common tasks and perform optimization analysis. It is not the most intuitive way to manage a project because there is no interaction with the graphic interface, but on the other hand, it allows to have complete control of every aspect of every design phase before mentioned.

Indeed, for each of them, several script input file can be created and successively read by the software that will execute consecutively the commands inside the script. At a more advanced level, more analysis can be executed consecutively without the intervention of the user, which has only to write a proper input file.

1.6 The company

“Egis is an international group offering engineering, project structuring and operations services. In engineering and consulting, its sectors of activity include transport, building, urban development, industry, water, environment and energy. In

roads and airports, its offer is enlarged to encompass project structuring, equity investment, facilities delivery and operations.

The Group additionally deploys its expertise in areas such as new mobility services and turnkey energy systems.

It is the only French construction-engineering group among the top ten European groups and the world's top twenty in the construction sector.

In the ranking published in December 2016 by ENR (Engineering News-Record) the international benchmark guide for engineering, Egis appears in 23rd place in the Top 150, in 8th position in the top 20 in the "Transportation" category, also 8th in the TOP 10 in the Regions category in Africa, and 3rd in the Top 5 in the "Highways" category.

The rise in turnover generated outside France comes as a confirmation of the increasingly international profile of the Group and its activities.

Egis Industries undertakes projects that represent a strong challenge and require high levels of technical skill: innovative projects, processes that are far-reaching or that have strong implications for buildings, protection of the environment, safety and security, limit conditions, aggressive environments, etc.

Founded in 1929 as "Séchaud & Metz", Egis Industries' long experience is focused on structures exposed to exceptional stresses (earthquake, airplane crash, explosion) or requiring special skills (long span, vibration, ground/structure interaction).

The firm's core of excellence was developed in the industrial and nuclear sectors, the latter being an area where Egis Industries has been making a contribution to France since the first atomic pile, Zoé. Combining all this experience with our excellence in the management of projects and of costs and deadlines, we undertake missions that extend from expert appraisal to full engineering (architect engineer, EPCM) and from design to dismantling.

Therefore, the initial historical activity of Séchaud and Metz focused on nuclear structures and provided a foundation of technical expertise in the field of complex structures and calculations that naturally extended to civil structures and architectural constructions. Séchaud and Metz later became Egis Industries."

2. Contact mechanics

Contact elements represent the core of this study, and in this chapter, a brief description of the physical behaviour and their mathematical characterization will be given. The starting point is an introduction of these particular elements, followed by the description of the procedure utilized to solve the contact problems. Next, the various contact resolution methods will be discussed and the differences between them will be discussed.

2.1 Introduction

In the real world, any interaction between two bodies implies a contact: walking, running, driving a car or a bicycle. Any contact implies the transfer of loads, heat or electricity, but the physics behind these phenomena is not so easy because of the multiscale and multiphysics nature of the problem. Furthermore, when contact occurs, the deformability of the bodies and the entity of the loads makes it difficult to detect the contact area, which is one of the principal variables of these kinds of problems, making them highly non-linear even for a very simple problem. (Wriggers 06)

Over time, mathematics tried to create models able to describe the phenomenon by means of measurable variables like the friction coefficient, the heat transfer coefficient and the contact area mentioned before. Then, these models have been integrated into numerical procedures in order to study the development of the previous quantities belonging to a particular system. There is to say that both mathematic and numerical methods are based on strong simplification and so, the correct evaluation of the results is not easy. (Yastrebov 13)

Nowadays, contact mechanics helps to solve problems of different nature in several fields. The majority of the problems fall in mechanical engineering like the design of gears, the cold forming of a metal sheet, the rolling of a tyre on the pavement or car crash simulation. Other applications are present in biomechanics or industrial process.

In civil engineering, it helps the evaluation of uplift and sliding of a superficial foundation under an eccentric load, a seismic event or an impact. Also, it can be used studying the connection between structural elements of a steel structure. In

geotechnical engineering, it can be used studying piles foundations or the slope instability.

Since the nature of the problems can be very different, a good contact algorithm has to take into account nonlinear materials, large deformations, time-dependent response and multi-fields capability. This level of complexity requires high robustness of the computational method and a good mastering of engineering techniques. (Wriggers 06)

Besides that, mathematically a mechanical problem can be solved by means of differential equations solvable with appropriate boundary conditions; this condition is called *strong form*. Then, when we need to create a numeric procedure, we use to write the energetic balance of the virtual works, which is the base of the FEM; this new interpretation is called *weak form*. Contacts are treated as finite elements, and since their math is based on inequalities, it is difficult to integrate it in a weak form. Thanks to variational principles, it is possible to pass to variational inequalities, easier to manage but that requires new solution techniques. (Yastrebov 13)

Other troubles lie on the discretization of the contact domain and the linearization of the variational inequalities. Then, if it is present also the friction, things become even more complicated. Usually, most of the contact algorithms rely on Coulomb's friction law which states that the resistance sliding force depends on the normal contact pressure and so on the contact area. But, as mentioned before, this last is not known a priori, increasing the computational effort to obtain a valid solution. (Yastrebov 11)

The previous difficulties are related at the resolution phase, that is only the last one; previously there are the detection phase and the discretization phase, each of one has its own problems. At the begin, could seem that each phase is independent or is more important of another one, indeed they are strictly related and a good result of a single-phase contribute on the overall final result. In the next paragraph, they will be discussed in detail. (Yastrebov 11)

2.2 Numerical procedure for contact problems

Contact elements belong to a particular family of finite elements that works like "link elements" between separated but possibly interacting surfaces. Like the other elements, they are composed of nodes and edges, and usually, they are overlapped on already existing classic elements which define two different bodies.

Every contact element has its own unknown vector, tangential matrix and residual vector, which are expanded and assembled with the unknown, tangential and residual matrixes of the classic structural elements. The number of the unknown parameters depend by the resolution algorithm chosen. This phase is known as contact discretization.

The previous step is contact detection, and play an important role in the contact resolution. During this phase, the algorithm creates the link between a defined master node and a proximal slave node. There are several criteria to do this, and if it is not so efficient, the dimension of the matrix mentioned before could be too big, increasing the computational time of the calculator or to an erroneous estimation of the results.

Then, during the resolution step, the unknowns of the problem are determined. The reliability of the results depends upon the previous phases and the resolute algorithm that the user chooses to use: some of them are more accurate but need more computational time, while others are quicker but more sensitive to the set of parameters.

2.2.1 Contact detection

Since contact resolution logic is based on eliminating penetration of one body in another simpling applying a repulsive force, first, such a penetration need to be detected. So, this phase consists of an algorithm which determines which nodes are going to penetrate. Once the penetration is detected, the algorithm creates the contact between a master and a slave entity which can be a node, a segment or a surface.

First of all, these algorithms are realized differently according to the type of resolution utilized:

- **Implicit:** the probable penetration has to be evaluated before the resolution phase and at every solution step;
- **Explicit:** first the penetration has to be detected and then the repulsive force applied.

For the study under examination, only the implicit solver will be used and so only the techniques related to it will be explained.

Another difference lies in the physic of the problem and in the numerical approach used to solve the problem. Two branches can be defined:

- **Spatial search:** the detection is made on different bodies rather than on discretized one. It is widely used in problems involving multi-body systems like those composed of sand, stones or snow and generally any particles system;

- **Local contact detection:** more suitable for large displacements and large deformation problems and for the finite element method. Computationally it is heavier than the previous because big changes in the geometry may occur.

This phase is also strictly dependent on the discretization method that will be explained in the following paragraph.

After this brief overview of the detection techniques, now the detection strategies will be introduced; basically, there are two possible paths to follow:

- **All-to-all method:** it is the simplest one and consist of projecting the slave nodes on a predefined entity (nodes or segment) and then create the contact link with the closest one. Hence, there are two procedures:
 - **Node-to-Node (NTN)**
 - **Node-to-Segment (NTS)**
- **Bucket sort method:** the bases are the same as the previous method, but the research of the closest point is optimized reducing the area of interest and adding more verifications. In this way, the computational time increase but the contact area is evaluated more accurately.

2.2.2 Contact discretization

The contact discretization defines between which entities the constraint equation will be established, and so, from it depends how will be transferred the various effort from one element to another. There are different procedures to do that:

- **Node-to-Node (NTN):** it is the oldest and simplest one and it does not allow any finite sliding or large deformation. It is applicable only for linear or quadratic elements. It requires conforming mesh;

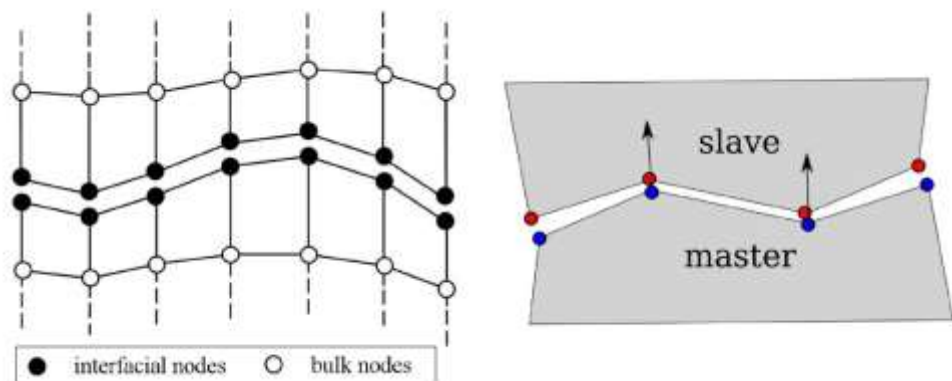


Figure 2.1 Node to Node discretization

- **Node-to-Segment (NTS):** it is suitable for non-conforming meshes and large deformation/sliding, but at the same time it is not stable for some mesh configuration;

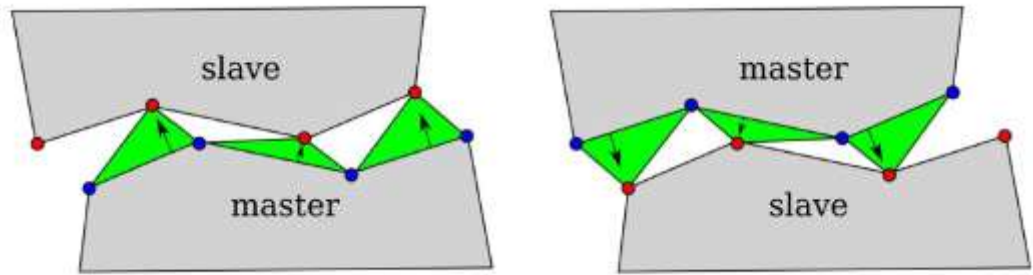


Figure 2.2 Node to Segment discretization

- **Segment-to-Segment (STS):** it allows to use high order shape functions and overcome the problems of the previous discretization, so it is supported by non-conforming meshes and avoid the formation of spurious modes; on the other hand, it is very difficult to implement.

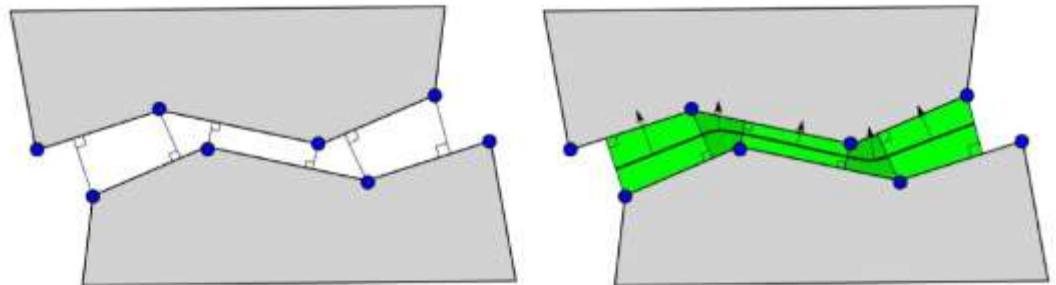


Figure 2.3 Segment to Segment discretization

2.2.3 Contact resolution

As mentioned before, during the exact contact resolutions some variational inequalities subjected to geometrical constraints need to be solved. These constraints result in additional terms in the objective energy functional.

Such an operation converts the constrained optimization, where constraints are given as inequalities, into an unconstrained or partly unconstrained one. If one supposes the active contact zone to be known, then the variational inequality can be replaced by variational equality, which finally results in an unconstrained problem written in a standard form of variational equality (Wriggers 06).

The problem so formulated is easier to implement in a finite element framework; the instruments necessary to solve it are a non-linear solver, like the Newton-Rapson method implemented in ANSYS (Bathe 96), and an optimization algorithm used to minimize the energetic balance of the problem.

Between these last, along the time several methodologies have been developed and adapted to solve contact problems. The most utilized are:

- Penalty method
- Lagrange method
- Augmented Lagrange method

Every method has its own pro and cons, so it chooses has to be coherent with the physical problem and its dimensions. The differences between them will be presented in the next paragraphs.

2.2.3.1 Penalty method

With this method, the contact energy depends by a penalty term ε . The expression of the contact energy is the following:

$$\Pi_c^{PM} = \frac{1}{2} \int_{\Gamma_c} (\varepsilon_N (g_N)^2 + \varepsilon_T (g_T)^2) dA$$

To respect the non-penetration criteria, at the interface a negative pressure σ_N arises.

$$\sigma_N = \varepsilon_N (-g_N)$$

Logically, the higher is the contact pressure and the better the Hertz's conditions are fulfilled. In this optic, the parameter ε_N can be seen as the stiffens of springs, and so the master surface can be approximated as a bed of springs which are opposing to the penetration of another body defined by the slave nodes. It is clear that the penetration will never be zero utilizing this method, otherwise, there would not be an opposing force to the penetration.

The greatest advantage of this method is that no DOF are added in the matrix involved, so the computational effort is not so high which means less analysis time. Then, thanks to its simple interpretation it is easy to implement this algorithm in a numerical procedure. On the other hand, the solution is not exact and will depend by the stiffness of the spring (Penalty factor): if too low there will be too much penetration, while if it is too high an ill-conditioning of the global stiffness matrix may occur.

2.2.3.2 Lagrange method

Respect to the previous formulation, this time the contact energy depends by a parameter called Lagrange multiplier λ . The contact contribution in the energetic balance become:

$$\Pi_c^{LM} = \int_{\Gamma_c} (\lambda_N g_N + \lambda_T g_T) dA$$

The base idea of this method consists of the search of the stationary points of a functional $\mathcal{L}(u, \lambda)$ appositely assembled and called Lagrangian. It is so assembled:

$$\mathcal{L}(u, \lambda) = \Pi(u) + \Pi_c^{LM}(\lambda)$$

The minimum points of the functional are given by the condition $g_N = 0$ that means zero penetration. Then, the λ multiplier is seen as a pressure exerted from the contact necessary to maintain at zero the penetration. Physically, this modelization is more correct, but on the other hand, the number of unknowns passes from N (degree of freedom) to $N + N_\lambda$ (number of λ multipliers).

These unknowns lead to a modification of the stiffness matrix. Addind new terms into it could lead to ill-conditioning of the problem and consequently to convergence difficulties. Moreover, even if it does not happen, the computational time involving a bigger matrix is longer respect to the other alghoritms.

However, despite all the previous cons mentioned before, Lagrange method is the only one that give an exact solution.

2.2.3.3 Augmented lagrange method

The idea behind this formulation is to combine the Penalty and Lagrange methods. Indeed, inside the energetic expression there are both the λ and the ε parameters:

$$\Pi_c^{ALM} = \begin{cases} \int_{\Gamma_c} (\lambda_N g_N + \frac{\varepsilon_N}{2} g_N^2) d\Gamma & \text{for } \widehat{\lambda}_N \leq 0 \\ \int_{\Gamma_c} -\frac{1}{\varepsilon_N} |\lambda_N|^2 & \text{for } \widehat{\lambda}_N \geq 0 \end{cases}$$

The approach to solve the problem is similar to Lagrange one, but this time the functional is written like:

$$\mathcal{L}(x, \lambda) = F(x) + \Pi_c^{LM}(\lambda)$$

“As λ can be considered as a force, so it will push x_i closer to the solution and vice versa: if $g(x_i) > 0$, the Lagrange multiplier should be increased to pull x_i to the solution. If $g(x_i)$ gradually tends to zero, λ_i converges to the solution.” [VLAD 13]

This hybrid formulation has both pro and cons of the two methods: on one hand the number of unknowns is increased but on the other hand the convergence problem are overcome thanks to the Penalty factor ε_N and the solution is near to the

exact one. There is only a slight dependence by the contact stiffness ε_N but not so strong like in the pure Penalty method.

3 Study cases presentation

This chapter contains the description of the models (geometry, elements, mesh setting) utilized during the various phases of the project and their boundary conditions (loads, constraints). Initially, a very simple model has been adopted, in order to be as close as possible to the Newmark's assumption. Then its complexity has been gradually increased up to define a valid and reliable procedure that could be applied to a real structure.

3.1 The test cases

In order to develop and validate a correct ANSYS procedure for stability analysis, several load conditions have been tested, the same already used to validate the VBA macro for the NE method. For each of them has been defined as an accelerogram (variable for intensity, direction and sign) and the conditions of the soil surrounding the building. The scheme below shows sides numbering and the soil layout valid for each load case:

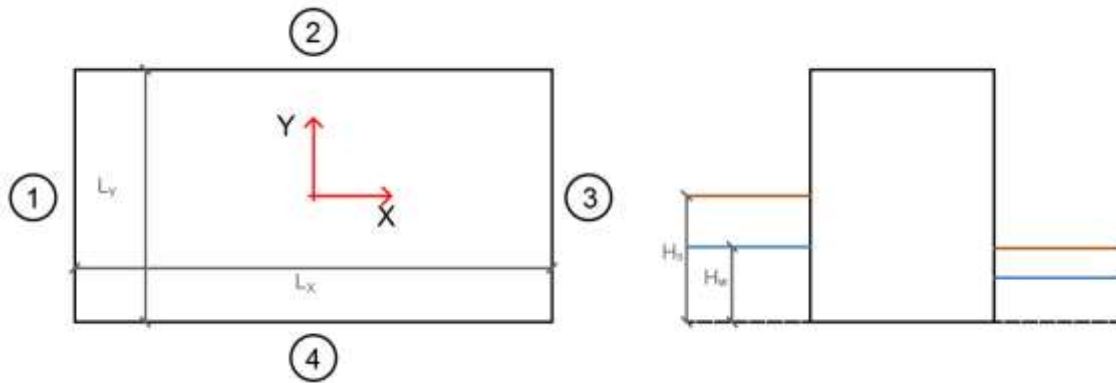


Figure 3.1 Boundary condition for the surrounding soil

For each case has been defined, for every side of the model, the height of the ground (H_s) and of the groundwater table level (H_w).

3. Study cases presentation

- CASE 1**

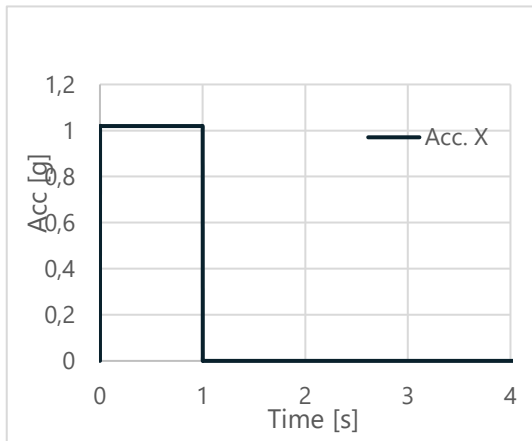


Figure 3.2 Accelerogram Case 1

SIDE	Application	H _s [m]	H _w [m]
1	N	-	-
2	N	-	-
3	N	-	-
4	N	-	-
Vertical	N	-	-

Table 3.1 Case 1 / Surrounding ground conditions

- CASE 2**

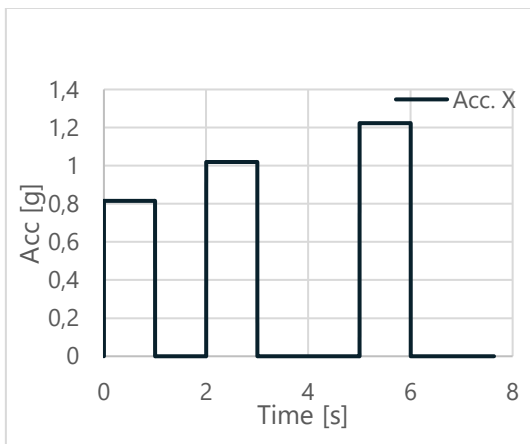


Figure 3.3 Accelerogram Case 2

SIDE	Application	H _s [m]	H _w [m]
1	N	-	-
2	N	-	-
3	N	-	-
4	N	-	-
Vertical	N	-	-

Table 3.2 Case 2 / Surrounding ground conditions

- CASE 3**

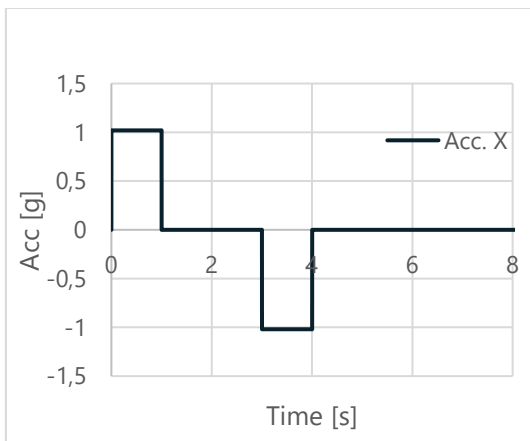


Figure 3.4 Accelerogram Case 3

SIDE	Application	H _s [m]	H _w [m]
1	N	-	-
2	N	-	-
3	N	-	-
4	N	-	-
Vertical	N	-	-

Table 3.3 Case 3 / Surrounding ground conditions

• **CASE 4**

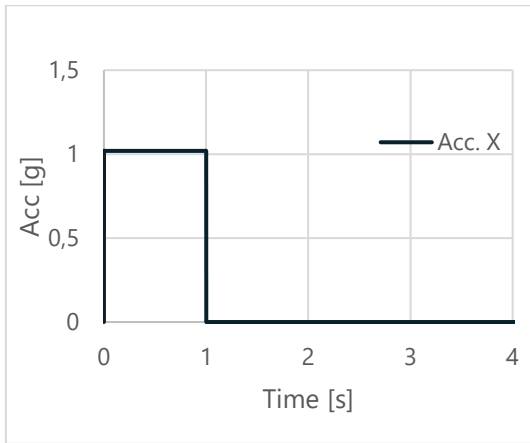


Figure 3.5 Accelerogram Case 4

SIDE	Application	H_s [m]	H_w [m]
1	N	-	-
2	N	-	-
3	N	-	-
4	N	-	-
Vertical	Y	-	5

Table 3.4 Case 4 / Surrounding ground conditions

• **CASE 5**

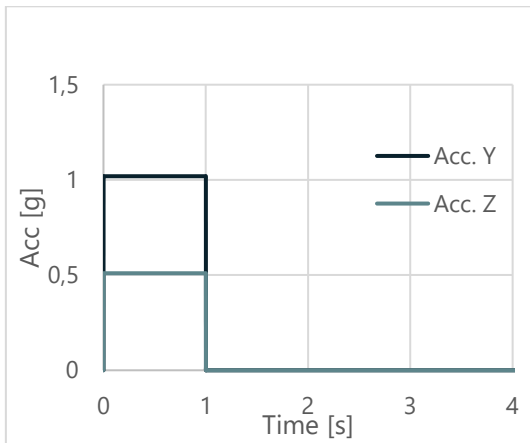


Figure 3.6 Accelerogram Case 5

SIDE	Application	H_s [m]	H_w [m]
1	N	-	-
2	N	-	-
3	N	-	-
4	N	-	-
Vertical	N	-	-

Table 3.5 Case 5 / Surrounding ground conditions

• **CASE 6**

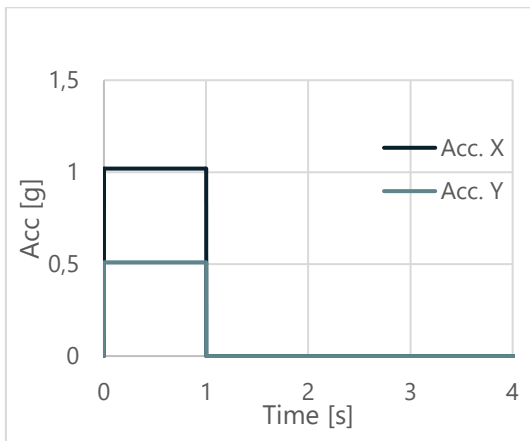


Figure 3.7 Accelerogram Case 6

SIDE	Application	H_s [m]	H_w [m]
1	N	-	-
2	N	-	-
3	N	-	-
4	N	-	-
Vertical	N	-	-

Table 3.6 Case 6 / Surrounding ground conditions

• **CASE 7**

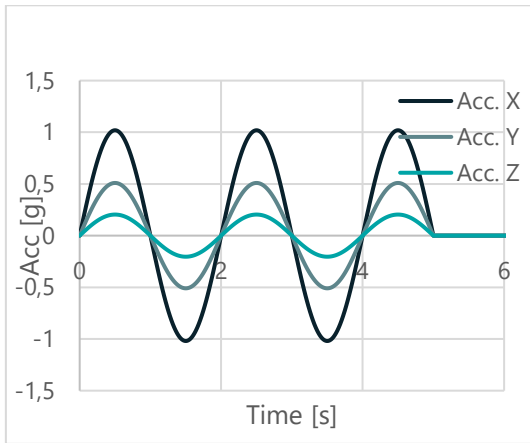


Figure 3.8 Accelerogram Case 7

SIDE	Application	H_s [m]	H_w [m]
1	Y	3	2
2	Y	3	-
3	N	-	-
4	N	-	-
Vertical	N	-	-

Table 3.7 Case 7 / Surrounding ground conditions

• **CASE 9**

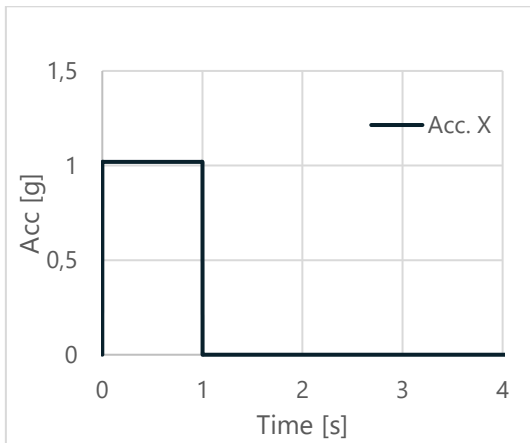


Figure 3.9 Accelerogram Case 9

SIDE	Application	H_s [m]	H_w [m]
1	Y	3	-
2	N	-	-
3	N	-	-
4	N	-	-
Vertical	N	-	-

Table 3.8 Case 9 / Surrounding ground conditions

• **CASE 10**

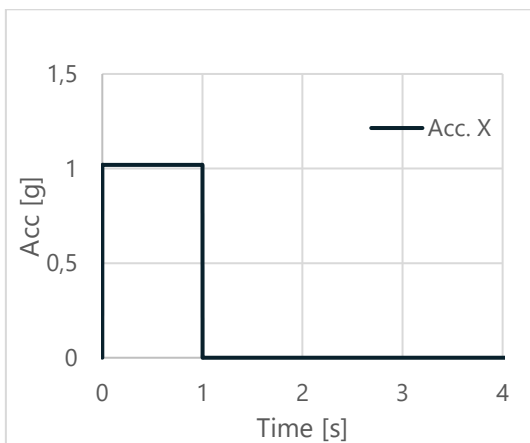


Figure 3.10 Accelerogram Case 1

SIDE	Application	H_s [m]	H_w [m]
1	Y	3	2
2	N	-	-
3	N	-	-
4	N	-	-
Vertical	N	-	-

Table 3.9 Case 10 / Surrounding ground conditions

3. Study cases presentation

- **CASE 11**

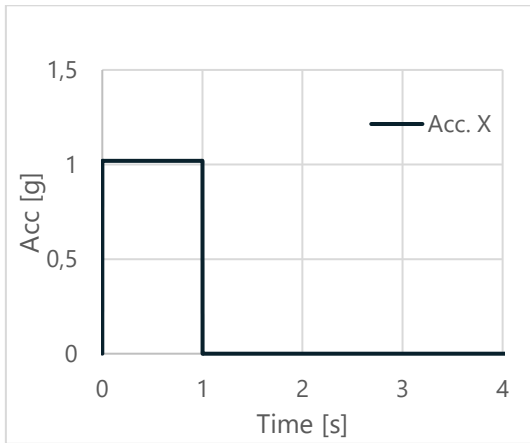


Figure 3.11 Accelerogram Case 11

SIDE	Application	H_s [m]	H_w [m]
1	Y	3	2
2	Y	4	-
3	N	-	-
4	N	-	-
Vertical	N	-	-

Table 3.10 Case 11 / Surrounding ground conditions

- **CASE 12**

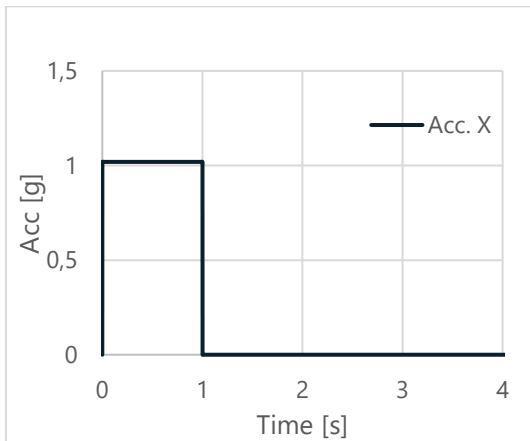


Figure 3.12 Accelerogram Case 12

SIDE	Application	H_s [m]	H_w [m]
1	Y	3	-
2	N	-	-
3	Y	3	-
4	N	-	-
Vertical	N	-	-

Table 3.11 Case 12 / Surrounding ground conditions

- **CASE REAL**

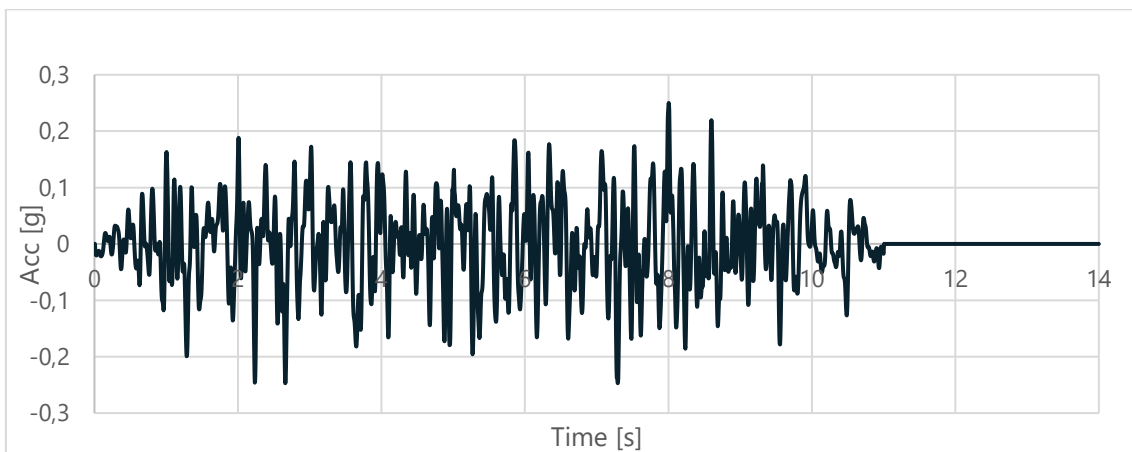


Figure 3.13 Accelerogram Case Real / X-direction

3. Study cases presentation

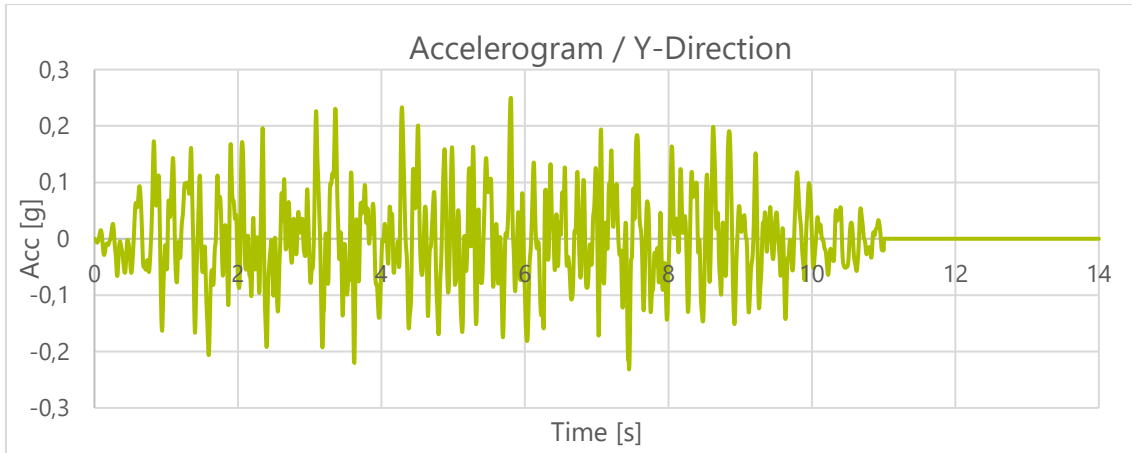


Figure 3.14 Accelerogram Case Real / Y-direction

SIDE	Application	H_s [m]	H_w [m]
1	Y	3	2
2	Y	3	-
3	N	-	-
4	N	-	-
Vertical	N	-	-

Table 3.12 Case Real / Surrounding ground conditions

3.2 Models

3.2.1 Model 1

1.7.1.1 GEOMETRIC MODEL

The first model has been used to replicate the Newmark's methodology and so to compare the VBA macro's results with ANSYS's solutions. The method does not take into account the geometry of the structure and so, as shown in the fig.XXX and so the model is composed by a cube of unitary dimensions (1 x 1 x 1). The ground instead, as it has to be a rigid surface, it is represented by a square big enough to contain the cube sliding on it.

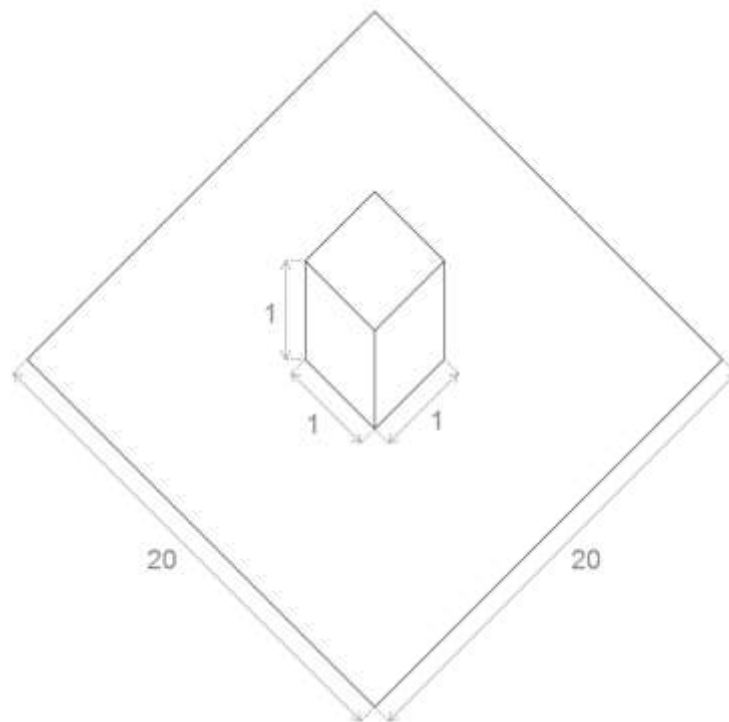


Figure 3.15 Geometry Model 1

1.7.1.2 Numerical Model

- **Rigid block**

The element used to mesh the rigid block is the *SOLID 185* (Figure 3.16):

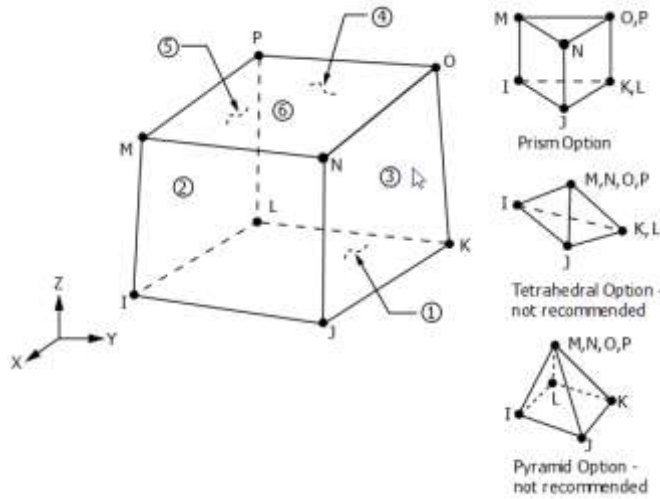


Figure 3.16 SOLID 185 scheme

It is a 3D eight-node element with three degrees of freedom at each node (translations in the x , y , and z directions). The element has plasticity, hyperelasticity, stress stiffening, creep, large deflection, and large strain capabilities. It also has a mixed formulation capability. (Ansys Help)

This element has several Keyoptions, but for the problem under examination, the default options are used.

- **Rigid surface**

Regarding the sliding plane, as it has to be a rigid surface, the geometry has meshed only with the *TARGE 170* mentioned above. Even in this case, all the default options are suitable for the problem under examination.

- **Contact surface**

The contact surface has been defined meshing the element *CONTA 173* on the bottom face of the already meshed rigid block. In this way, the two elements have common nodes and the effects are transferred from one to the other and vice versa. Between the various element options and real constant before mentioned, for the case under examination have been modified the following parameters showed in the tables:

Table 3.13: Keyoptions for CONTA173

KEYOPT	FUNCTION	VALUE	DESCRIPTION
1	Select DOF	0	I want to utilise only U_x , U_y , U_z . Others options are not interesting for this problem.
2	Contact algorithm	0/4	0 = Augmented Lagrange (Penalty) 4 = Pure Lagrange

3. Study cases presentation

5	CNOF/ICONT auto	0	Eliminate automatically small gaps or penetrations adjusting the two Real Constant CNOF and ICONT. I do not want any automatic adjustment from the software. Further explanation will follow below
9	Effect of initial penetration	1	Exclude the initial penetration/gap. I do not want to take into account the effect of an eventual initial penetration due to a numerical approximation. Otherwise, an erroneous approximation of the contact forces could occur, leading to no-convergence problem or false results.
12	Contact behaviour	2	No separation: uplift is not allowed. In this phase, we would just duplicate the N-E method which does not consider uplift.

Table 3.14: Real Constant for CONTA173

Real Constant	FUNCTION	VALUE	DESCRIPTION
3	FKN (Penalty only)	1	Define a scalar value for the normal stiffness. This will affect the amount of penetration between the two bodies. As explained for the KEYOPT(9), too much penetration must be avoided. Further explanation will follow below
5	PINB	0.25	Define a scalar value for a circular region, of radius 2*underlying element, in which the code will assign a status (sliding, sticking, near field) for the contact element. This region is centred on the Gauss point of the contact element. If too big, false contact relation could be established, and computational time will increase.

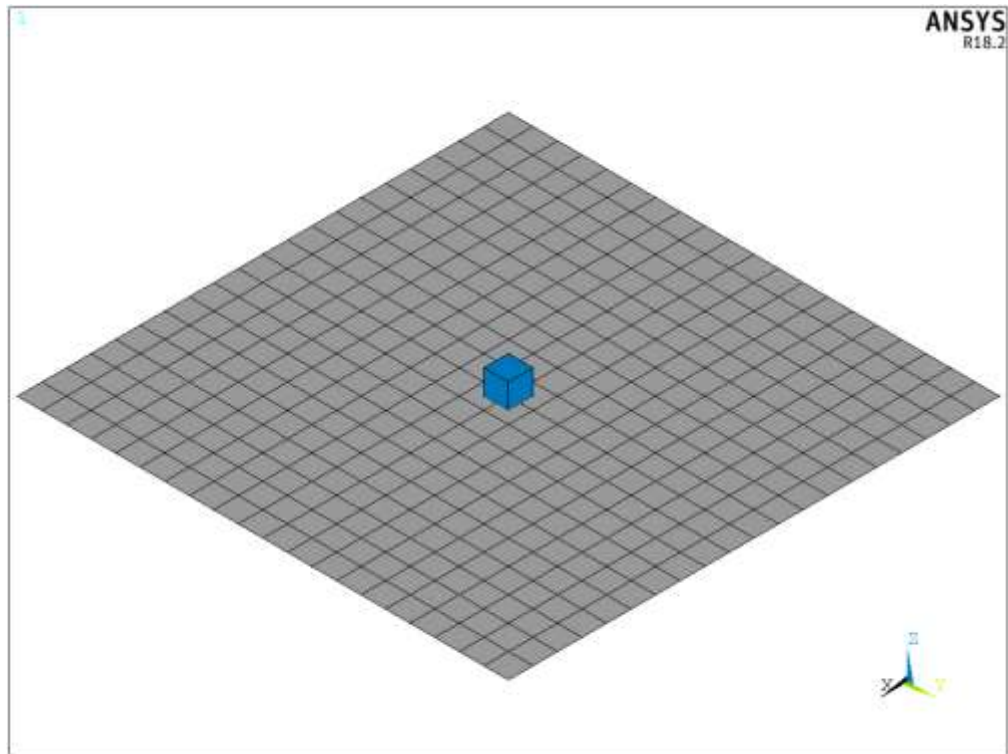


Figure 3.17 Model 1 meshed

3.2.2 Model 2

3.2.2.1 Geometric model

The second model is an optimization of the first and it has been utilized for the same scope. Geometrically, the ground is represented by a square area as in the previous model; only the rigid block has been modified, and now is represented by a unitary square area (there is no more the third dimension). In this way, every eccentricity from the sliding surface has been eliminated.

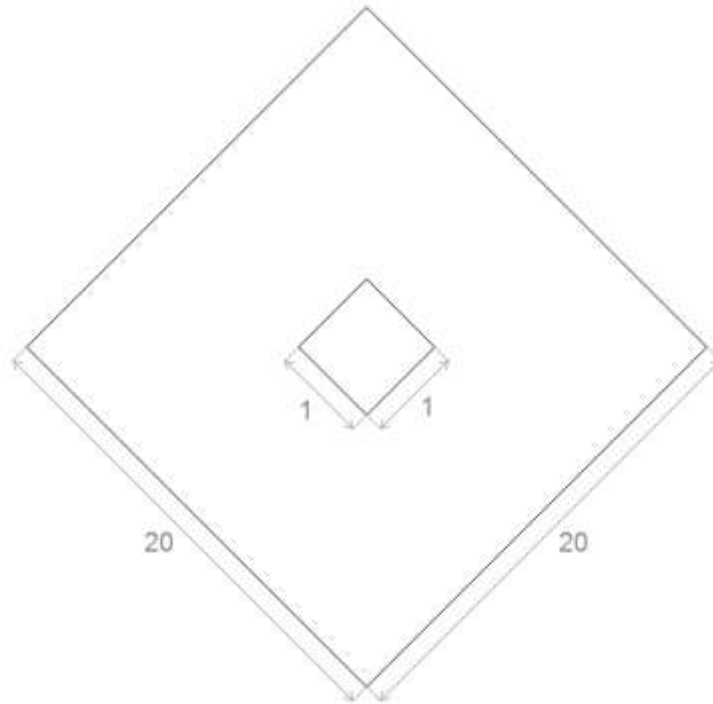


Figure 3.18 Geometry Model 2

3.2.2.2 Numerical model

- **Rigid block**

This time the rigid block has been modelled by means of more element; the base element is the *SHELL 181* (Figure 3.19):

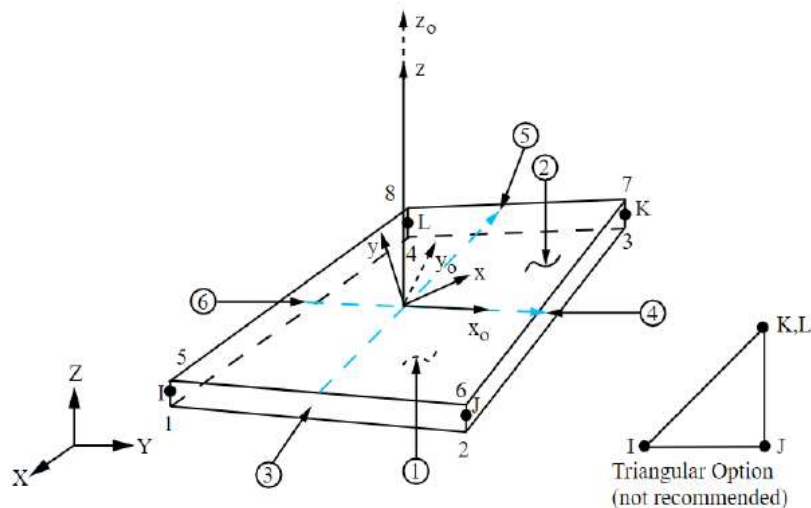


Figure 3.19 SHELL 181 scheme

It is a four-node element with six degrees of freedom for each node (translations in the x , y , and z directions and rotation around x , y , and z -axis). It is well-suited for linear, large rotation, and/or large strain nonlinear applications.

The element supports full integration with incompatible modes, and reduced integration method, with the control of the spure deformation. By default, this element uses the uniformly reduced integration for performance reasons in nonlinear applications (Ansys Help). For this application, default options are well suited.

Next, to be as close as possible to the NE model, all the mass has been concentrated in an additional node, placed at the centre of gravity, by means of a special element called *MASS 21* (Figure 3.20):

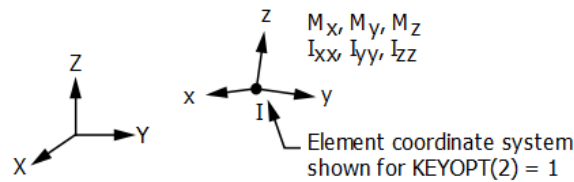


Figure 3.20 MASS 21 scheme

It is a point element having up to six degrees of freedom: translations in the nodal x , y , and z directions and rotations about the nodal x , y , and z -axes. A different mass and rotary inertia may be assigned to each coordinate direction (Ansys Help). Then, to assign the mass to the element, a real constant has been used; the table below shows the values assigned to this last:

Table 3.15: MASS 21 - Real Constant

Real constant	FUNCTION	VALUE	DESCRIPTION
1	MASS X	1000000	Mass in x-direction
2	MASS Y	1000000	Mass in y-direction
3	MASS Z	1000000	Mass in z-direction

In order to avoid any undesired deformation of the shell element, the four corner nodes have been linked to an additional node placed at the centre of gravity by means of rigid link element called *MPC 184*; these represent a general class of multipoint constraint elements that apply kinematic constraints between nodes (Ansys Help). In this case, the MPC element has been used as a rigid link/beam component used to transmit forces and moments coming from the inertia loads generated by the acceleration of the body.

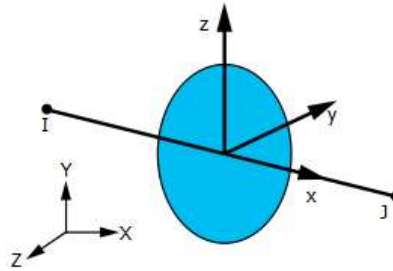


Figure 3.21 MPC 184 scheme

The (Figure 3.21) shows the geometry, node locations, and the coordinate system for this element. Two nodes define the element. The element x-axis is oriented from node I toward node J. The cross-sectional area of the element is assumed to be unitary and is relevant only for the output of bending moments when the element is used as a rigid beam (Ansys Help).

- **Target surface**

As for the previous model, the sliding surface has been modelled in the same way and with the same characteristic. No changes were necessary.

- **Contact surface**

The contact surface has been defined meshing the element *CONTA 173* on the bottom face of the shell element.

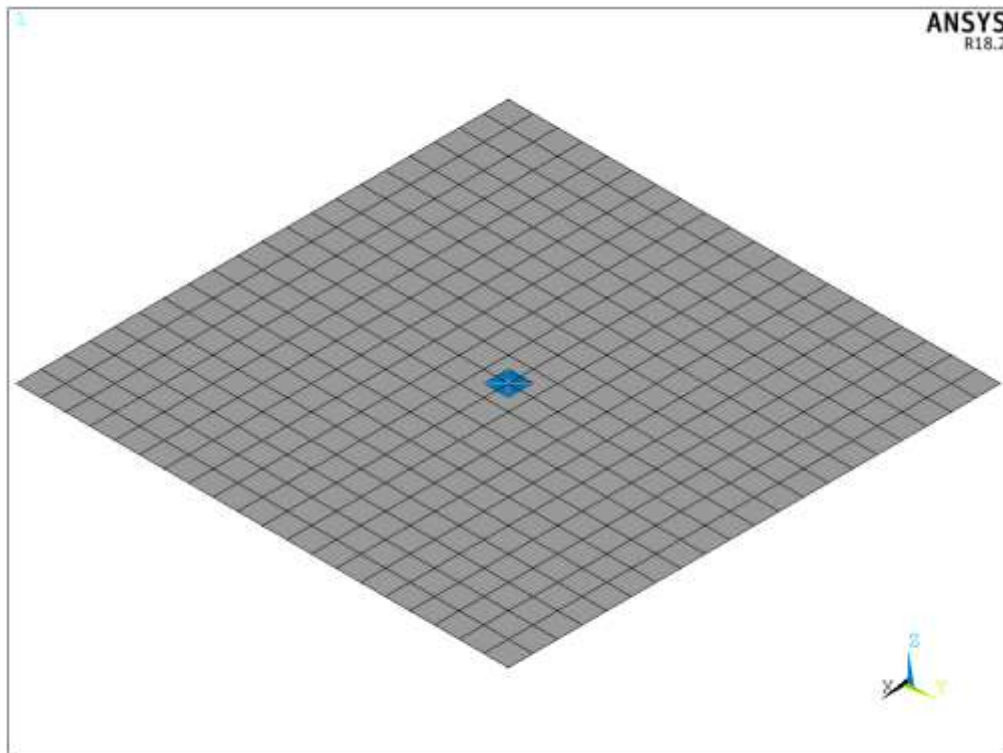


Figure 3.22 Model 2 meshed

3.2.3 Model 3

3.2.3.1 Geometric model

The third model is the most similar to a real structure model, but at the same time is geometrically simple to help the study of this delicate phase. It is a 2 storeys building, having a parallelepiped shape 16,5 m wide, 39,2 m long and of a height of 18,05 m, with a raft foundation at the base and some internal wall at ground floor. The external walls have a thickness of 1,6 m, while the internal ones of 0,6 m. Regarding the horizontal slabs, the raft is 1,5 m thick, the roof 1,3 m and the internal slab 0,6 m.

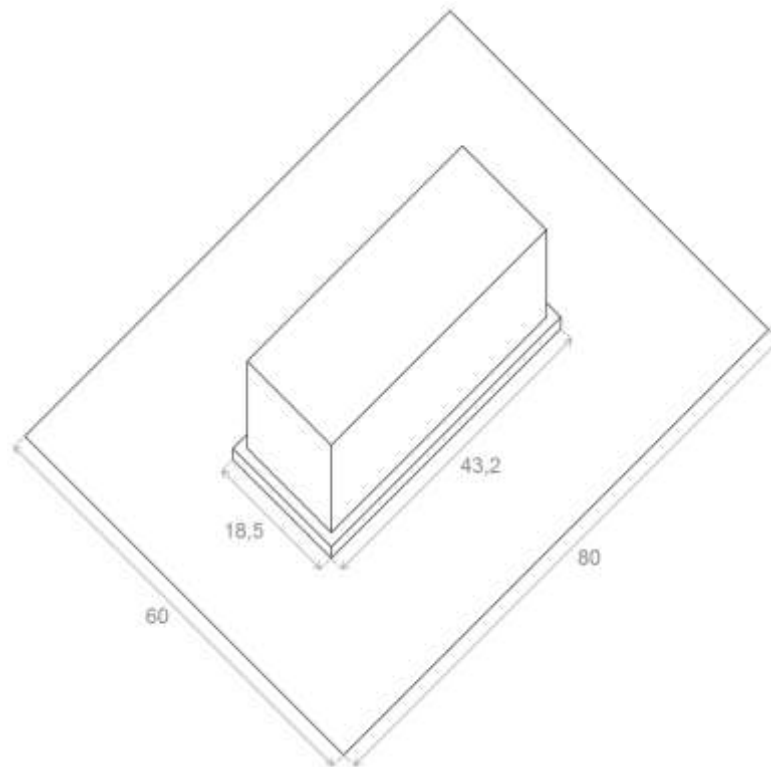


Figure 3.23 Assonometric view of the geometric Model 3

3.2.3.2 Numerical model

- **Building**

All the components of the building have been modelled with *SHELL 181* element. Then, to assign different thickness to every component, it has been created a real constant for each of them. Moreover, to simulate some additional mass present on the building, *MASS 21* elements have been added in some areas of the ground and the first-floor slab.

In order to calibrate the dimension of the mesh, it has been conducted some modal analysis with three different mesh size. Then, the frequency of the firsts three

modes has been compared so as to find the mesh size value where convergence was reached.

MODE	Mesh 0,5	Mesh 1
1	7.0378	7.0393
2	9.8001	9.8761
3	10.463	10.610
4	11.949	12.005
5	12.734	12.889

Table 3.16 Mode's frequencies for two different mesh size

- **Target surface**

As for the previous models, the sliding surface has been modelled in the same way and with the same characteristic. No changings are necessary.

- **Contact surface**

The contact surface has been defined meshing the element *CONTA 173* on the bottom face of the shell elements that compose the raft foundation.

The resulting model is the following:

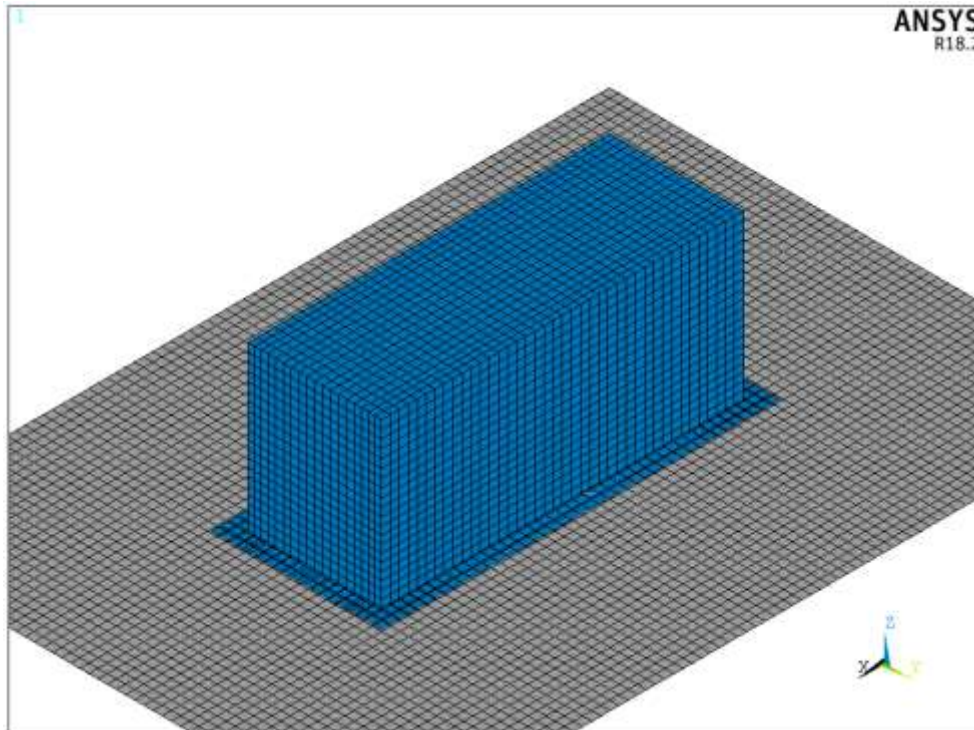


Figure 3.24 Model 3 meshed

3.3 Materials

3.3.1 Concrete

For all the three models, only the concrete has been used. This is not an infinite rigid material, as stated in NE method, but as the dimension of the block are not so big and the elements utilized for the mesh is only one, it is intrinsically rigid enough to respect that hypothesis. To verify this hypothesis, a horizontal force has been applied to the model in order to verify if there were differences in displacements between the bottom and top nodes. The results showed identical displacements so that it is possible to affirm that the hypothesis of the rigid block is verified.

Inside ANSYS environment, it is possible to define several kinds of material with different behaviours (isotropic, non-isotropic, non – linear constitutive law, etc.); concrete is a highly non – linear material, with high compressive resistance but an almost null traction resistance. However, since the goal of this project is to study the global stability, a linear constitutive law has been assumed.

To define an isotropic linear material, ANSYS requires only a few parameters:

- Elastic module
- Density
- Poisson coefficient

For this project, these values are given directly from the client of the building.

3.3.2 Friction model

The interaction between the soil and the structure is governed by the friction coefficient; in ANSYS is possible to define a Coulomb friction model: it defines an equivalent tangential stress τ_{eq} at which sliding on the surface begins. Before that, no movement occurs and the state is known as sticking. Once the τ_{eq} is exceeded, the two surfaces will slide relative to each other. This state is known as sliding (Ansys Help).

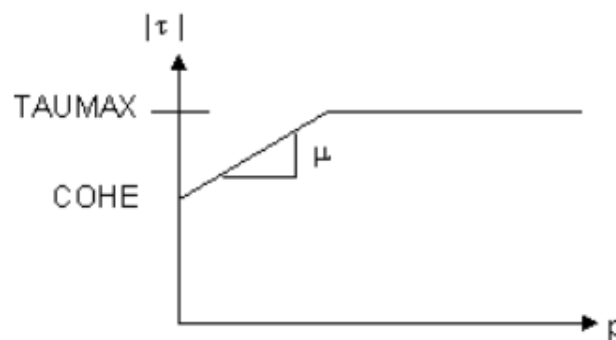


Figure 3.25 Coulomb's law

As shown in the picture, it is possible to modify the friction model by means of three parameters:

- TAUMAX: real constant which defines the maximum contact friction;
- CHOE: real constant which provides a sliding resistance with zero normal pressure
- μ : coefficient of friction governed by the following relation:

$$\mu = MU \cdot (1 + (FACT - 1) \cdot \exp(-DC \cdot V_{rel}))$$

Where:

MU: dynamic coefficient of friction;

FACT: the ratio of static to dynamic coefficients of friction (equal to 1 by default);

DC: decay coefficient (equal to 0 by default);

When all coefficients are the defaults one, the equation is rewritten as:

$$\mu = MU$$

The interface coefficient of friction, MU, is defined as a material property for the contact elements.

3.4 Load description

Usually, in the design of this kind of buildings, there are many loads to take in consideration, many of which coming from accidental and unpredictable situations. As this study born for a research purpose, only the most necessary loads have been taken into account.

3.4.1 Dead load

The permanent loads G_c include:

- Deadweight of the structure/building G_c :
 - Self-weight of structural elements and uniform permanent loads on slabs;
 - Weight of permanent non-modelled masses, such as non-structural walls, staircases and air ducts;
- Deadweight of fixed equipment, secondary frameworks and security doors;

3.4.2 Static lateral pressure due to earth

The load case G_G includes the permanent lateral pressure of earth σ_n presents besides the building. The static lateral earth pressure is calculated according to the following figure:

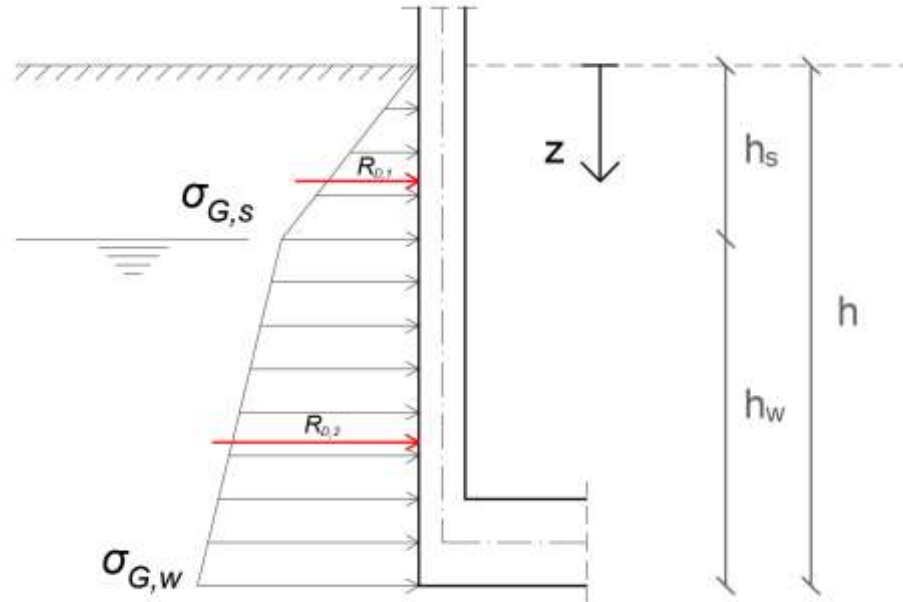


Figure 3.26 Static earth pressure

$$\sigma_{G,s} = K_0 \cdot \gamma \cdot z$$

$$\sigma_{G,w} = K_0 \cdot (\gamma \cdot h_s + \gamma' \cdot (z - h_s))$$

Where:

- K_0 earth pressure coefficient at rest, equal to 0.5
- h_s height between the ground level and the water level
- h_w height between the water level and the bottom face of the raft
- γ, γ' unit effective weight and unit wet weight of the soil

The resultant forces of the two pressures are given by:

$$R_{G,s} = \frac{1}{2} \cdot \sigma_{G,s} \cdot h_s \cdot L$$

$$R_{G,w} = \frac{1}{2} \cdot (\sigma_{G,s} + \sigma_{G,w}) \cdot h_w \cdot L$$

3.4.3 Permanent level of the groundwater table

The effect of the permanent level of the groundwater table on the nuclear power island is taken into account by considering the following water pressures:

- Vertical water pressure under the raft;

- Lateral water pressure.

The vertical and lateral water pressures due to the permanent level of the groundwater are calculated as showed in the following figure:

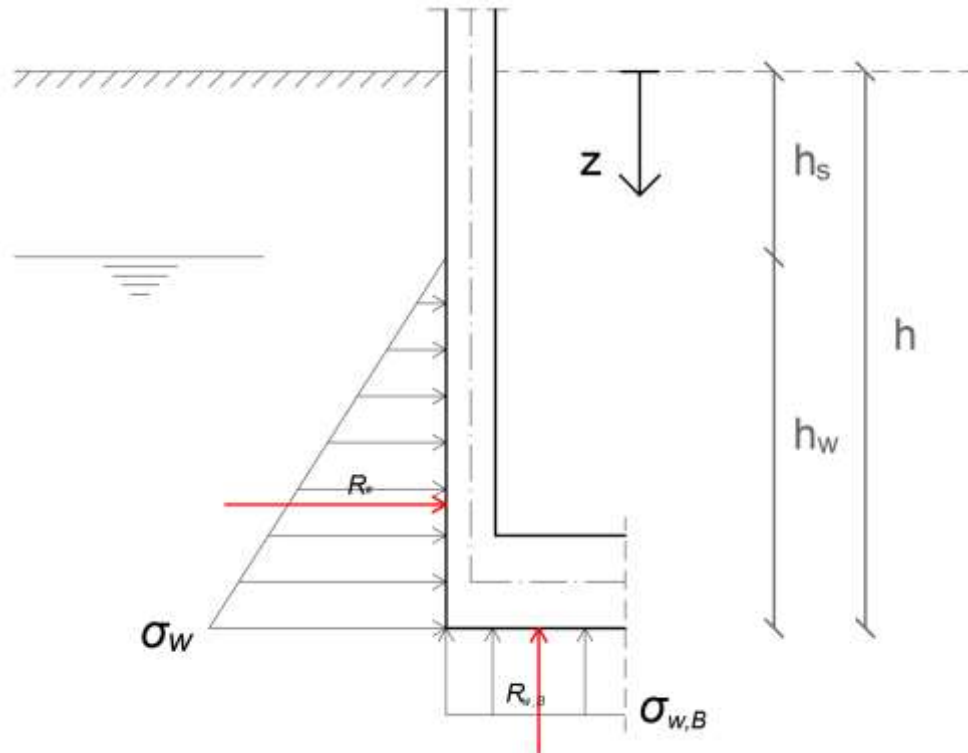


Figure 3.27 Static water pressure

$$\sigma_w = \gamma_w \cdot (z - h_s)$$

The resultant forces of the lateral and vertical pressures are given by:

$$R_W = \frac{1}{2} \cdot \sigma_w \cdot h_w \cdot L$$

$$R_{W,Ver} = \sigma_w \cdot A_{Raft}$$

3.4.4 Dynamic lateral earth pressure due to earthquake

The dynamic lateral earth pressure has to be combined with the seismic action. The action corresponds to four distinctive load cases:

- Load case $A_{d,E,g,1}$: earth pressure in the positive X-direction;
- Load case $A_{d,E,g,2}$: earth pressure in the negative X-direction;
- Load case $A_{d,E,g,3}$: earth pressure in the positive Y-direction;
- Load case $A_{d,E,g,4}$: earth pressure in the negative Y-direction.

The dynamic lateral earth pressure is defined by a uniform diagram in the following way:

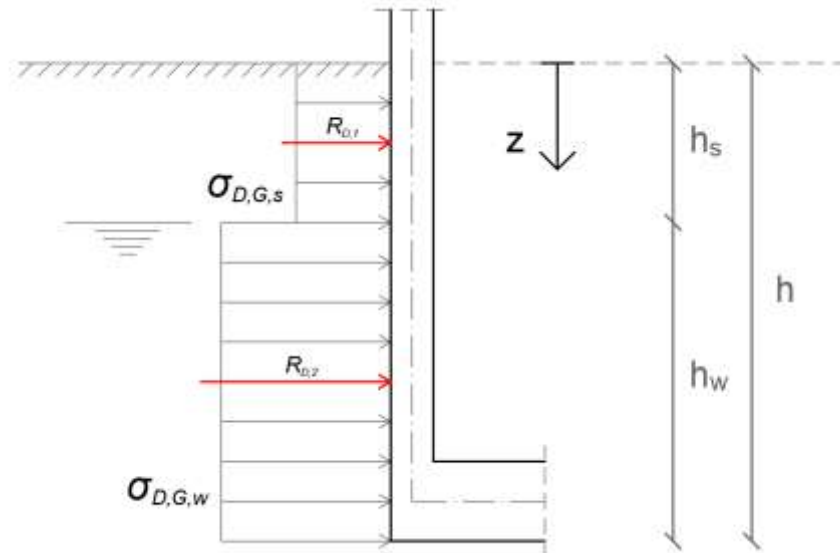


Figure 3.28 Dynamic earth pressure

$$\sigma_{D,G,s} = \alpha \cdot S \cdot \gamma \cdot h_s$$

$$\sigma_{D,G,w} = \alpha \cdot S \cdot \gamma' \cdot h_w + 2 \cdot \alpha \cdot S \cdot \gamma' \cdot h_s$$

Where:

- α ratio between the ground acceleration and the acceleration of gravity, taken equal to 1
- S parameter function of the soil class, taken equal to 1
- h_s height between the ground level and the water level
- h_w height between the water level and the bottom face of the raft
- γ, γ' unit wet and effective soil density, equal respectively to 23.2 kN/m³ and 13.4 kN/m³

The resultant forces of the two pressures is given by:

$$R_{D,G,s} = \sigma_{D,G,s} \cdot h_s \cdot L$$

$$R_{D,G,w} = \sigma_{D,G,w} \cdot h_w \cdot L$$

3.4.5 Hydrodynamic pressure of the groundwater

This hydrodynamic pressure of the groundwater has to be combined with the seismic action. This action corresponds to four different load cases:

- Load case $A_{d,E,g,w,1}$: water pressure in the positive X-direction;
- Load case $A_{d,E,g,w,2}$: water pressure in the negative X-direction;
- Load case $A_{d,E,g,w,3}$: water pressure in the positive Y direction;
- Load case $A_{d,E,g,w,4}$: water pressure in the negative Y direction.

The hydrodynamic lateral pressure of water is defined in the following way:

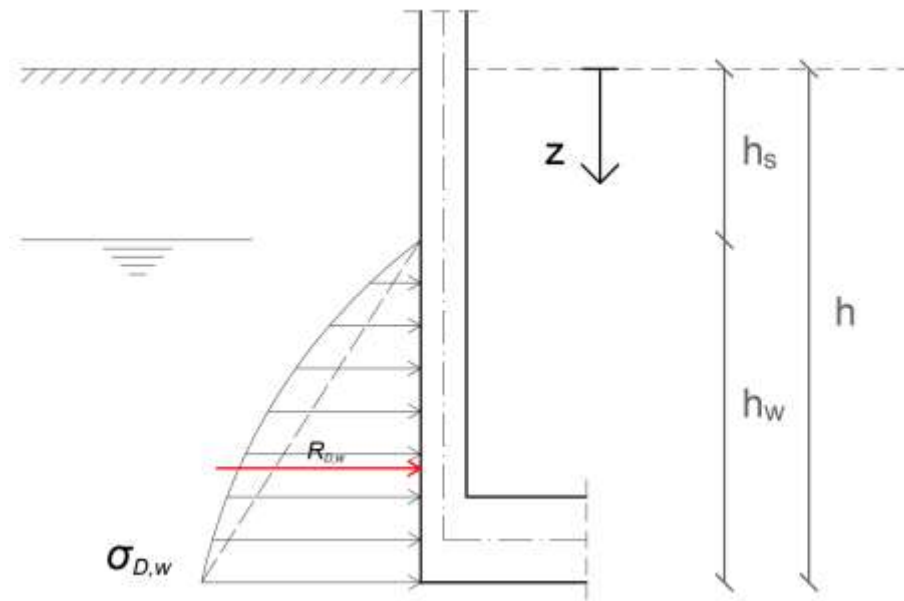


Figure 3.29 Dynamic water pressure

$$\sigma_{D,w} = \frac{7}{8} \cdot k_h \cdot \gamma_w \cdot \sqrt{h_w \cdot z}$$

Where:

- k_h horizontal seismic coefficient, taken equal to 1

As the area of that non – linear trend is not easy to obtain, the calculation of the resultant has been done assuming a triangular-shaped area:

$$R_{D,w} = \frac{1}{2} \cdot \sigma_{D,w} \cdot h_w \cdot L$$

3.5 Loads application

3.5.1 Inertia loads

All the inertia loads have been applied defining a global acceleration in X, Y or Z direction. The APDL command is the following:

ACEL, ACEL_X, ACEL_Y, ACEL_Z

When the value of the acceleration is constant, it is possible to specify it directly in the expression of the command. A typical example is the gravity acceleration:

ACEL, , , 9.81

When there is the necessity to apply a variable acceleration, the software requires to declare a table within which specify the value of the acceleration for every load step. Then, these are read from an external *.dat* file. To load a table, the command became:

ACEL, %acc_X%, %acc_Y%, 9.81

Moreover, the EC 8 require to decrease the variation of the Z-acceleration of 2/3; this operation can be done also with APDL commands, without the necessity to use other software. All the procedure has been parameterized and automatized inside the APDL environment.

3.5.2 Lateral static and dynamic earth/water action

Due to the differences between the models 1 / 2 from 3, the application of these loads has been done in a different way.

Generally, external forces in ANSYS can be applied in two different way: as concentrated forces or as surface loads. The commands relative to each of them are the following:

F, NODE, Lab, VALUE

SFE, Elem, LKEY, Lab, KVAL, VAL1

In both cases, the field value can be a constant value or a table containing the value of the force per each time – step.

If there is the necessity to specify a linearly varying surface load, such as hydrostatic or lateral earth pressure, the following command can be used:

SFGRAD, Lab, SLKCN, Sldir, SLZER, SLOPE

It defines the difference per unit length (*SLOPE*) along one direction (*Sldir*) in a specified reference system (*SLKCN*).

By default, if two forces (concentrated or distributed) are inserted one after the other, the second replaces the first. This option can be changed in order to cumulate them; this can be done with the following command:

FCUM, Oper, RFACT, IFACT

SFCUM, Lab, Oper, FACT, FACT2

This option is not valid when a force is inserted by a table.

After this brief introduction about loads' definition in ANSYS, below will be explained the different procedures utilized for every model:

- **MODEL 1**

Due to the simplicity of the model, only concentrated forces have been used. Firstly, for all the load condition (static and dynamic) resultants has been calculated. Secondly, inside a DO cycle, static forces have been summed to pseudo-static forces relative to the dynamic loads for every time step. This last is calculated multiplying the

resultant of the dynamic case with the acceleration at the time t divided by the PGA. The total value has been divided by the number of the nodes present on the upper face of the block and inserted in a table. Then, the table has been applied to each node of the upper face. The procedure has been executed for each planar direction.

- **MODEL 2**

For this model the same procedure before defined has been used; the only difference is that this time the forces are applied only on one node (the central one where all the mass is concentrated) and so, the forces do not need to be divided by the number of the nodes.

- **MODEL 3**

This time the various load cases have been applied in a different way; firstly, for every side of the building, a local coordinate system has been created in order to easily calculate the value of the forces depending by the boundary conditions. Then, due to the limitation of the cumulation of the loads, static and dynamic actions have been applied in different ways:

- **Static earth/water action**

Both have been applied as a surface load; first, the maximum pressure and the pressure at one meter from the base quote have been calculated; then, the gradient has been obtained from the difference between the two previous values.

Before the application of the action, it has to be noticed that the geometrical quotes of the upper surface of the soil and the groundwater table does not correspond with the mesh size in the model. Usually, this is not a problem because corrective nodal forces and moments (red arrows) can be applied.

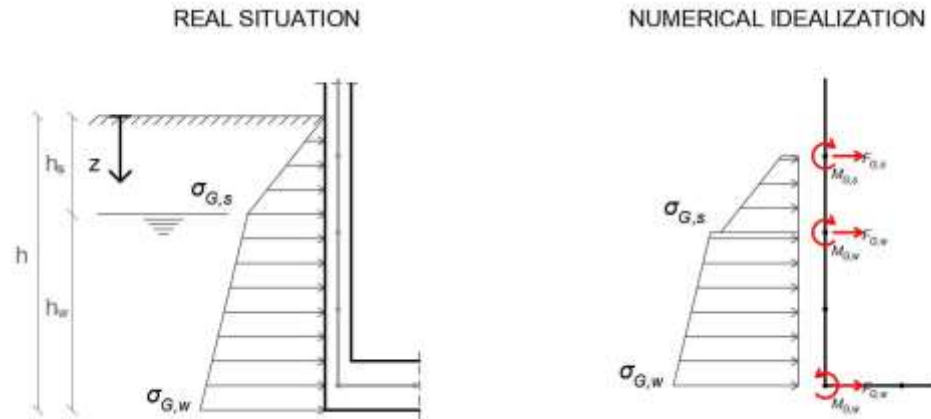


Figure 3.30 Real vs Numerical load

Unfortunately, for the limitations mentioned before, it is not possible to apply these corrective forces. To overcome the problem, pressures have been incremented by a percentage calculated with the ratio between the real resultant and the numerical one

NUMERICAL APPROXIMATION

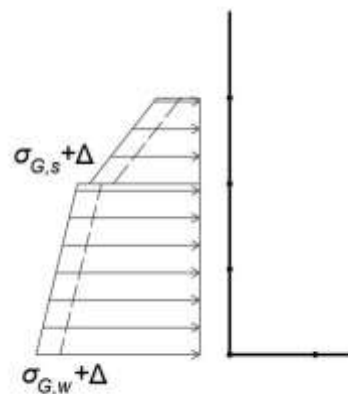


Figure 3.31 Static earth pressure simplification

Because of this, part of the information will be lost, but the approximation does not compromise the results.

○ **Dynamic earth/water action**

Since the distribution of these actions are constant along Z-direction, their application occurs by means of concentrated loads applied at every node. They are calculated dividing the total resultant by the number of nodes at each z-quote. Then, a table has been created for above and below groundwater level.

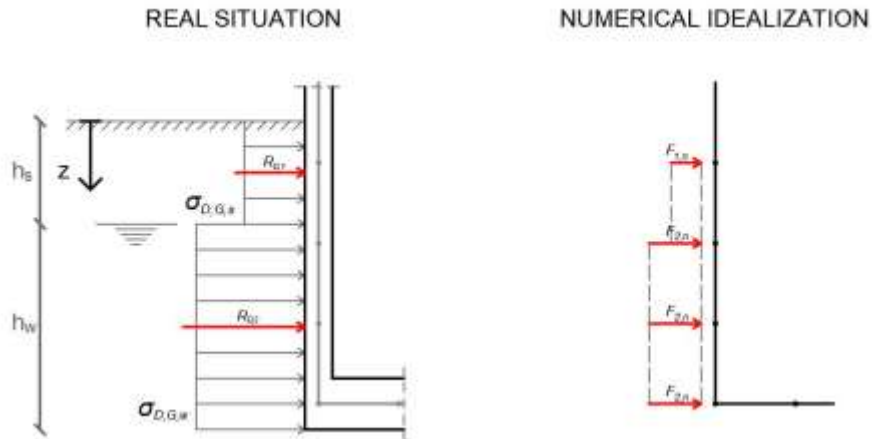
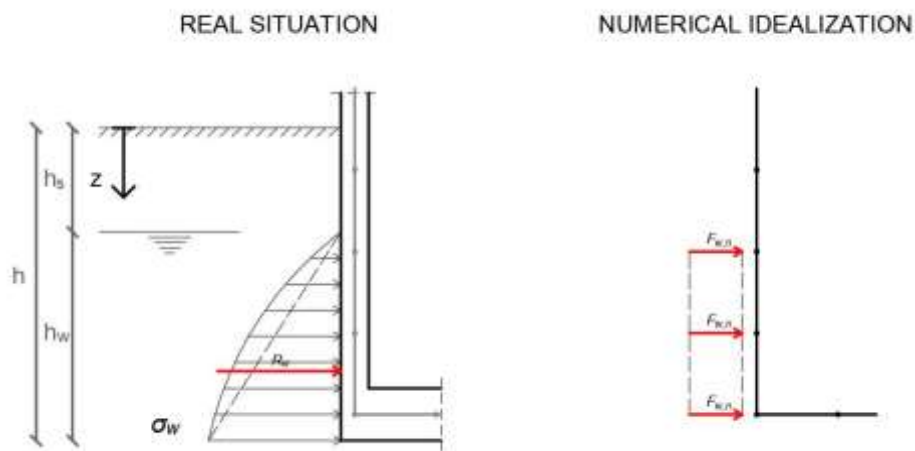


Figure 3.32 Dynamic earth pressure simplification

The last simplification regards the application of the dynamic water action. As shown before, this last has a parabolic trend with respect to the z -dimension. Theoretically, for each node level along z , should be created a table. This would require a much longer code and more computational time. So, for sake of simplicity, has been decided to divide the resultant of the parabolic trend by the number of nodes under the groundwater level.



3.6 Boundary condition

For all the tree models, the constraint between the building/block and the sliding surface is represented by the pair contact/target, while the sliding surface is constrained with the external environment by means of fully restrained DOF.

4 Case Study 1

This chapter contains results of the analysis conducted on the first model; the goal of this first part is to reproduce the Newmark – Elms theory and at the same time understand which parameters affect more the results and their accuracy.

The analysis has been conducted varying the FKN value, the sub-step time and the contact algorithm for each case test; the other parameters have been set as explained in the previous character. First, the absolute displacements of the block in function of the time will be shown, and then the maximum displacement for each FKN will be plotted in function of the sub-step time. In conclusion, critical comments on these results will be exposed.

4.1 Augmented Lagrange contact algorithm

4.1.1 Absolute displacements

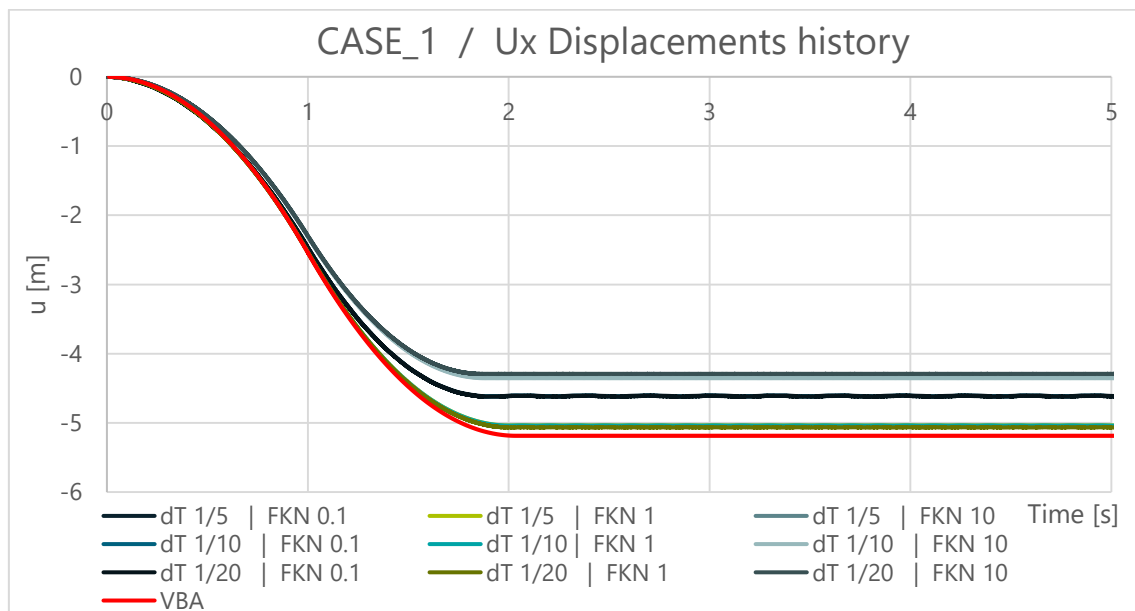


Figure 4.1 Case 1 / Ux displacements ALM

4. Case Study 1

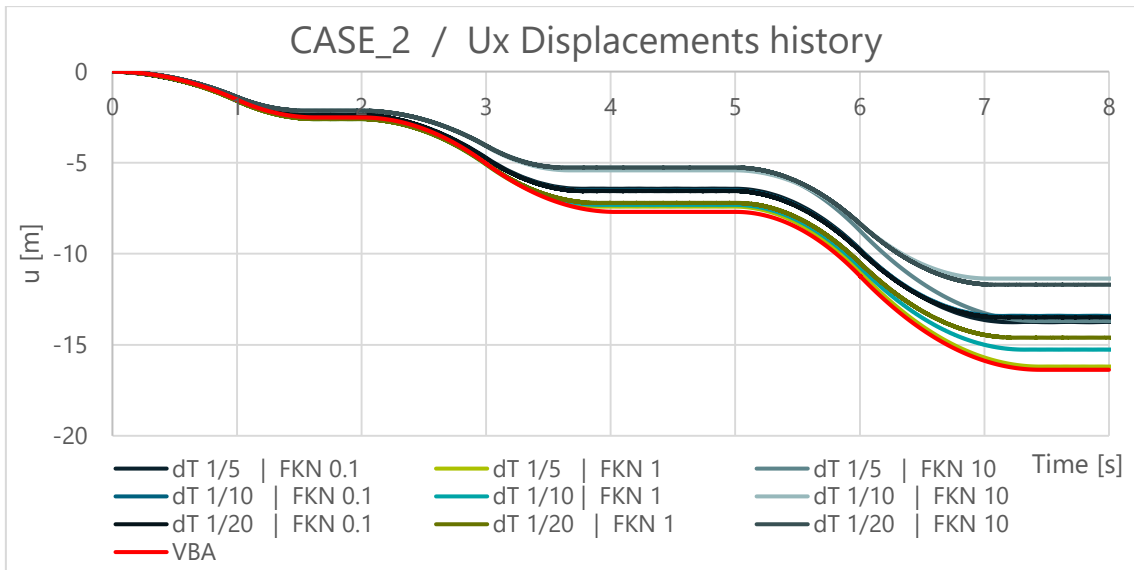


Figure 4.2 Case 2 / Ux displacements ALM

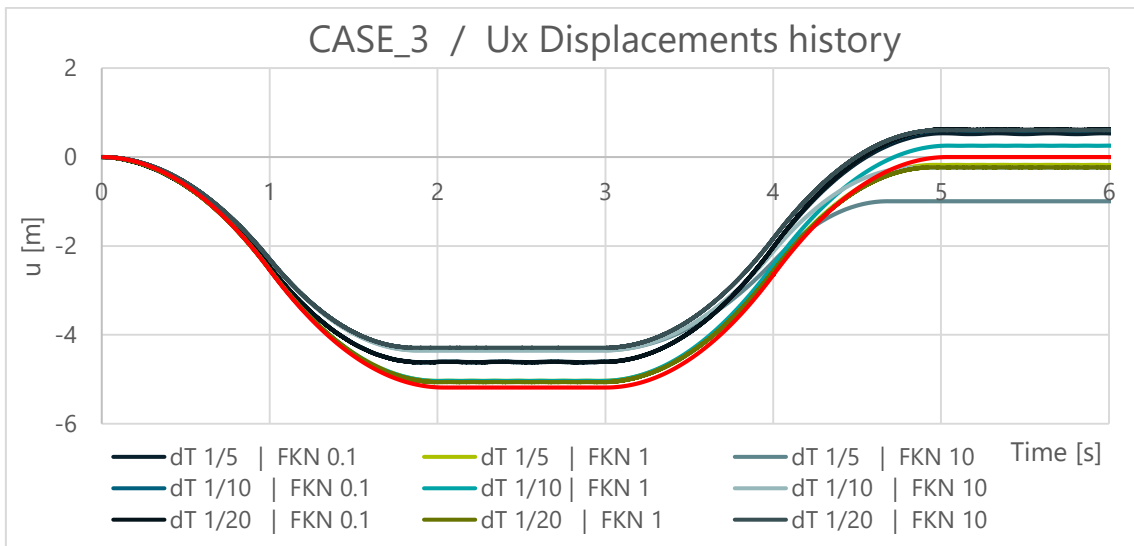


Figure 4.3 Case 3 / Ux displacements ALM

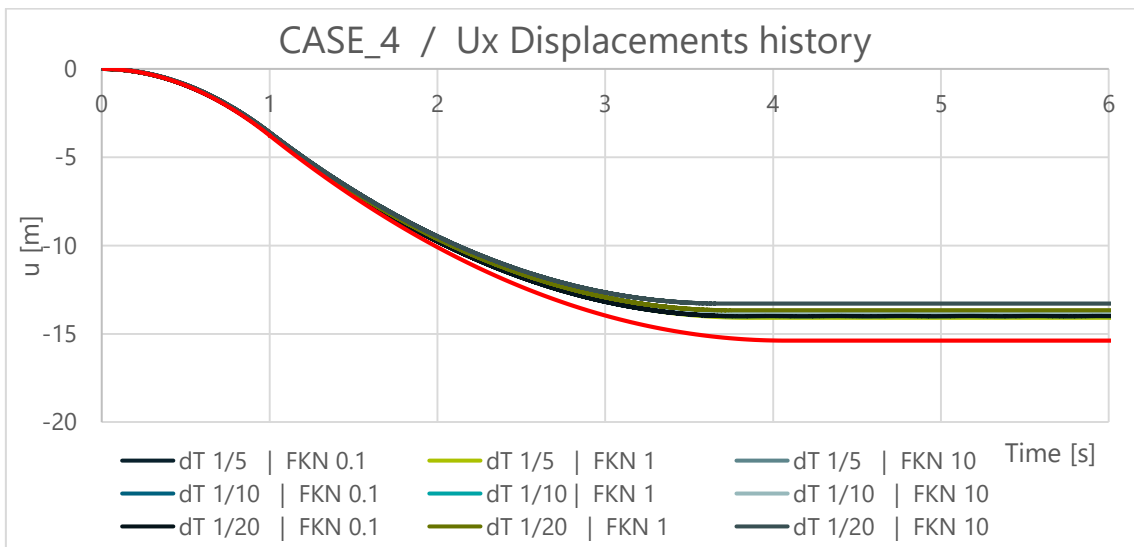


Figure 4.4 Case 4 / Ux displacements ALM

4. Case Study 1

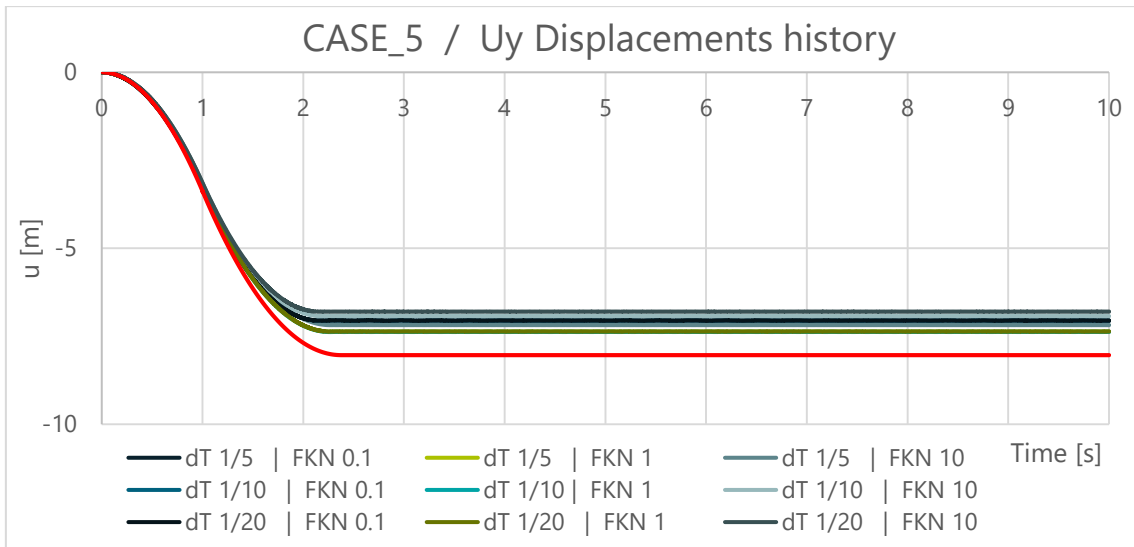


Figure 4.5 Case 5 / Uy displacements ALM

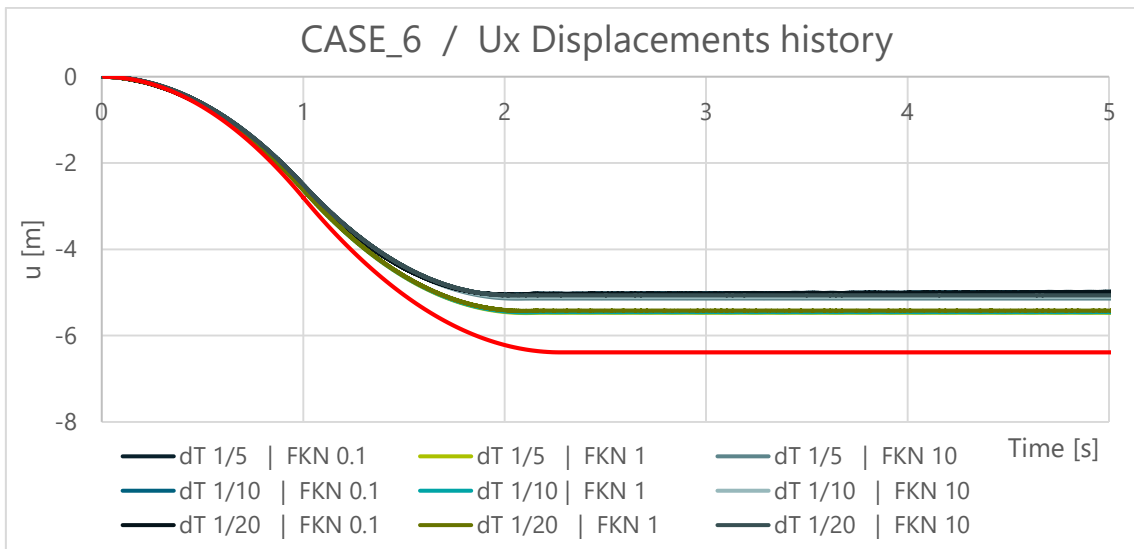


Figure 4.6 Case 6 / Ux displacements ALM

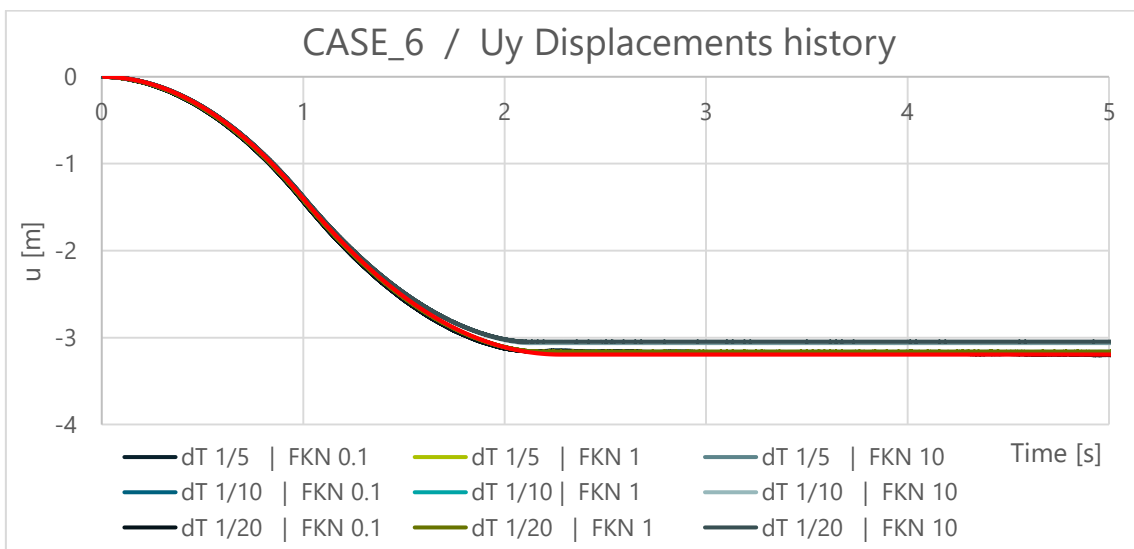


Figure 4.7 Case 6 / Uy displacements ALM

The graphs above show a big dependence on the results from both FKN value and Sub – step time. Generally, the accuracy is not so high; to better understand and quantify the best combination of the two factors, below will be plotted the maximum displacement in function of the two variables.

This will help to find a convergence value for the variable involved in the output:

4.1.2 FKN – Sub step interaction

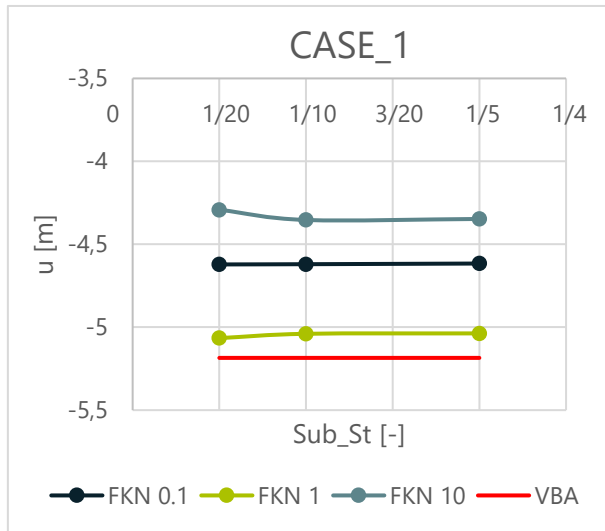


Figure 4.8 Case 1 / FKN - Sub step time relation

VBA - ANSYS Deviation / CASE_1			
sub_st	FKN 0.1	FKN 1	FKN 10
1/5	10.97%	2.85%	16.16%
1/10	10.89%	2.80%	16.04%
1/20	10.87%	2.30%	17.23%

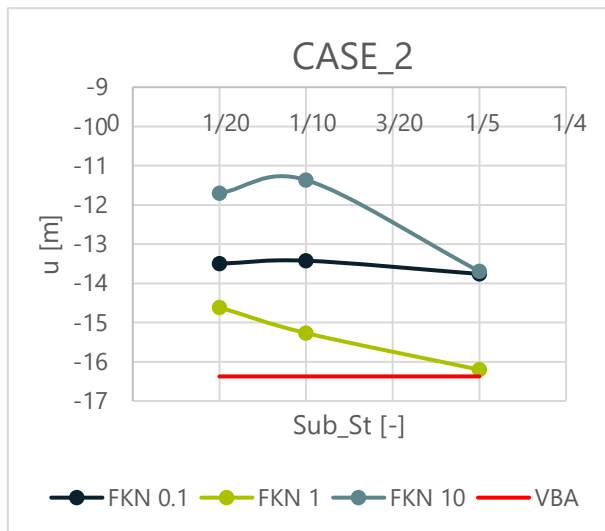


Figure 4.9 Case 2 / FKN - Sub step time relation

VBA - ANSYS Deviation / CASE_2			
sub_st	FKN 0.1	FKN 1	FKN 10
1/5	15.96%	1.05%	16.36%
1/10	18.02%	6.75%	30.57%
1/20	17.55%	10.76%	28.52%

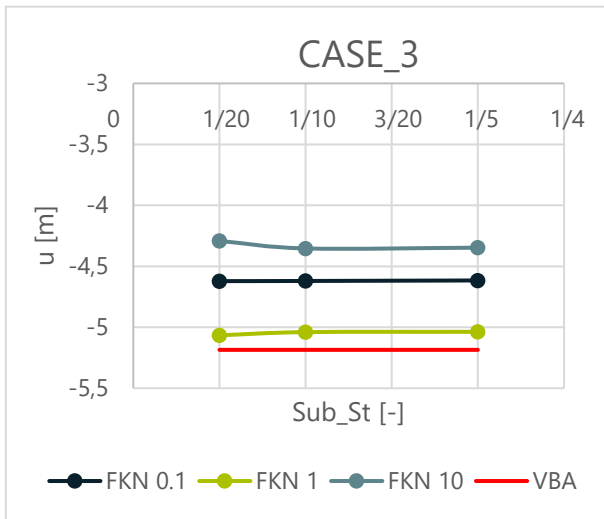


Figure 4.10 Case 3 / FKN - Sub step time relation

VBA - ANSYS Deviation / CASE_3			
sub_st	FKN 0.1	FKN 1	FKN 10
1/5	10.97%	2.85%	16.16%
1/10	10.89%	2.80%	16.04%
1/20	10.87%	2.30%	17.23%

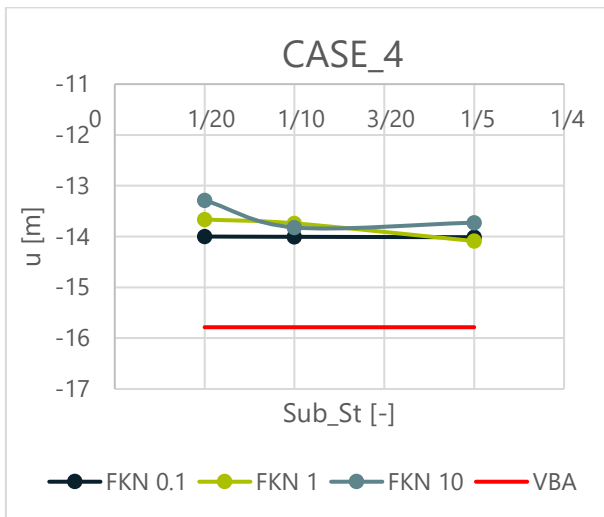


Figure 4.11 Case 4 / FKN - Sub step time relation

VBA - ANSYS Deviation / CASE_4			
sub_st	FKN 0.1	FKN 1	FKN 10
1/5	11.22%	10.75%	13.04%
1/10	11.27%	12.95%	12.44%
1/20	11.31%	13.43%	15.83%

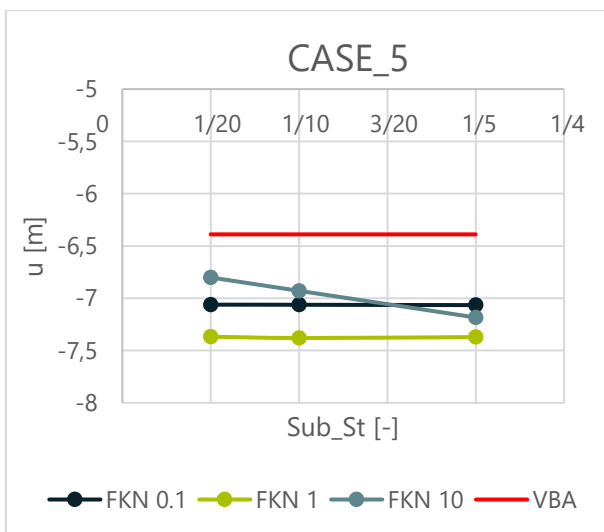


Figure 4.12 Case 5 / FKN - Sub step time relation

VBA - ANSYS Deviation / CASE_5			
sub_st	FKN 0.1	FKN 1	FKN 10
1/5	-10.59%	-15.37%	-12.44%
1/10	-10.53%	-15.50%	-8.45%
1/20	-10.52%	-15.31%	-6.45%

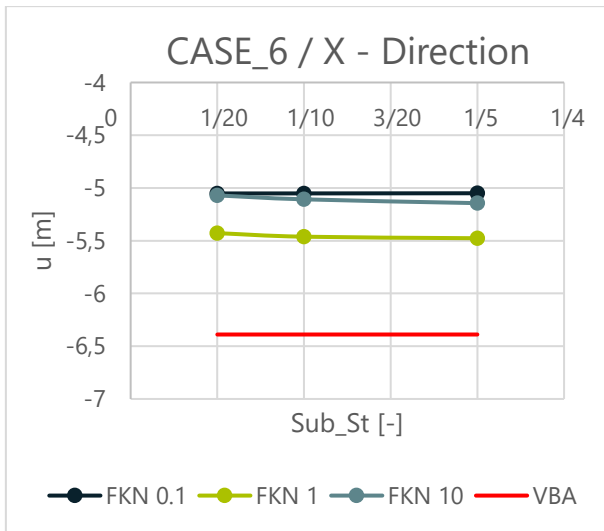


Figure 4.13 Case 6 / FKN - Sub step time relation

VBA - ANSYS Deviation / CASE_6			
sub_st	FKN 0.1	FKN 1	FKN 10
1/5	20.96%	14.28%	19.49%
1/10	20.93%	14.51%	20.05%
1/20	20.93%	15.04%	20.64%

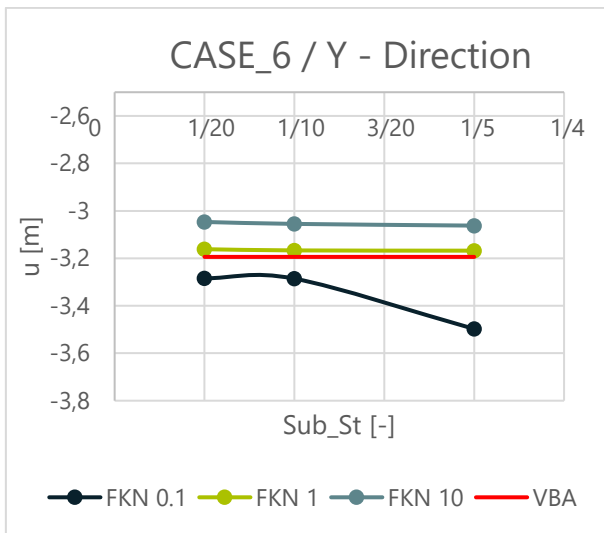


Figure 4.14 Case 6 / FKN - Sub step time relation

VBA - ANSYS Deviation / CASE_6			
sub_st	FKN 0.1	FKN 1	FKN 10
1/5	-9.50%	0.82%	4.13%
1/10	-2.87%	0.86%	4.35%
1/20	-2.83%	1.02%	4.61%

The previous plot gives a better idea of how the FKN and Sub – Step time influence the results. From a first overall view, it is clear that a smaller Sub – Step time does not affect the precision of the results, the maximum displacement remains constant or suffers small variation. However, this is not negative because a bigger Sub – Step time means less step analysis and so less computational effort from the computer; at the end, this is translated in fast analysis, which takes not more than 4 minutes for an accelerogram of 10 seconds

On the other hand, it is not possible to affirm the same regard the FKN value: with the same Sub – Step time it is possible to assist to big variations from one FKN to another. This phenomenon is more evident especially in more complex cases, such as 2 / 3 / 6, where the variation can reach differences on the maximum displacements up to

15 %. For the remaining cases, the gap is still big but less wide, with differences not more than 8 %.

The closest results to the VBA macro have been obtained with FKN 1, the same suggested by the software house and already set as default value. Nevertheless, the accuracy is still too low, with a deviation that can reach also 15 %.

Further investigation has been done on the contact diagnostic file in order to better understand why these differences occur:

- Plotting the maximum penetration over time, it is possible to notice that the more the penetration is low and the more the FKN value is high, as stated in the theory reference book.

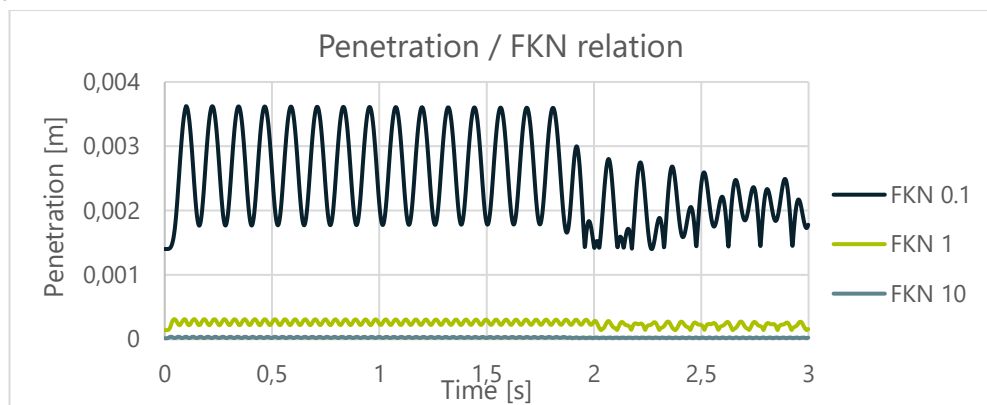


Figure 4.15 Penetration history

Higher penetration value could affect in a negative way the final displacement because this effect is not taken into account inside NE theory. On the other hand, also a too much high stiffness has not a positive effect because the risk is to overestimate the tangential stiffness that depends on it.

- From the FKN value depends also on the contact force calculated at the interface between the raft and the rigid surface;

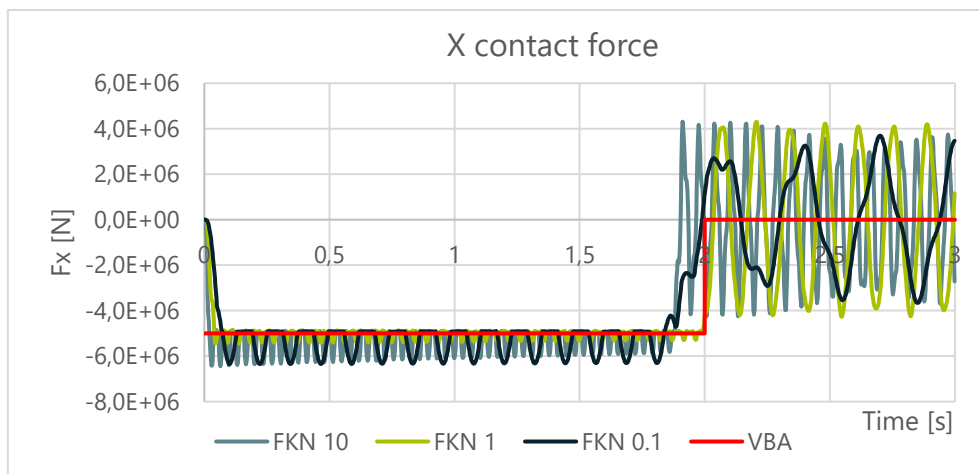


Figure 4.16 Contact force in X-direction

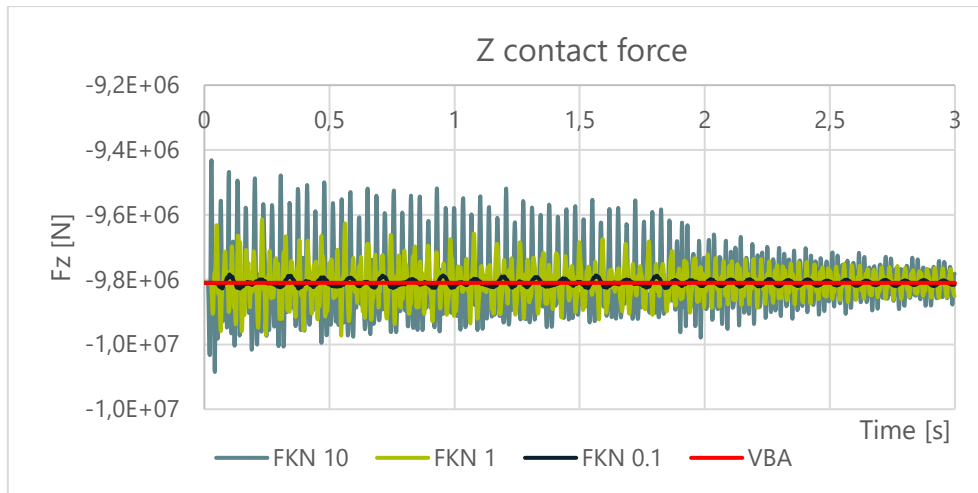


Figure 4.17 Contact force in Z-direction

By the X – force seems that FKN 1 is the most closed to the theoretical value, and so the most suitable for the problem, but then, looking at the Z – force the situation is not the same; this time the most closed is FKN 0,1.

In conclusion, utilizing the Penalty method is not easy to identify the right value for FKN if no other references are available to compare the results. The Lagrange method should overcome this problem so in the next phase it will be tested.

4.2 Pure Lagrange contact algorithm

4.2.1 Absolute displacements

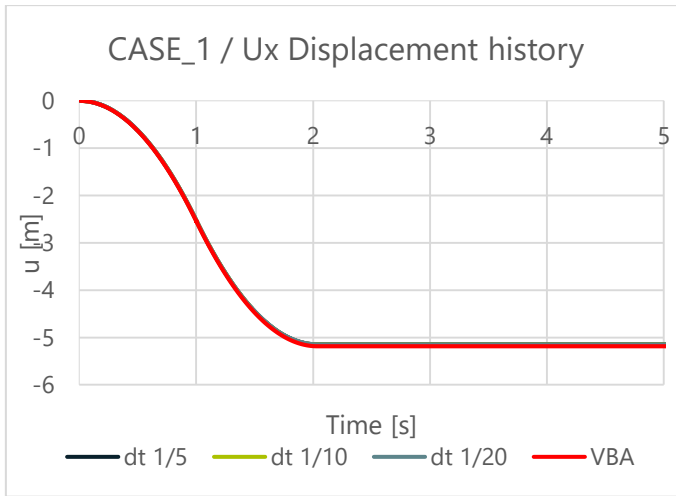


Figure 4.18 Case 1 / Ux displacements LM

VBA - ANSYS Deviation	
sub_st	FTOLN 1
1/5	0.79%
1/10	0.73%
1/20	0.73%

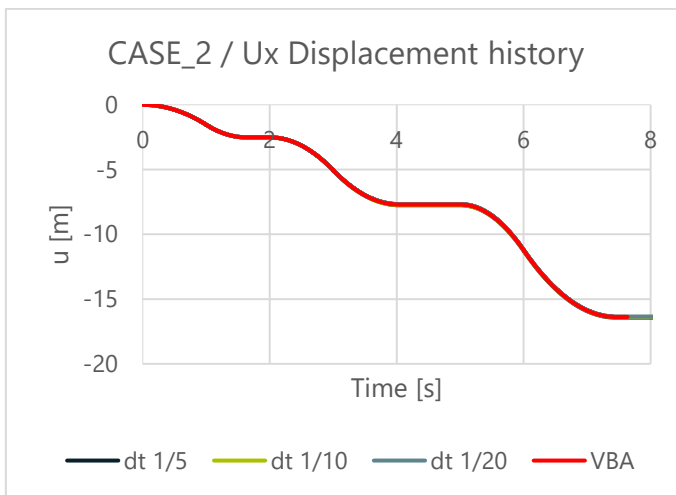


Figure 4.19 Case 1 / Ux displacements LM

VBA - ANSYS Deviation	
sub_st	FTOLN 1
1/5	-0.95%
1/10	-0.70%
1/20	-0.53%

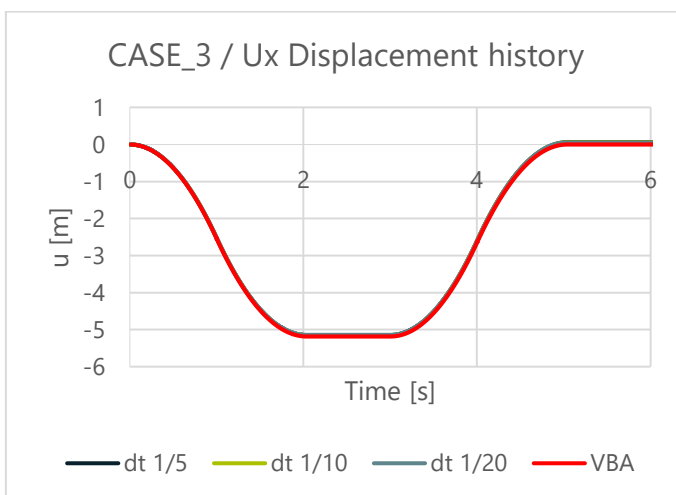


Figure 4.20 Case 3 / Ux displacements LM

VBA - ANSYS Deviation	
sub_st	FTOLN 1
1/5	0.79%
1/10	0.73%
1/20	0.73%

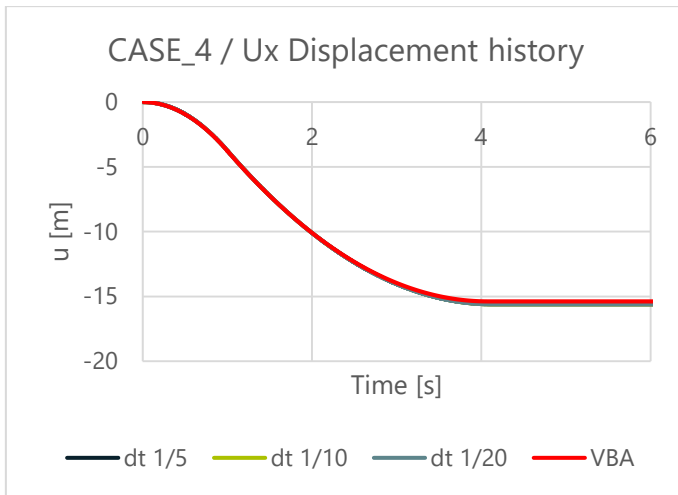


Figure 4.21 Case 1 / Uy displacements LM

VBA - ANSYS Deviation	
sub_st	FTOLN 1
1/5	-1.44%
1/10	-1.48%
1/20	-1.46%

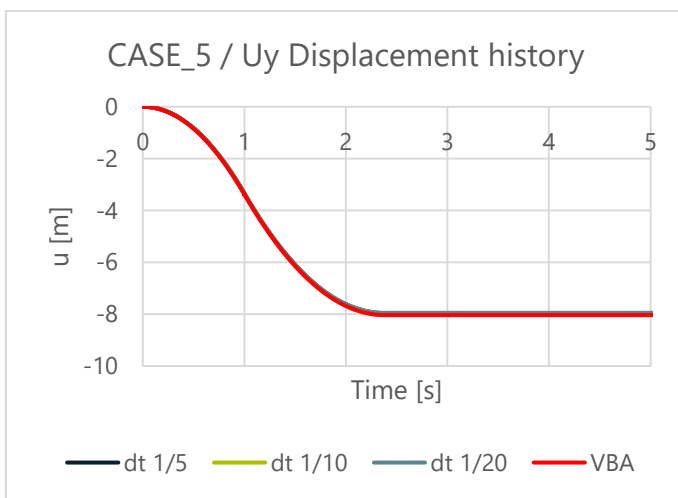


Figure 4.22 Case 5 / Uy displacements LM

VBA - ANSYS Deviation	
sub_st	FTOLN 1
1/5	1.00%
1/10	0.87%
1/20	0.96%

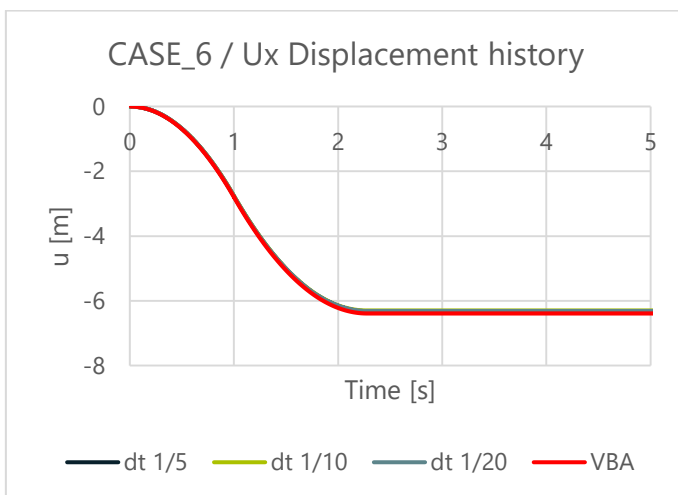


Figure 4.23 Case 6 / Ux displacements LM

VBA - ANSYS Deviation	
sub_st	FTOLN 1
1/5	1.12%
1/10	1.42%
1/20	1.17%

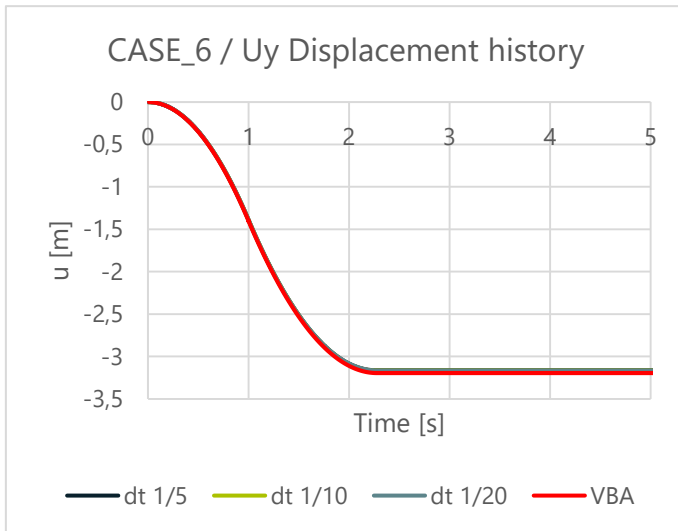


Figure 4.24 Case 6 / Uy displacements LM

VBA - ANSYS Deviation	
sub_st	FTOLN 1
1/5	1.00%
1/10	0.89%
1/20	0.87%

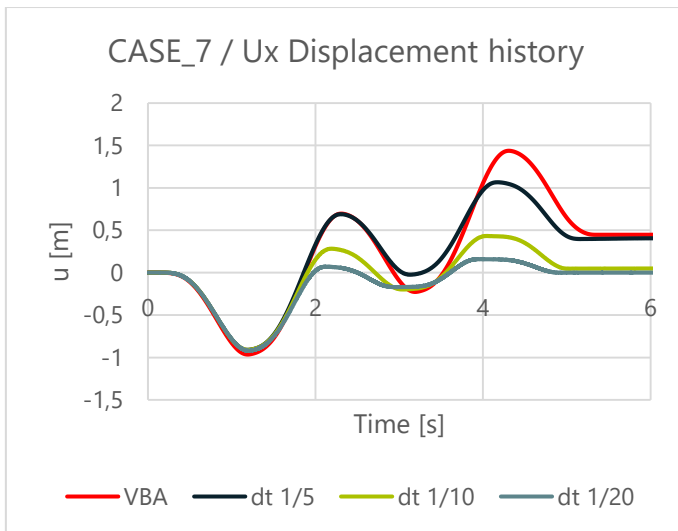


Figure 4.25 Case 7 / Ux displacements LM

VBA - ANSYS Deviation	
sub_st	FTOLN 1
1/5	5,65%
1/10	5,53%
1/20	4,57%

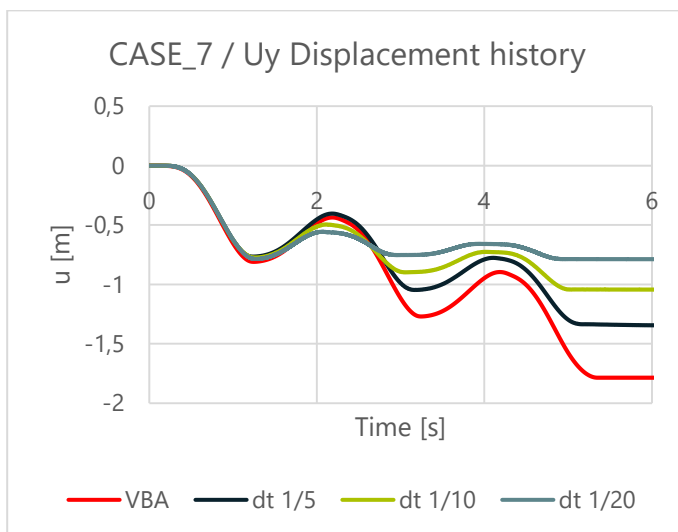


Figure 4.26 Case 7 / Uy displacements LM

VBA - ANSYS Deviation	
sub_st	FTOLN 1
1/5	24,71%
1/10	41,52%
1/20	55,87%

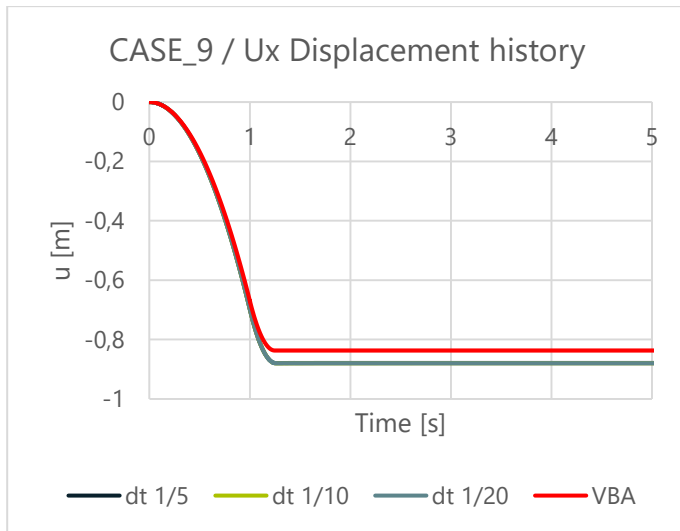


Figure 4.27 Case 9 / Ux displacements LM

VBA - ANSYS Deviation	
sub_st	FTOLN 1
1/5	-5,07%
1/10	-5,13%
1/20	-5,14%

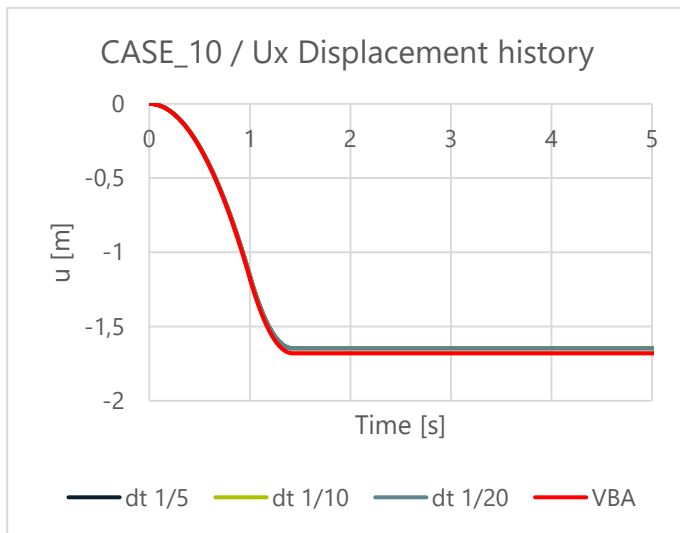


Figure 4.28 Case 10 / Ux displacements LM

VBA - ANSYS Deviation	
sub_st	FTOLN 1
1/5	2,05%
1/10	2,01%
1/20	1,98%

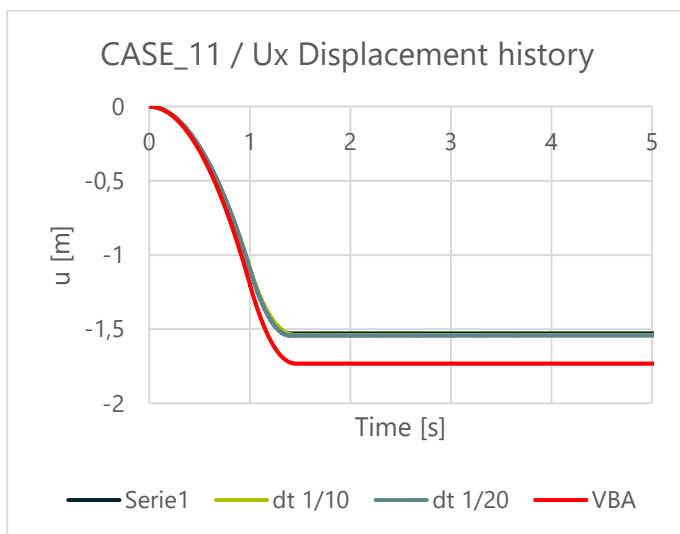
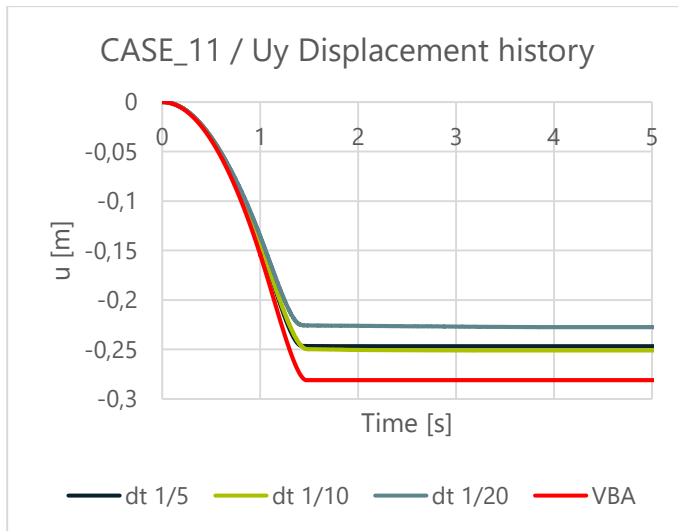


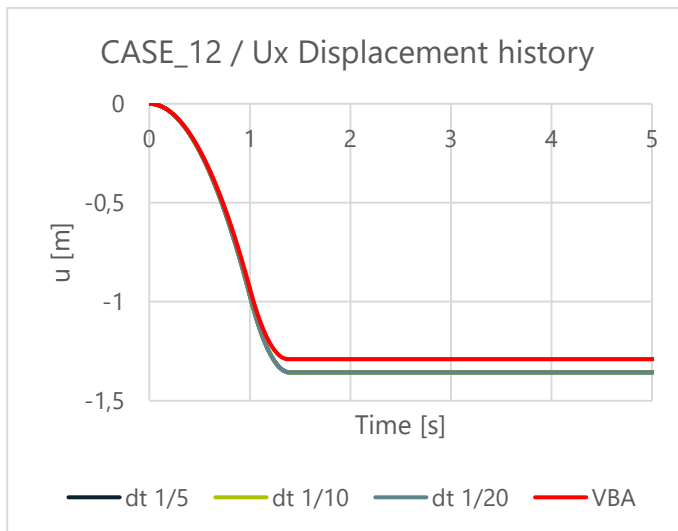
Figure 4.29 Case 11 / Ux displacements LM

VBA - ANSYS Deviation	
sub_st	FTOLN 1
1/5	11,71%
1/10	11,03%
1/20	10,84%



VBA - ANSYS Deviation	
sub_st	FTOLN 1
1/5	12,20%
1/10	10,69%
1/20	19,06%

Figure 4.30 Case 6 / Uy displacements LM



VBA - ANSYS Deviation	
sub_st	FTOLN 1
1/5	-5,15%
1/10	-5,20%
1/20	-5,20%

Figure 4.31 Case 12 / Ux displacements LM

It is evident that the Lagrange algorithm provides more accurate results; in this case the Sub – Step time does not affect the results, the curves are graphically coincident and the analytical calculation of the deviation confirm what shown in the graphs: between two consecutive Sub – Step time the difference is maximum of 0,40 % (Case 2)

Furthermore, the accuracy respect to the VBA macro is clearly improved; for the simplest cases (1 to 6) the average gap is of 1 %, while for cases where are present lateral forces only along one direction it rises up to 5 %.

Despite these first good results, for the two most complex cases (7 and 11), namely, where are present forces acting along two directions, displacements show remarkable deviations respect to the VBA reference curves. For the last case, a strong

dependency from the Sub – Step time come back again, with deviations ranging from 25 % up to 55 %.

Of course, this is not considered acceptable from an engineering point of view and so, further investigations have been conducted on the most unfavourable case:

- Plotting the penetration it is evident that it is almost zero, small fluctuations are present but not so big to influence the results;

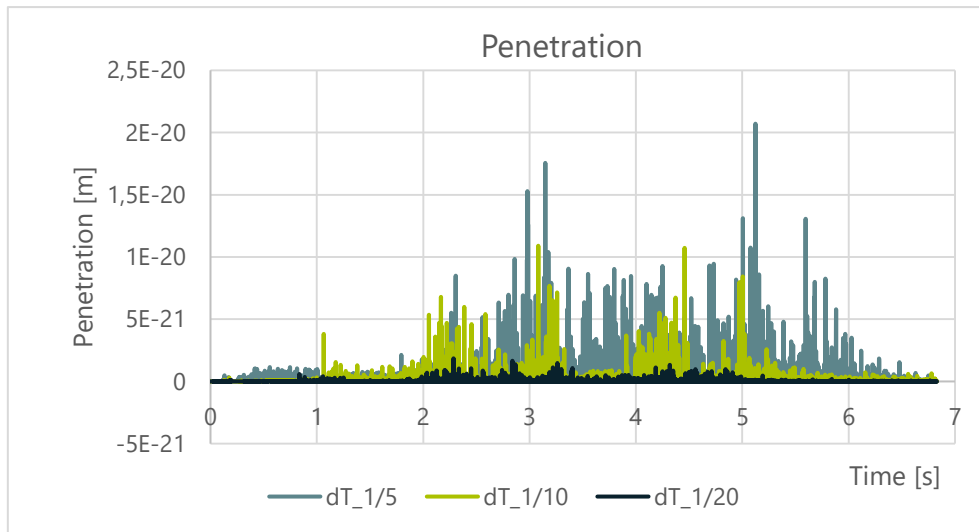


Figure 4.32 LM penetration history

- Another interesting effect has been figured out plotting the contact pressure; the image below shows it in three different times:

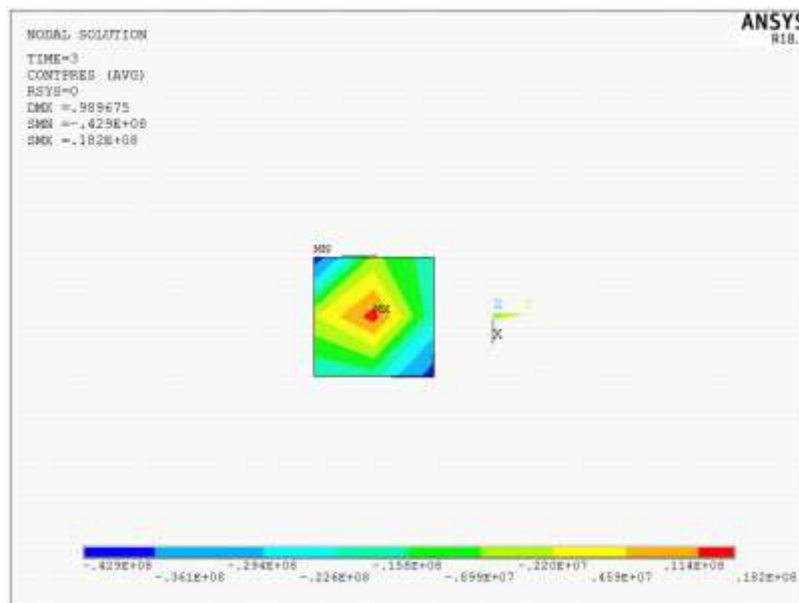


Figure 4.33 Contact pressure t=3 s

4. Case Study 1

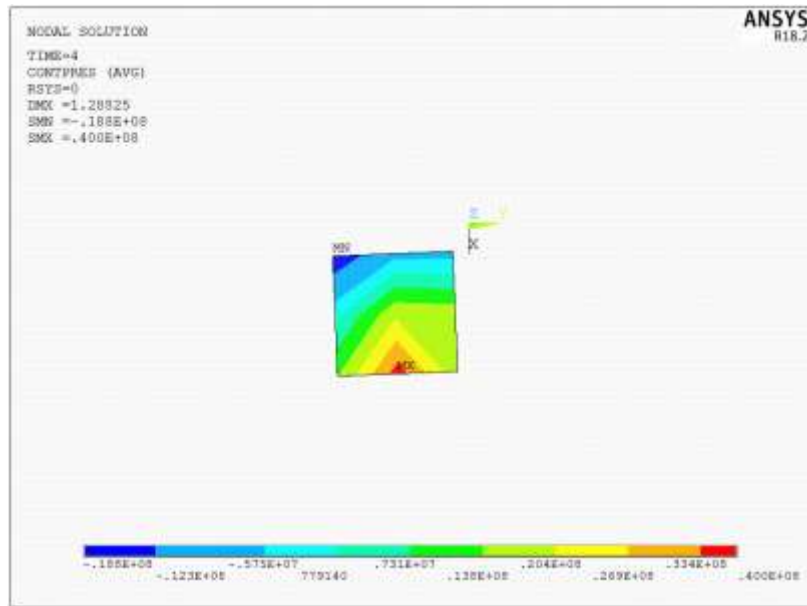


Figure 4.34 Contact pressure t=4 s

We can see that the pressure under the block varies due to eccentricity of the load both inertial and lateral external forces; in some instant, it even reaches negative pressure which means that it would uplift but as the option is deactivated, the software keeps it down reacting with downward pressure. Below it is present the graph of the resultant force along the Z-axis:

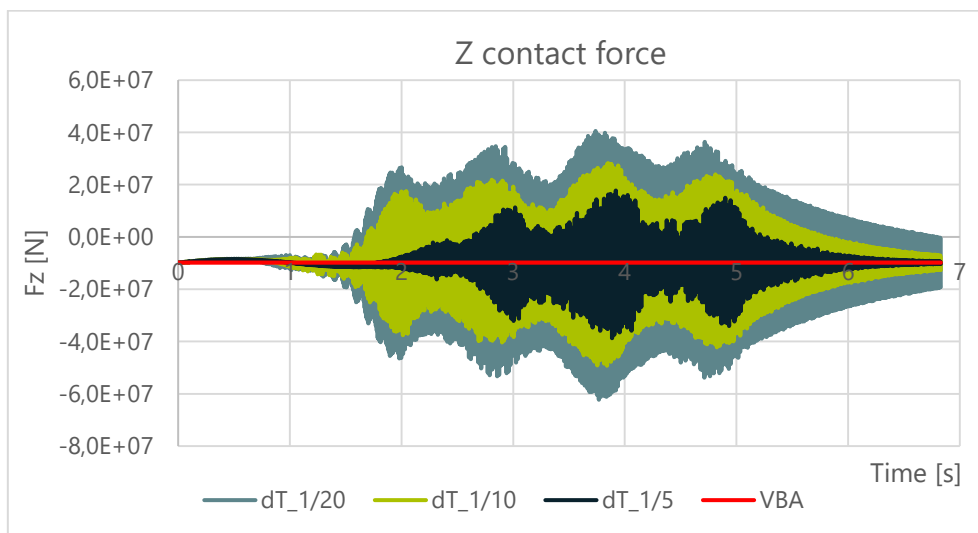


Figure 4.35 Contact force in Z-direction

The plot shows a further detail: when the negative pressure prevails on the positive one, the resultant force became negative; then, the frictional resisting force, which depends on the F_N , increase and as a result, a braking effect is generated.

- Looking at the image XXX, it is evident that the block rotates due to the different intensity of the forces acting along the two planar axis; this effect is not taken into account in the NE theory, and it is another probable cause of the deviation between the two results.

After these two phases, several aspects come out; the penalty method has too much dependence by the FKN factor, while utilizing Lagrange, even if the accuracy improved, other problems arise. Therefore, it indicates that the differences are not caused by the contact setting but also from the model; so, a revise of it has been necessary.

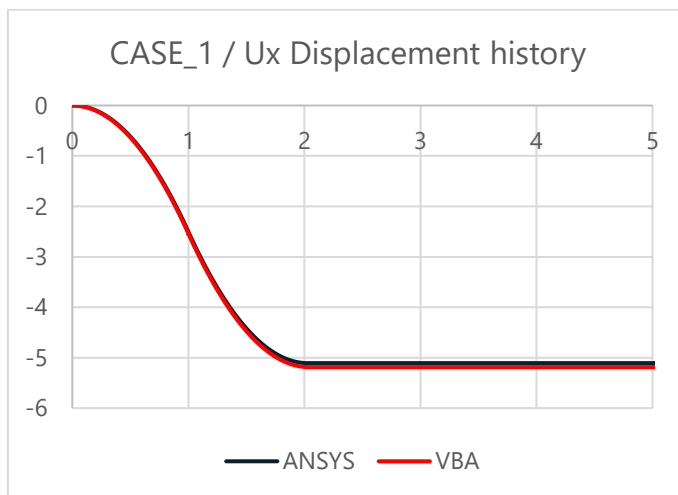
5 Case Study 2

This chapter contains results of the analysis conducted on the second model; since some incongruences come out with the first model, some changes in the base concept has been needed, leading to the necessity of a new model.

After the good results of the Pure Lagrange algorithm, the analysis has been conducted only with this last; the only variable parameter is the sub-step time. The exhibitions of the results will follow the same methodology before used.

5.1 Pure Lagrange contact algorithm

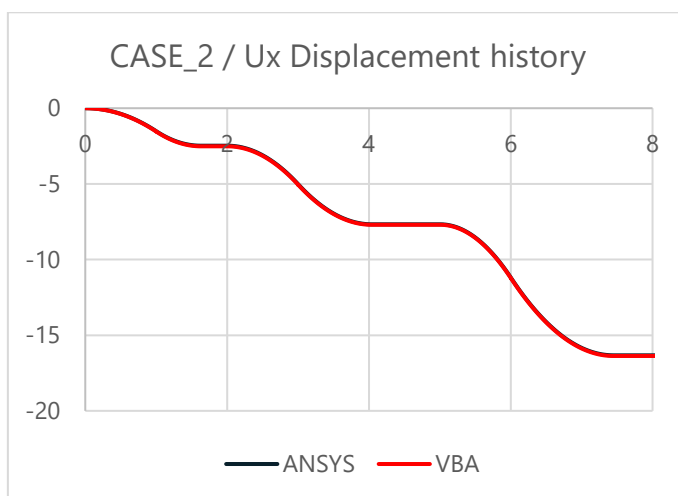
5.1.1 Absolute displacements



**VBA – ANSYS Deviation
t = 5 [s]**

1.51%

Figure 5.1 Case 1 / Ux displacements LM



**VBA – ANSYS Deviation
t = 8 [s]**

0.27%

Figure 5.2 Case 2 / Ux displacements LM

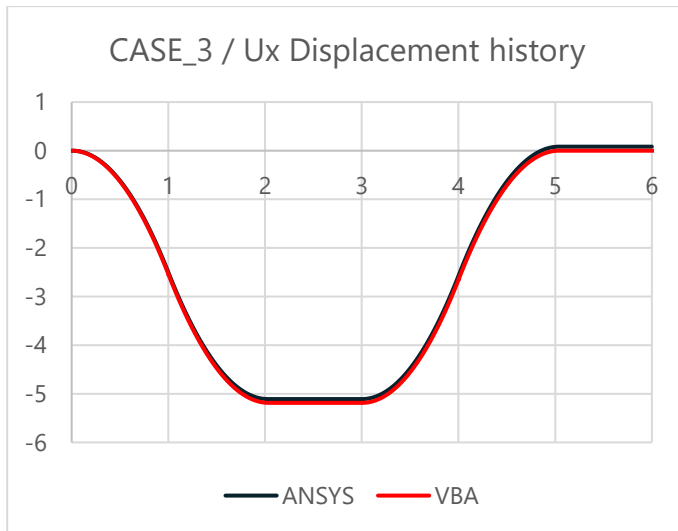


Figure 5.3 Case 3 / Ux displacements LM

VBA – ANSYS Deviation
t = 2,5; 6 [s]

1.51%

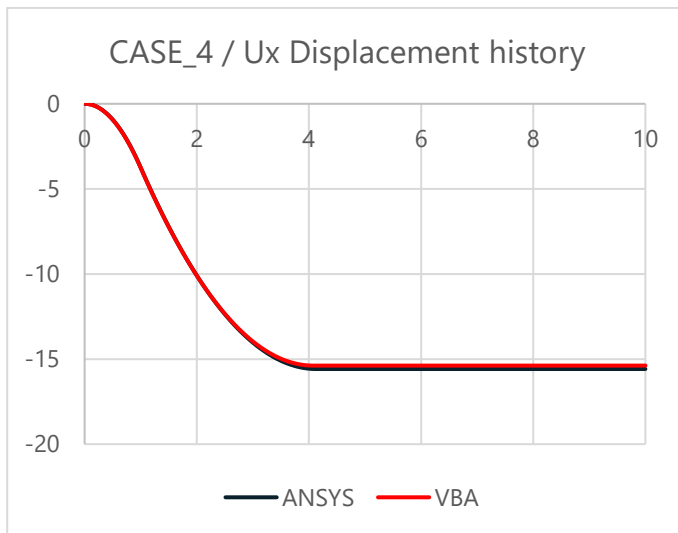


Figure 5.4 Case 4 / Ux displacements LM

VBA – ANSYS Deviation
t = 10 [s]

-1.30%

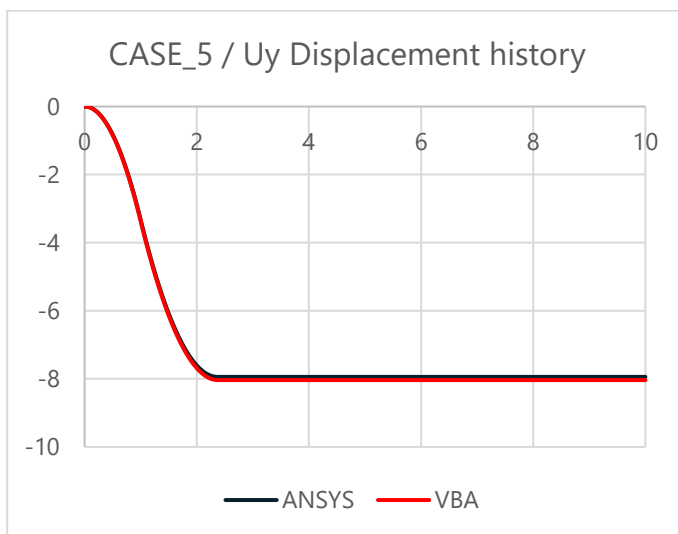


Figure 5.5 Case 5 / Ux displacements LM

VBA – ANSYS Deviation
t = 10 [s]

1.17%

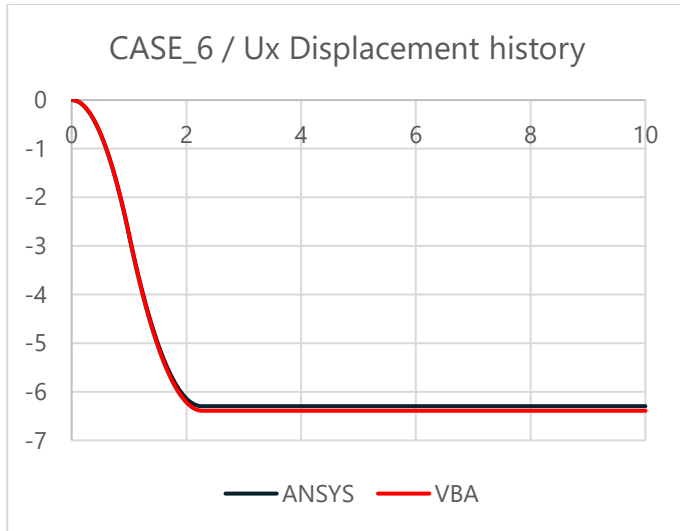


Figure 5.6 Case 6 / Ux displacements LM

**VBA – ANSYS Deviation
t = 10 [s]**

1.46%

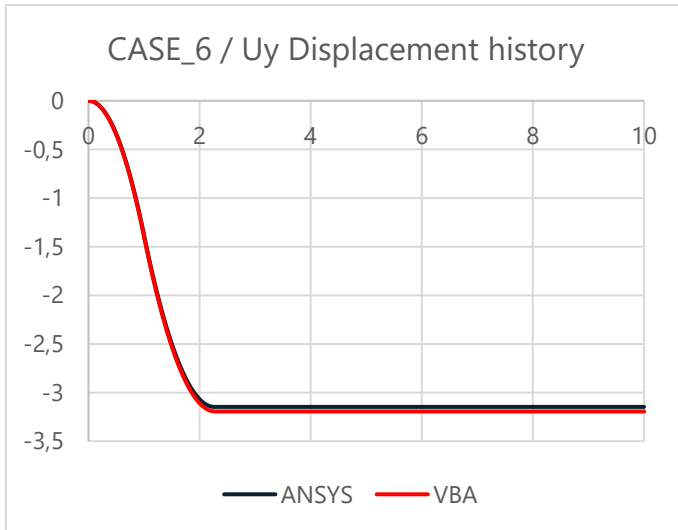


Figure 5.7 Case 6 / Uy displacements LM

**VBA – ANSYS Deviation
t = 10 [s]**

1.46%

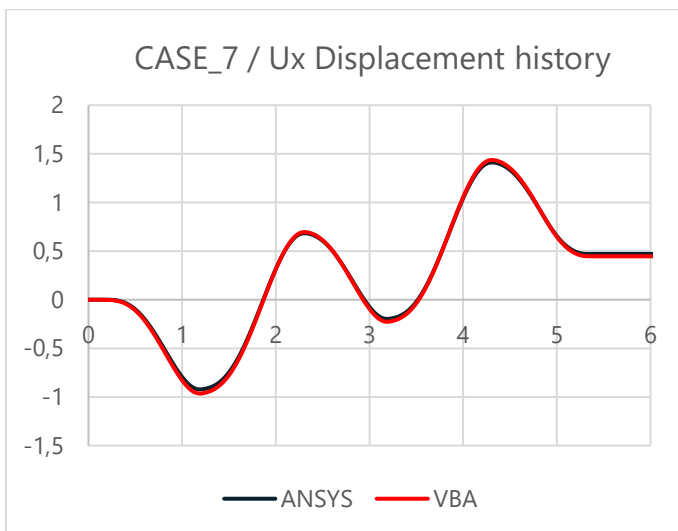
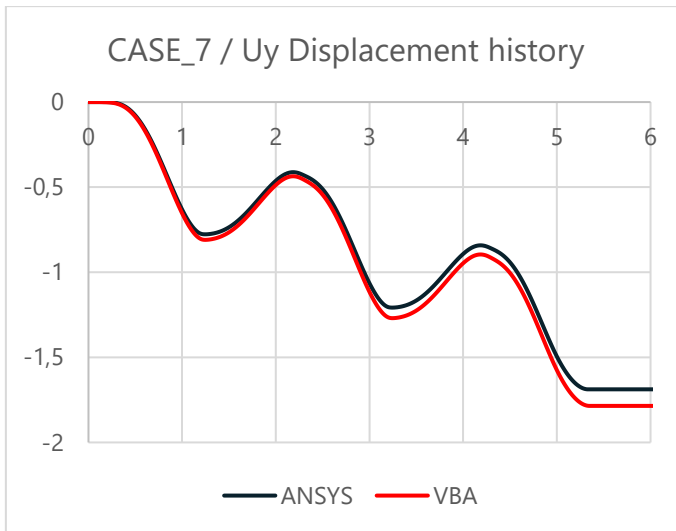


Figure 5.8 Case 7 / Ux displacements LM

**VBA - ANSYS Deviation
t = 6 [s]**

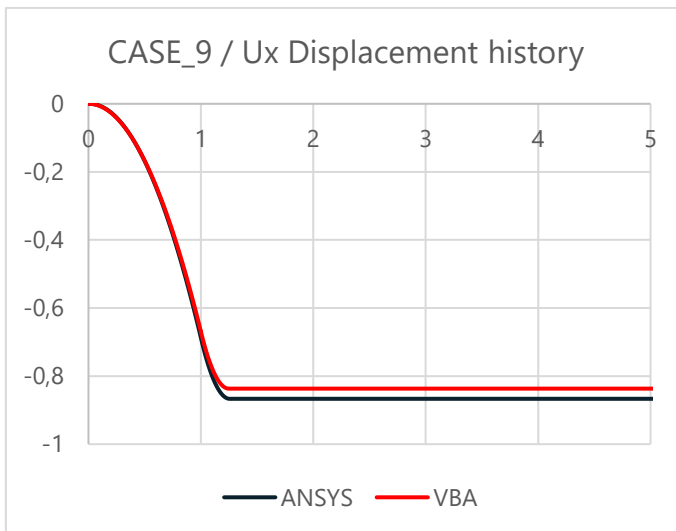
-5,39%



VBA - ANSYS Deviation
t = 6 [s]

5,45%

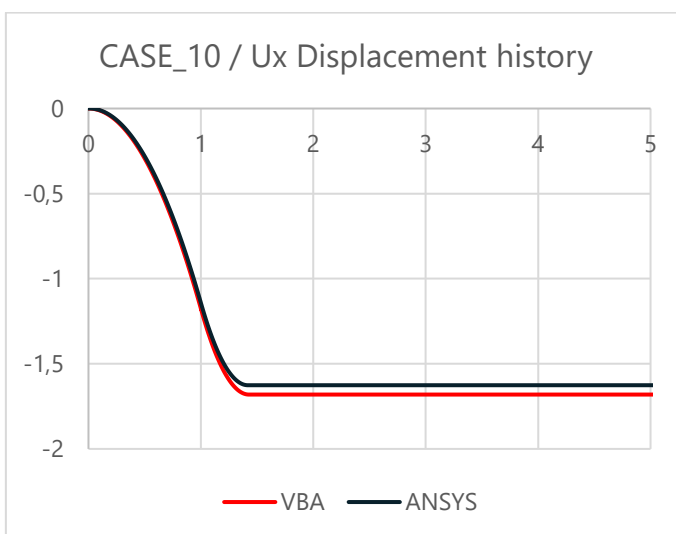
Figure 5.9 Case 7 / Uy displacements LM



VBA - ANSYS Deviation
t = 5 [s]

-3,58%

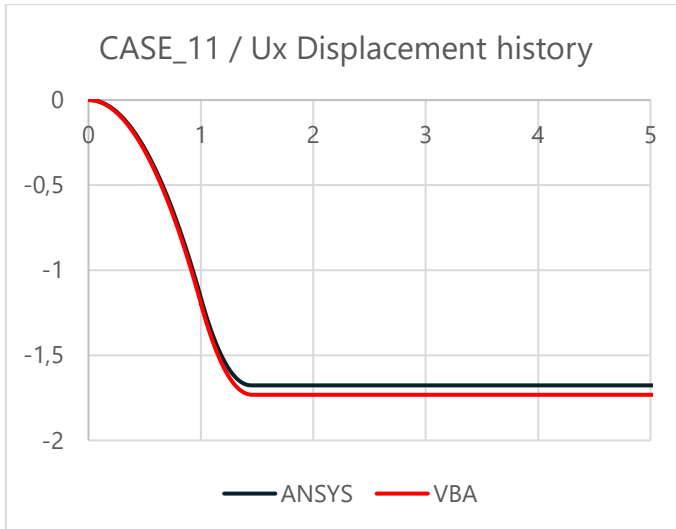
Figure 5.10 Case 9 / Ux displacements LM



VBA - ANSYS Deviation
t = 5 [s]

3,27%

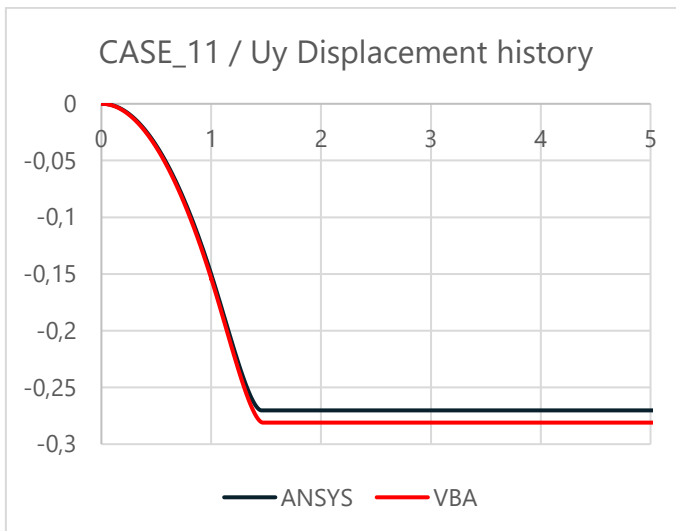
Figure 5.11 Case 10 / Ux displacements LM



VBA - ANSYS Deviation
t = 5 [s]

3,19%

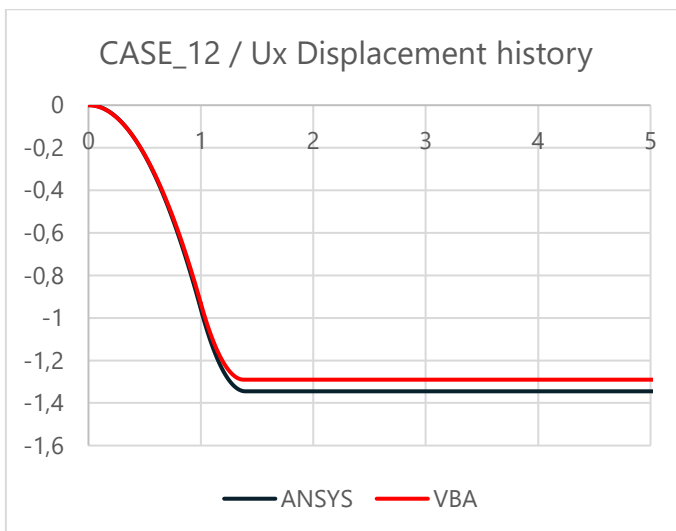
Figure 5.12 Case 11 / Ux displacements LM



VBA - ANSYS Deviation
t = 5 [s]

3,83%

Figure 5.13 Case 11 / Uy displacements LM



VBA - ANSYS Deviation
t = 5 [s]

-4,23%

Figure 5.14 Case 12 / Ux displacements LM

5. Case Study 2

The plots of the displacement history show that the accuracy of this new model is much higher than the last one; for cases 1 to 6, those without external forces, the average deviation from the VBA macro is 1%. The lowest value is only 0,27%, while the highest stop at 1,50%. For the remaining cases, figures are slightly higher, rising until an average value of 4%. The difference could be caused by the approximation done in the calculation of the resultants; nevertheless, it can be considered a great result.

Next, the previous model showed some incongruences from the NE hypothesis; below are present the plot of the case 7 in order to verify if the problems are still present:

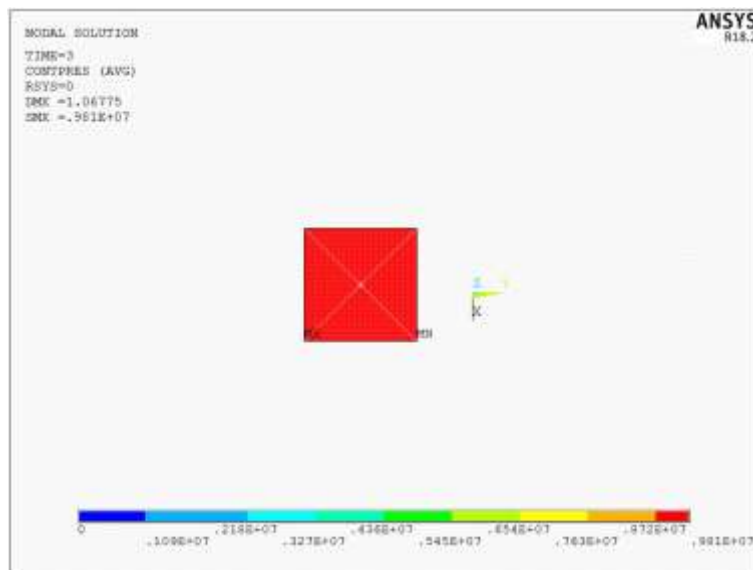


Figure 5.15 Contact pressure t = 3 s

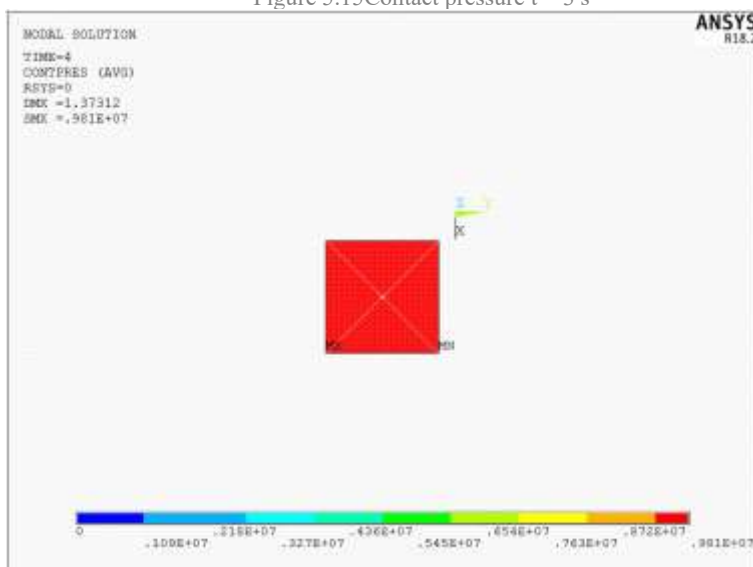


Figure 5.16 Contact pressure t = 4 s

It is possible to notice that with this model all the negative aspects previously mentioned are absent:

- ❖ Due to the absence of eccentricity between the mass element and the contact interface, the pressure on this last is always constant;
- ❖ Thanks to the rigid links that link the four corners of the element, any deformation is prevented.

Since the previous results have given a good response, the same model has been used for analysis with a real accelerogram:

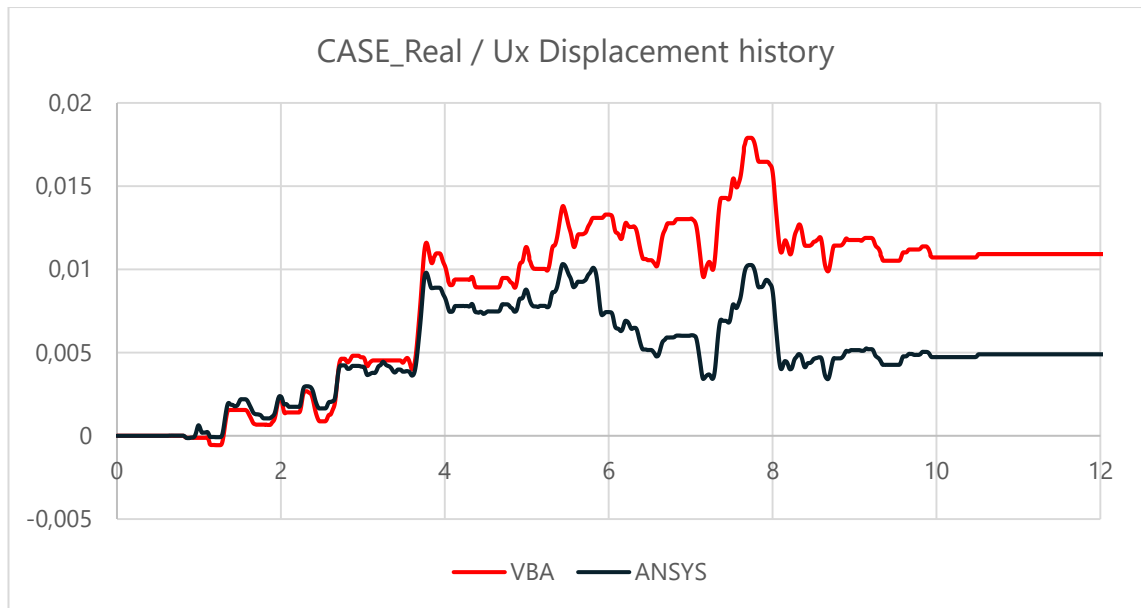


Figure 5.17 Case Real / Ux displacements LM

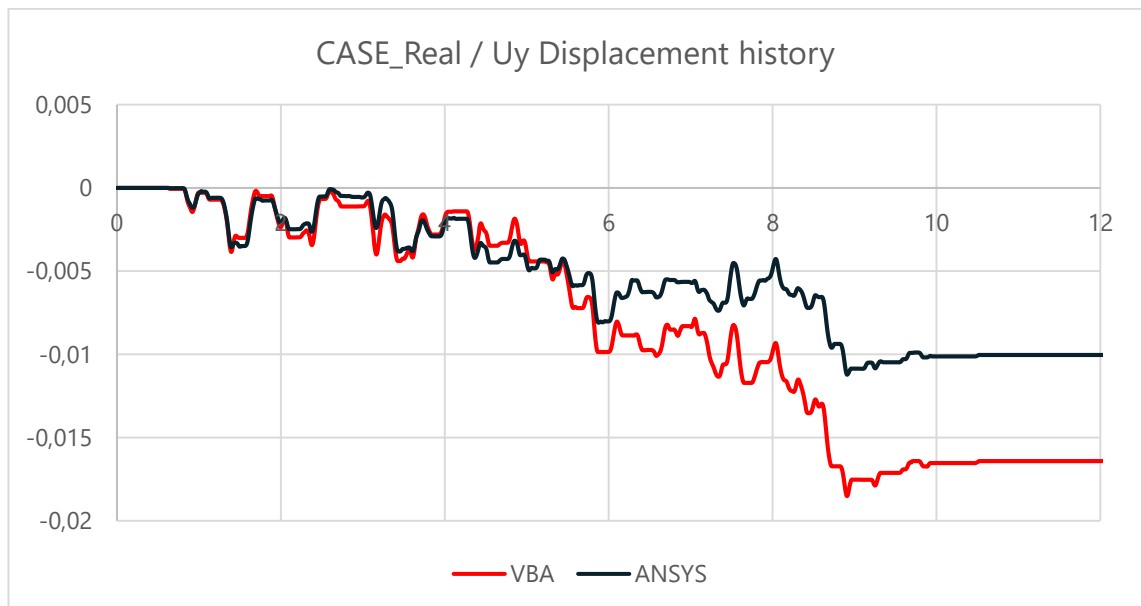
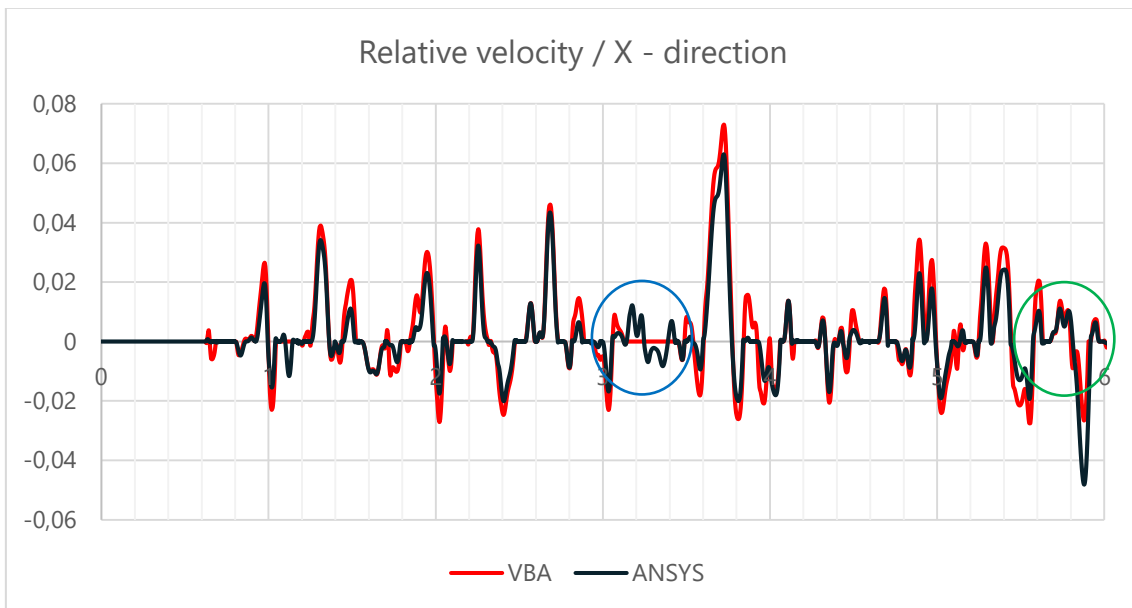
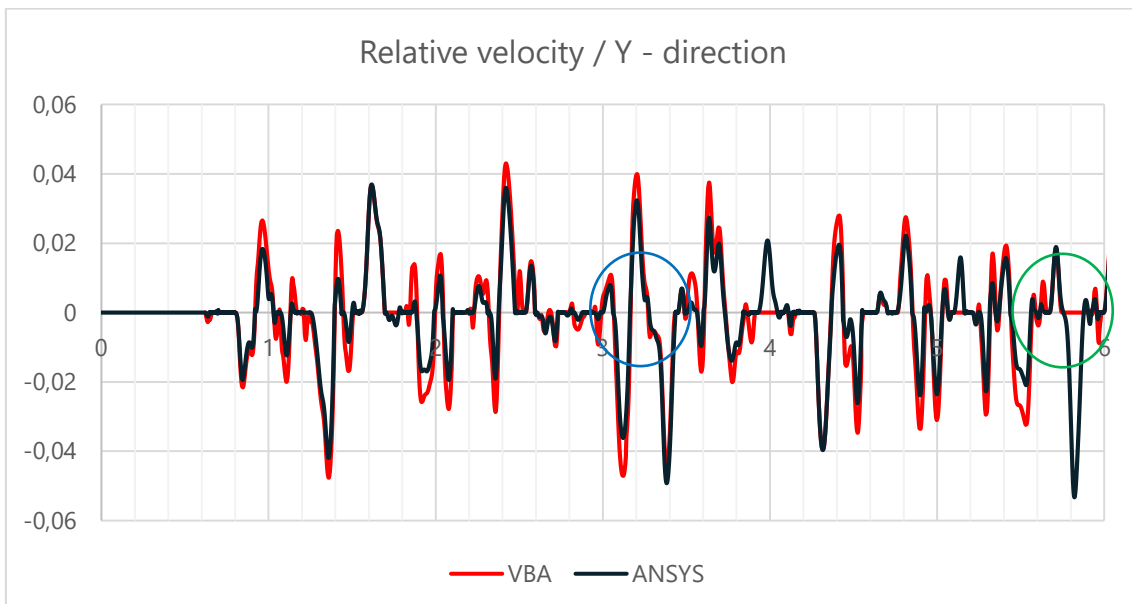


Figure 5.18 Case Real / Uy displacements LM

This time the accuracy is not so high respect to the one achieved with the test cases; the peak points are coincident (they occur at the same instant), but displacements are generally overestimated by the VBA macro. After a deep investigation on the NE numerical procedure implemented in VBA, an interesting aspect has been figured out. In the following graphs, the relative velocities between the block and the ground calculated by numerical integration have been overlapped.

Figure 5.19 Case Real / U_x velocities ALM vs VBAFigure 5.20 Case Real / U_y velocities ALM vs VBA

By a first overview, it is possible to observe that the two curves have the same peak, but again, the velocity of the NE method is always overestimated. This phenomenon obviously leads to an overestimation of the displacements and so to a

divergence of the results. This deviation is probably caused by the different integration method: we need to remember that ANSYS uses the Newmark integration method, while in the VBA macro has been implemented a finite difference integration. The two methods have been discussed in the contact mechanic paragraph.

Furthermore, looking at the blue (green) circles, in X (Y) – direction is clearly visible that VBA velocity is constantly equal to 0 m/s while in ANSYS there is a change in the sign. In the same range of time, along the Y(X)-direction the sliding is calculated. In this way, it is clear that part of the information is lost. The explanation at this phenomenon falls inside an assumption in the numerical methodology of Newmark: when sliding occurs, the velocities are calculated separately along the two directions and so there are two starts and finish sliding time. For sake of simplicity, the greater one is kept; the images 5.19 and 5.20 show the hypothesis just explained. The problem is that the eventual negative (or positive) relative velocity until tend of the smaller of the two velocities is lost, and since the calculation of the displacement depends directly by the velocity, a lack of information in the first has an impact on the second.

6 Case Study 3

This chapter contains results of the analysis conducted on the third model, the most similar to a real structure that will help to study the feasibility of this new methodology to be applied inside the Hinkley Point project.

After the experience acquired in the first two studies, the following analysis has been conducted always with both the contact algorithms, but in order to avoid eventually brake effect the no separation option has been disabled and so the uplift will be taken into account. This is not coincident with the NE hypothesis, but after all, would be impossible to replicate them on very different model respect to the one idealized by Elms.

6.1 Augmented Lagrange contact algorithm

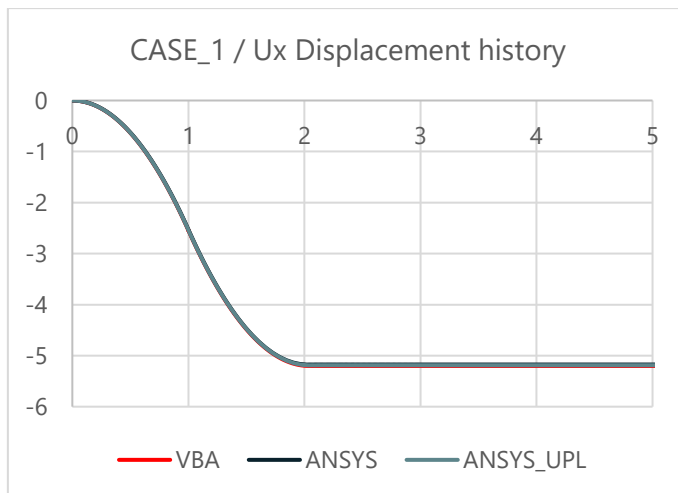


Figure 6.1 Case 1 / Ux displacements ALM

VBA – ANSYS Deviation t = 2,5 [s]	
No UPL	0.51%
UPL	0.23%

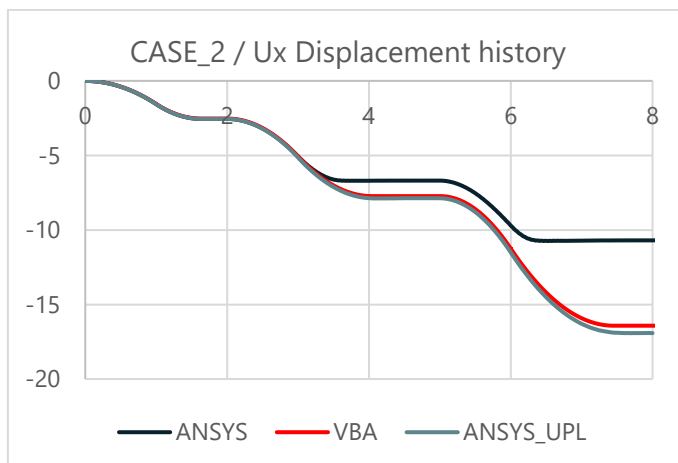
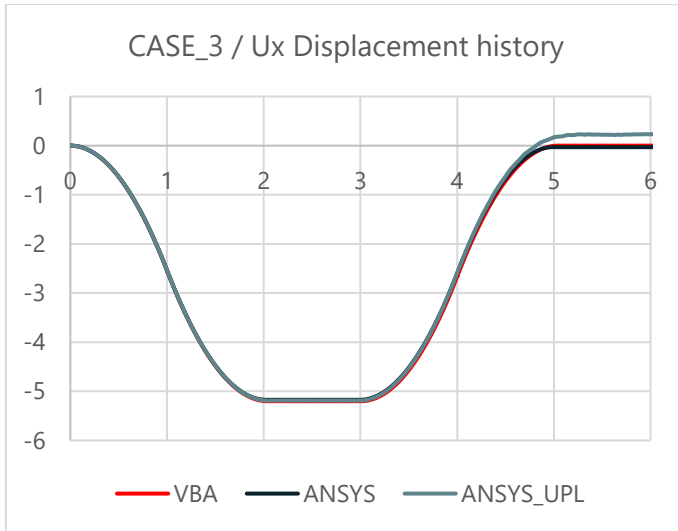


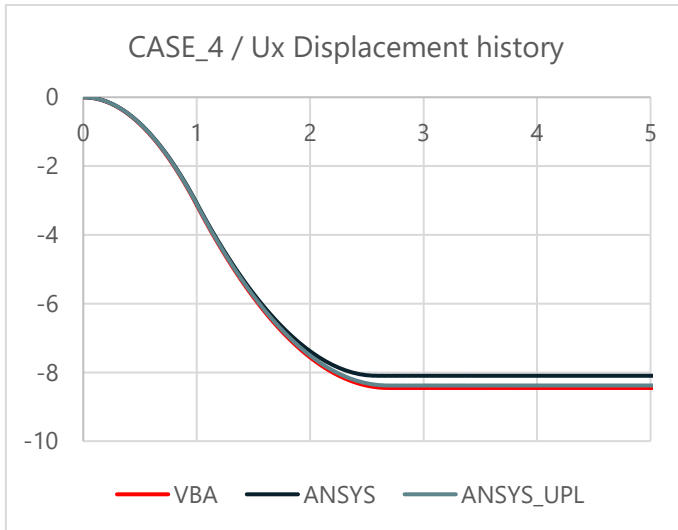
Figure 6.2 Case 2 / Ux displacements ALM

VBA – ANSYS Deviation t = 8 [s]	
No UPL	34.59%
UPL	-3.04%



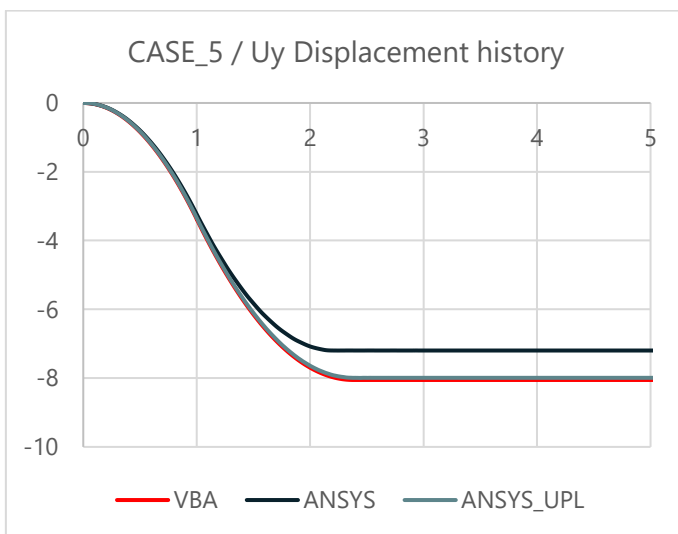
	VBA – ANSYS Deviation t = 2,5 [s]
No UPL	0.52%
UPL	0.23%

Figure 6.3 Case 3 / Ux displacements ALM



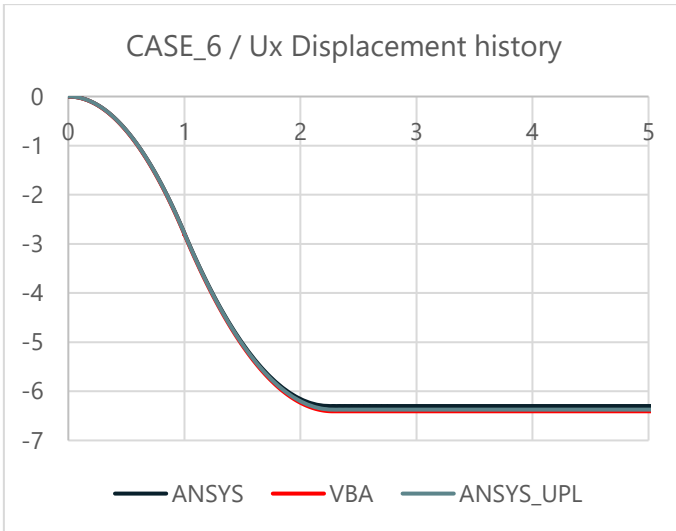
	VBA – ANSYS Deviation t = 3 [s]
No UPL	4.18%
UPL	0.83%

Figure 6.4 Case 4 / Ux displacements ALM



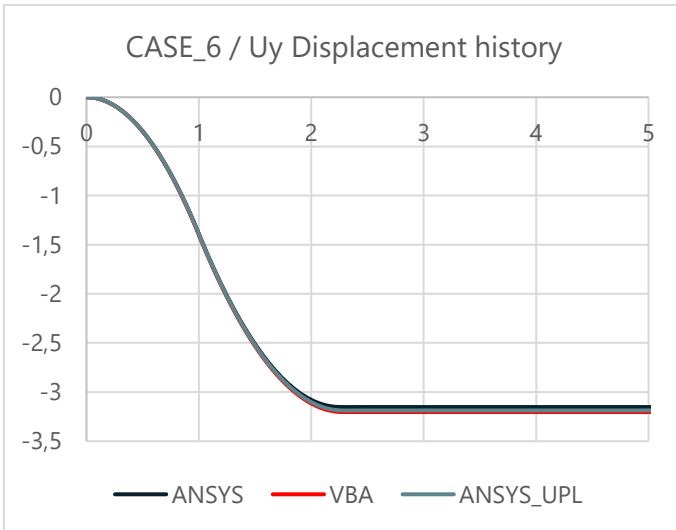
	VBA – ANSYS Deviation t = 3 [s]
No UPL	10.62%
UPL	0.74%

Figure 6.5 Case 5 / Ux displacements ALM



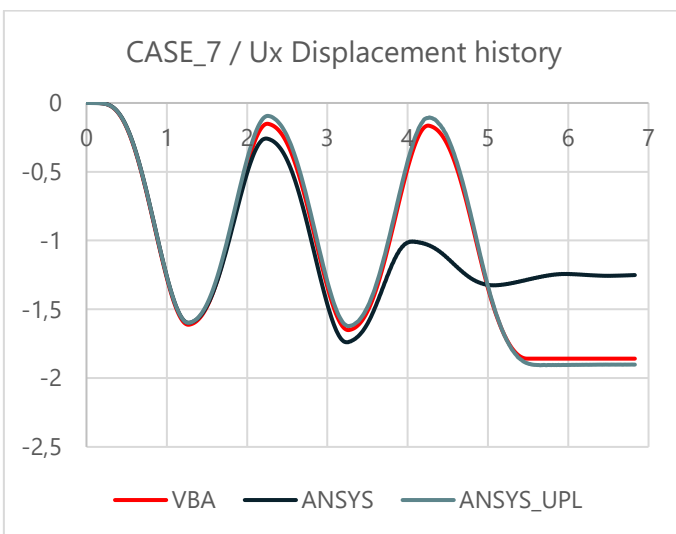
VBA - ANSYS Deviation	
t = 3 [s]	
No UPL	1.66%
UPL	0.51%

Figure 6.6 Case 6 / Ux displacements ALM



VBA - ANSYS Deviation	
t = 3 [s]	
No UPL	1.56%
UPL	0.47%

Figure 6.7 Case 6 / Uy displacements ALM



VBA - ANSYS Deviation	
t = 6 [s]	
No UPL	32.37%
UPL	-2.60%

Figure 6.8 Case 7 / Ux displacements ALM

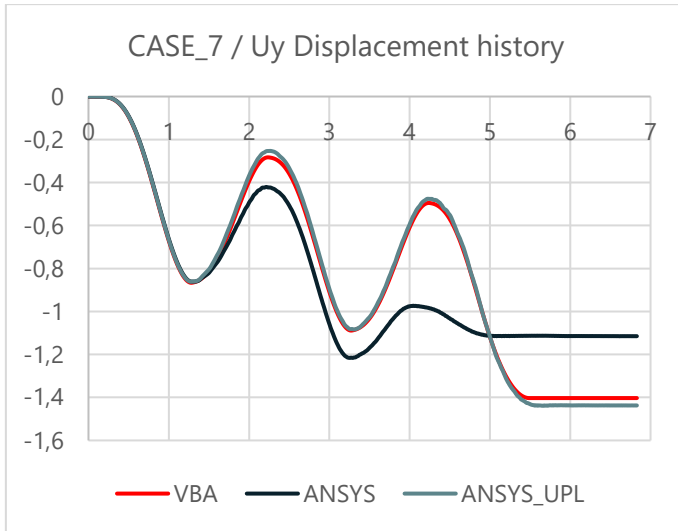


Figure 6.9 Case 7 / Uy displacements ALM

VBA - ANSYS Deviation	
t = 8 [s]	
No UPL	20.52%
UPL	-2.55%

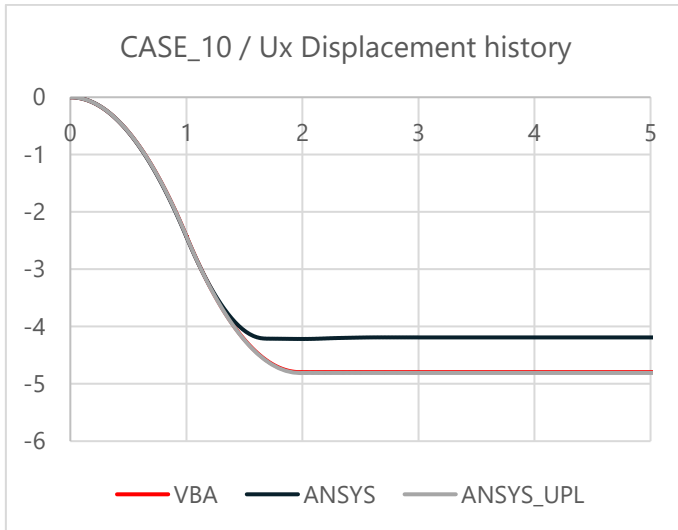


Figure 6.10 Case 10 / Ux displacements ALM

VBA - ANSYS Deviation	
t = 3 [s]	
No UPL	12.06%
UPL	-0.33%

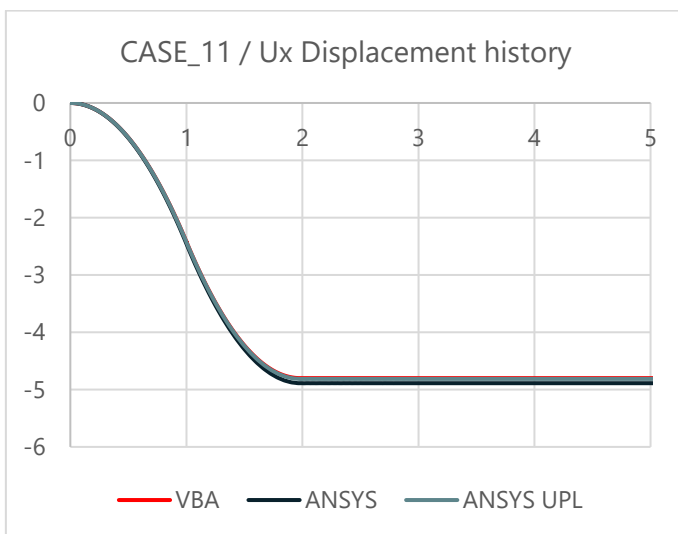
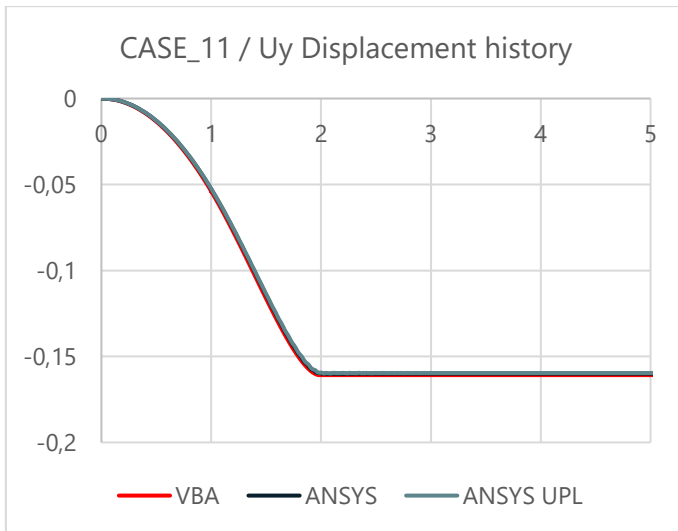


Figure 6.11 Case 11 / Ux displacements ALM

VBA - ANSYS Deviation	
t = 8 [s]	
No UPL	-1.86%
UPL	-0.31%



VBA - ANSYS Deviation t = 3 [s]	
No UPL	0.42%
UPL	0.61%

Figure 6.12 Case 11 / Uy displacements ALM

In the previous plots have been overlapped the displacement histories of the analysis conducted with and without uplift.

When it is disabled, for most of the cases the average deviation is of 1,5 % but for the remaining cases (2/4/5/10/7) curves show a remarkable difference, with gap ranging from 4% to even 34% for the case 2.

When uplift is taken into account, the situation is totally different; this time the deviation is below 1 % for almost all the cases, and only of 3 % and 2,6 % for cases 2 and 7 respectively.

Remembering that, from the case study 1, in some situation a braking effect could occur, below will be plotted the pressure on the contact interface and the respective resultants of case 2, those who showed the biggest deviation.

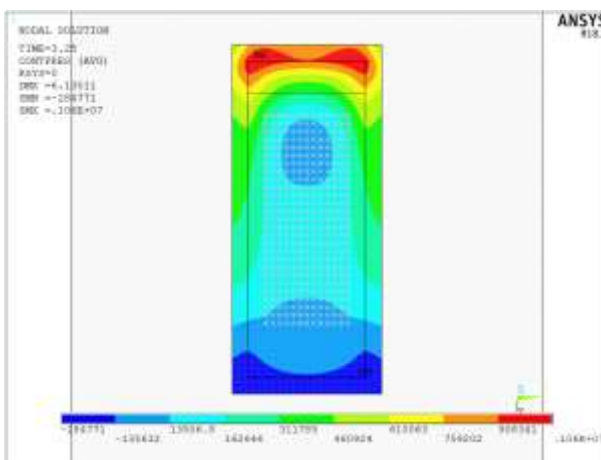


Figure 6.13 Contat pressure Case 2 No UPL / t=3,25 s

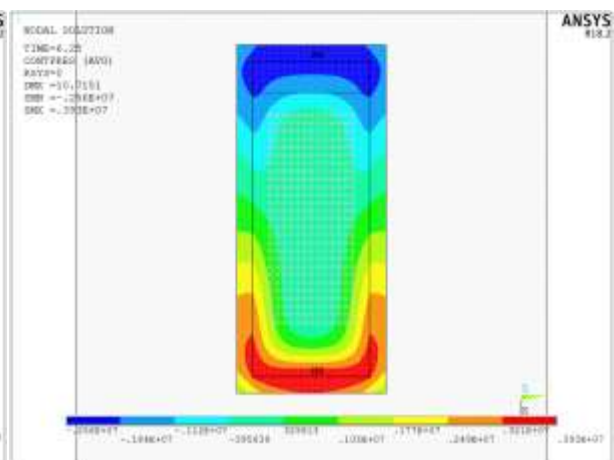


Figure 6.14 Contat pressur Case 2 No UPL / t = 6,25 s

6. Case Study 3

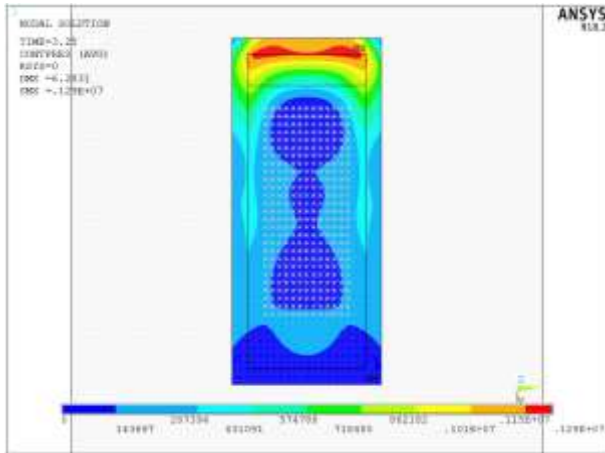


Figure 6.15 Contat pressure Case 2 UPL / $t = 3,25$

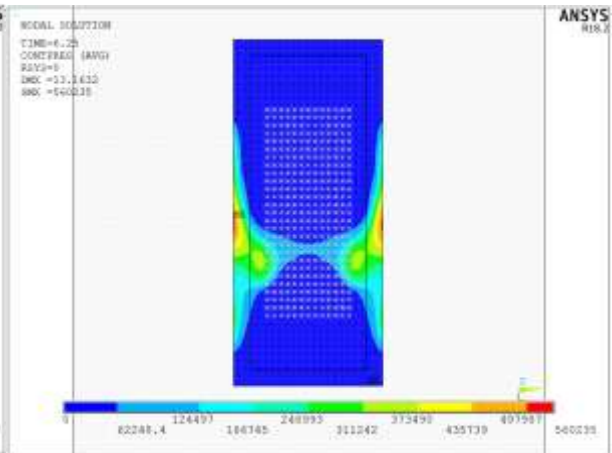


Figure 6.16 Contat pressure Case 2 UPL / $t = 6,25$

The figures 6.13 and 6.14, relative to the no – uplift case, show a relevant negative pressure area due to the software’s algorithm which wants to prevent uplift inserting forces in the opposite direction of the uplift.

In the images 6.15 and 6.16, since the uplift is allowed, the pressure is never negative: when it reaches zero, the software assigns the opened status and calculate the amount of uplift. In the images below is it possible to see the areas where it happens:

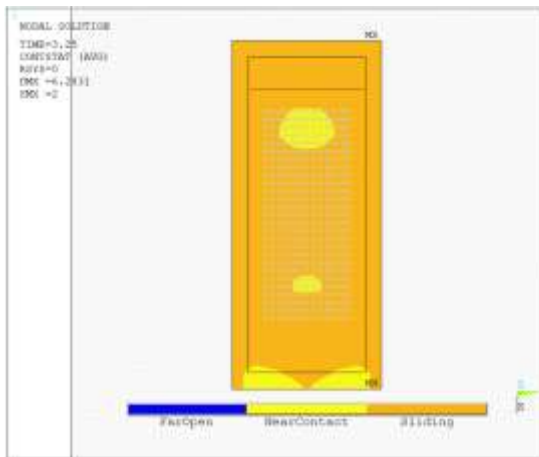


Figure 6.17 Contat status Case 2 UPL / $t = 3,25$

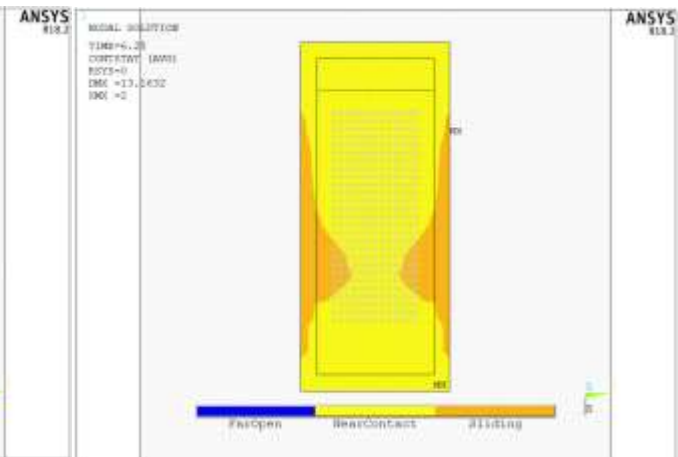


Figure 6.18 Contact status Case 2 UPL / $t = 6,25$

It is interesting to note that the opened status takes place in the same area where the pressure is zero.

Below are presented the graph relative to the resultant force in Z – direction relative to the distribution of the pressure under the contact:

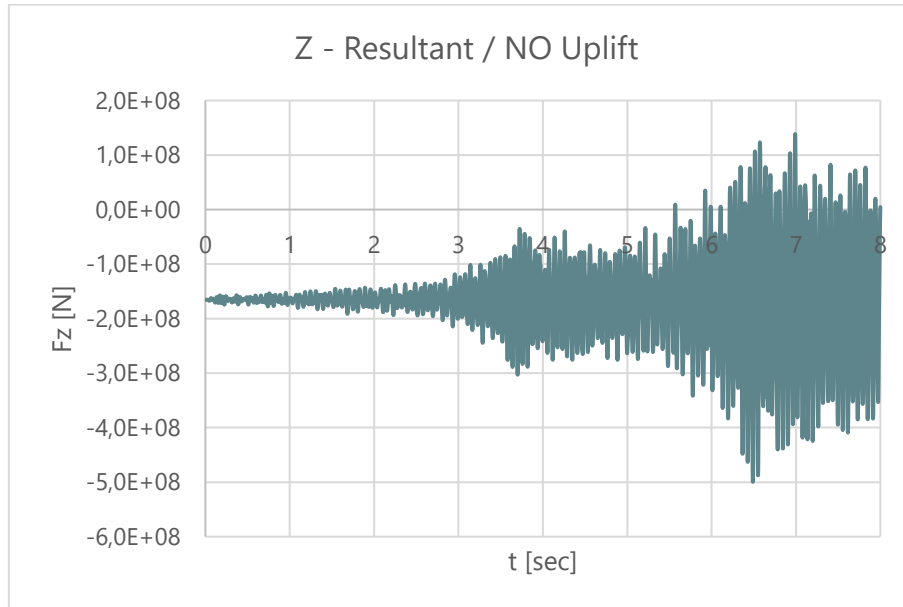


Figure 6.19 Time – History contact resultant force Z - direction / NO Uplift

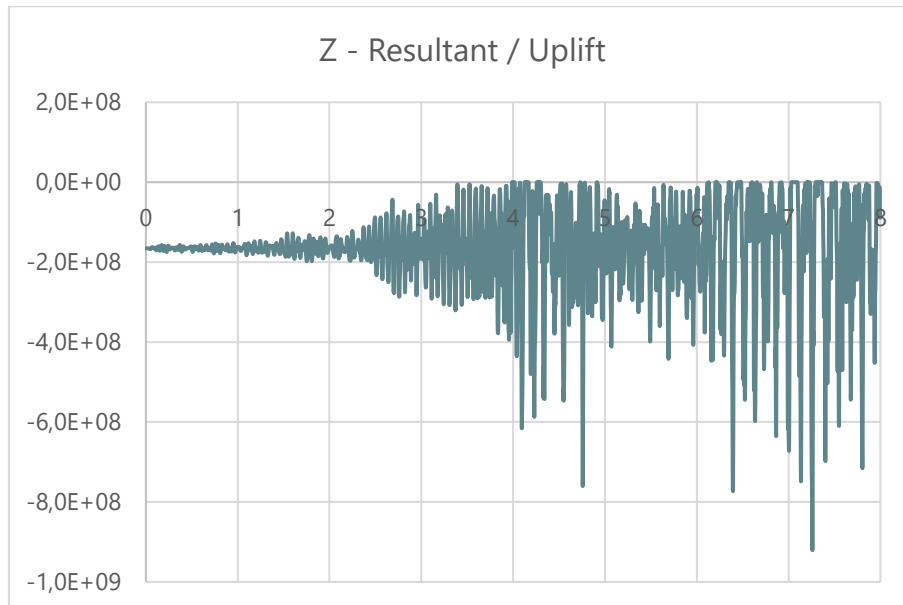


Figure 6.20 Time – History of contact resultant force Z - direction / Uplift

Looking at the first graph, it is possible to notice that until 3 seconds, when the fluctuation of the resultant is small, the displacement curve is coincident with the reference one; after that, the amplitude of the fluctuations increase and displacements curves start to diverge.

The plot of the resultant confirm what figured out in the first phase: when the resultant of the negative pressure prevails on those positive, the total contact resultant can assume positive value, increasing the resistance sliding force and braking the building.

Meanwhile, when the uplift option is active since it is impossible to have negative pressure, the resultant force never goes over the zero.

To sum up, this phenomenon can cause a big underestimation of the displacements for cases where the uplift has a relevant influence, so it has to be set according to the real physic of the problem, not only on the assumption of a simplified model.

Subsequently, is interesting to show the graphs relative to the percentage of the negative pressure area and the uplift area:

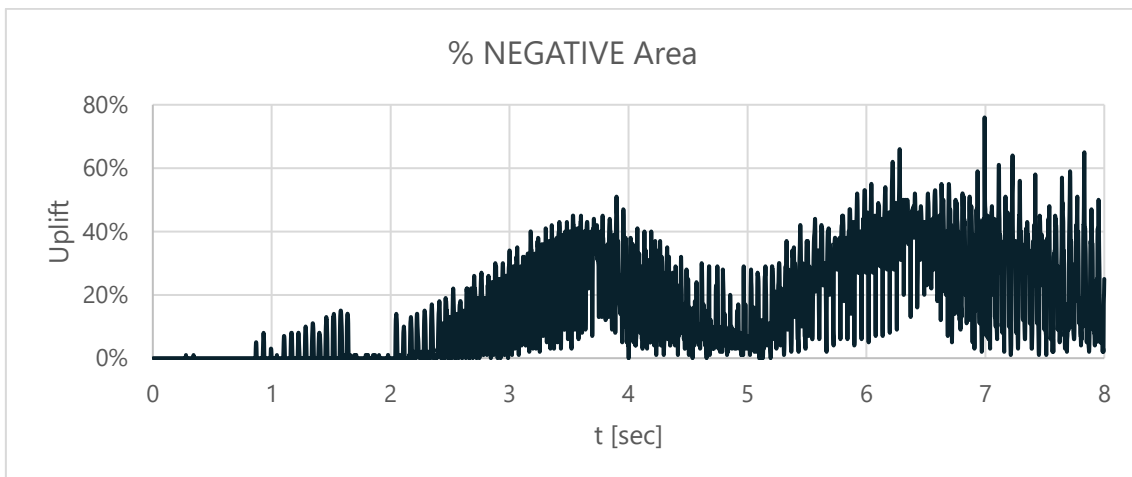


Figure 6.21 Time – History of the area percentage with negative pressure / Case 2

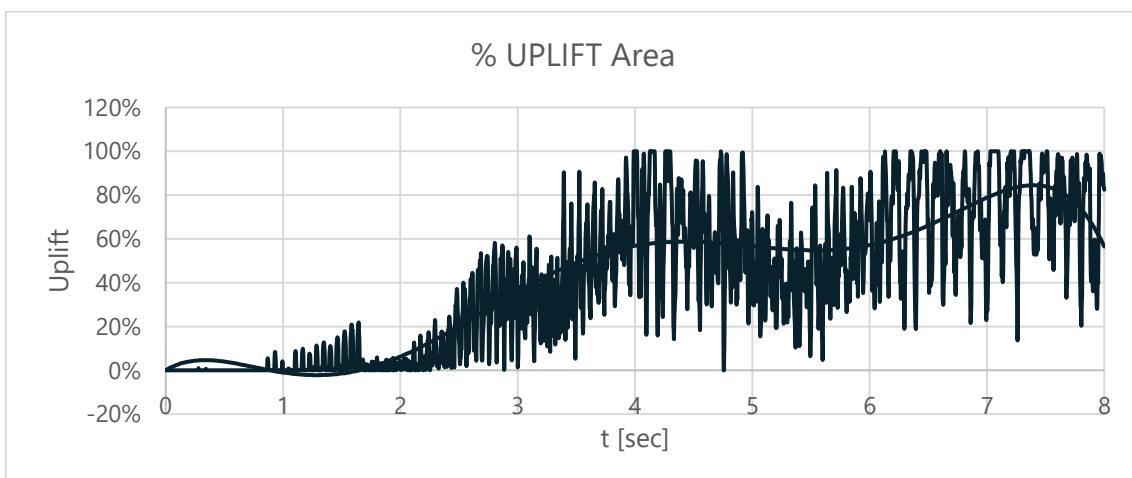


Figure 6.22 Time – History of the uplifted area percentage / Case 2

In both, it is possible to observe a rapid fluctuation of the value from one time step to the subsequent caused by the numerical contact algorithm.

The trend of the two graphs is similar, but while in the first the amplitude of the fluctuations is not so wide and it is possible to define a unique value per each time step, in the second it is much bigger. With peak value up to 100 % and rapid change of the same entity in a small amount of time, it is difficult to estimate an exact uplifted area.

The explanation at these not realistic values falls inside the “gap” calculation, namely the distance between the contact and target detection node calculated when the software assigns the status “opened”. Below will be shown two pictures about the gap calculated in two different instant:

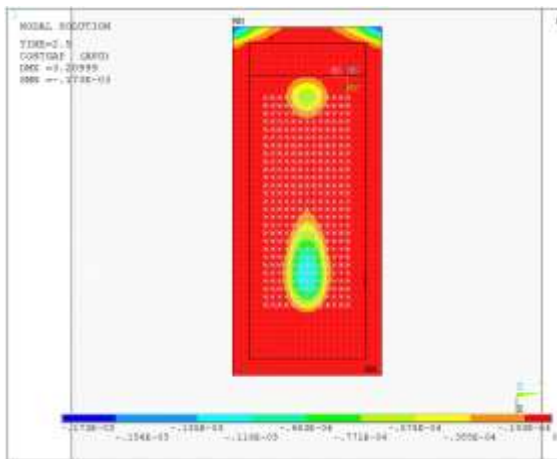


Figure 6.24 Contat gap Case 2 UPL / $t = 2,5$ s

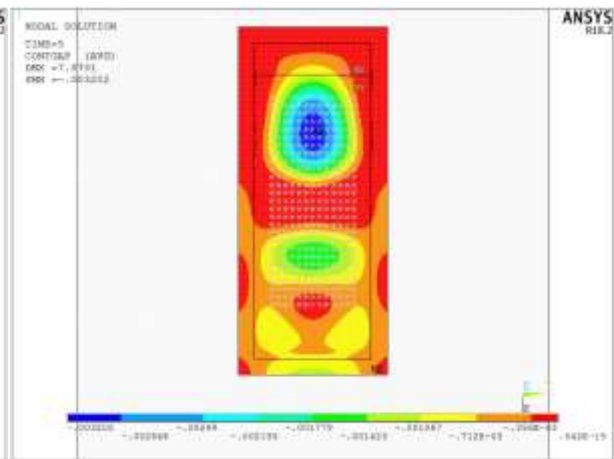


Figure 6.23 Contat gap Case 2 UPL / $t = 5$ s

It is possible to note, especially in the first picture, that the magnitude of the gap is very small: if neglected, it could lead to a better and less variable estimation of the uplifted area. Several attempts have been done in order to exclude it from the calculation, varying several real constant and contact option, but the results did not change.

6.2 Pure Lagrange contact algorithm

The algorithm that with model two showed the best results, this time has shown severe convergence problems with all the academic case tests. Different options have been tested, but no one has conducted to acceptable results.

It has been noticed that decreasing the friction coefficient the convergence was faster but then the problem recurred and the analysis fails. Increasing the number of iteration per sub-step time the convergence was achieved but to wrong values and so, meaningless results. Since this algorithm modifies the stiffness matrix of the structure, an ill-conditioning of it arises, leading to no – convergence problems.

Interesting results have been obtained with the real accelerogram; below are shown the results:

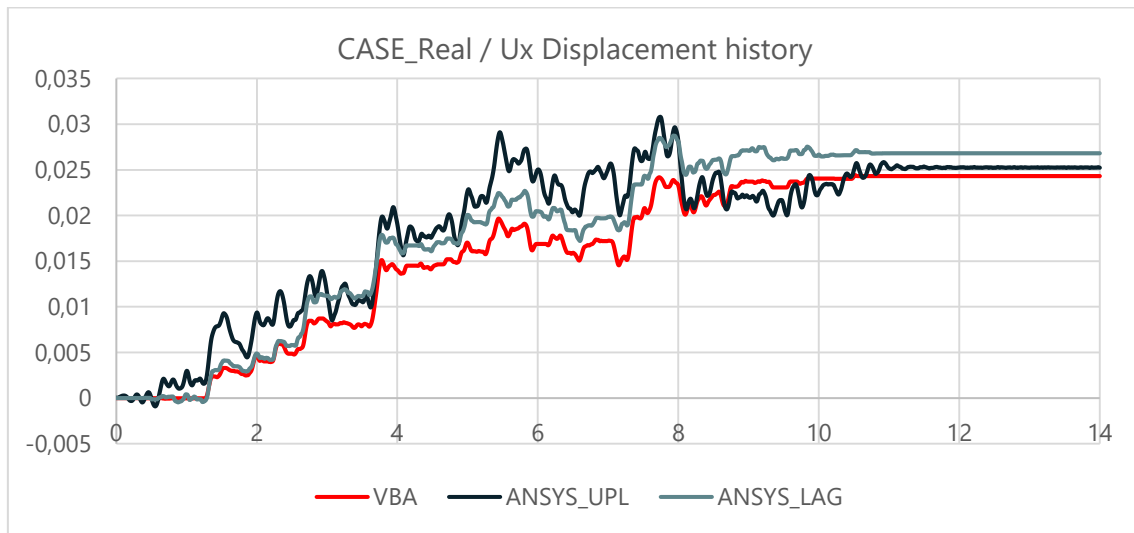


Figure 6.25 Case Real / Ux displacements comparison

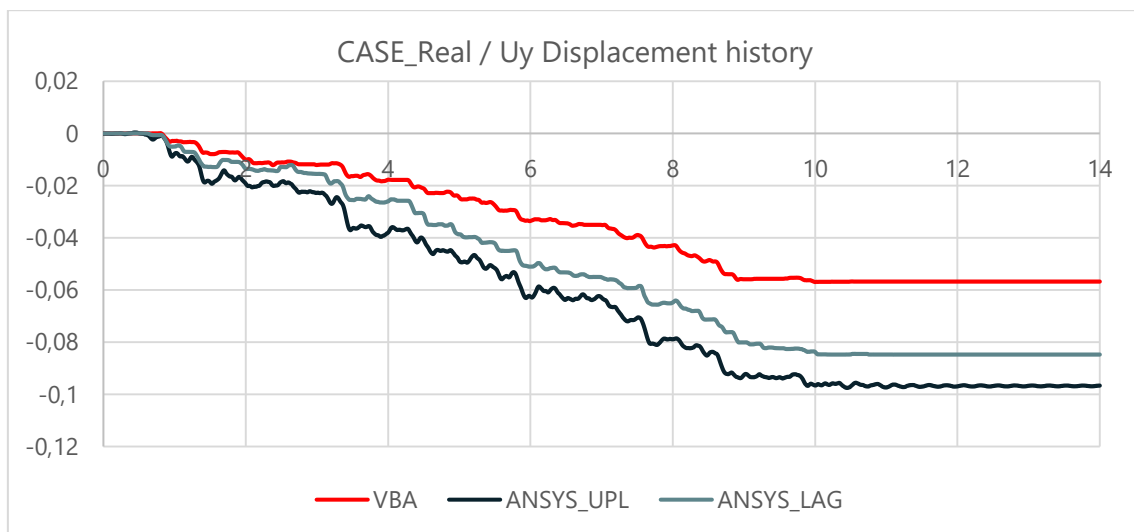


Figure 6.26 Case Real / Uy displacements comparison

In the previous plots have been overlapped, with the usual VBA reference curve, the responses relative to the two different contact algorithm; it is possible to see that:

- ❖ The Lagrange algorithm follow more tightly the VBA curve, the peak points are coincident and there are not wide fluctuation; until 2 seconds the curves are almost coincident and then, after a slight gap, it remains constant until the end;
- ❖ The Penalty curve is not so distant from the other two, but shows bigger fluctuation and is generally the more overestimated;
- ❖ Along the Y – direction, both curves show a big deviation. It could be caused by the eccentricity of the mass centre respect to the geometric centre or by the length of the side along Y-axis; a further investigation will be showed nextly.

Furthermore, it is interesting to analyse the variation of the relative velocity along the time:

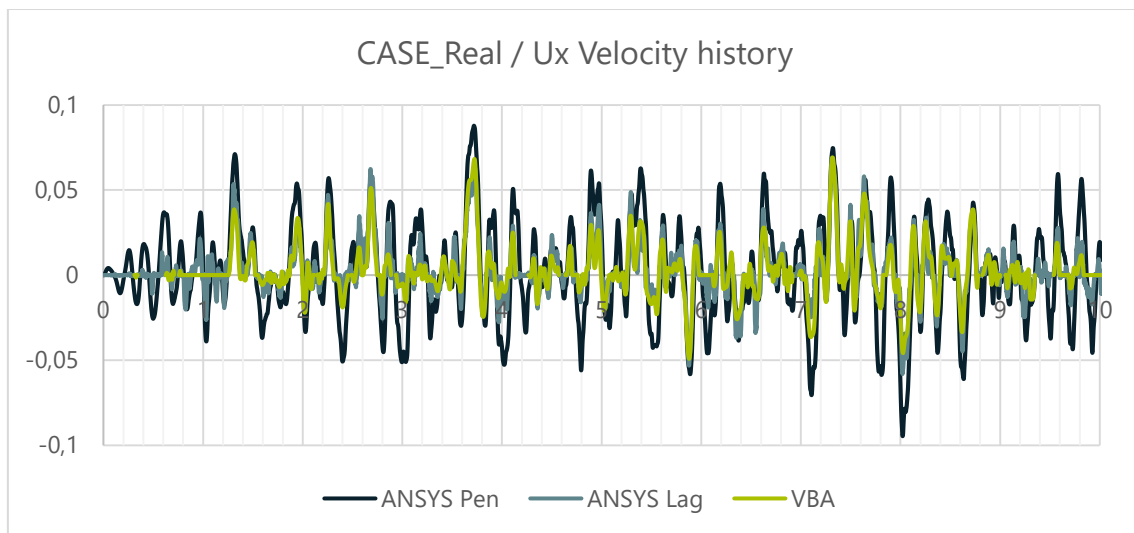


Figure 6.27 Case Real / Ux velocities comparison

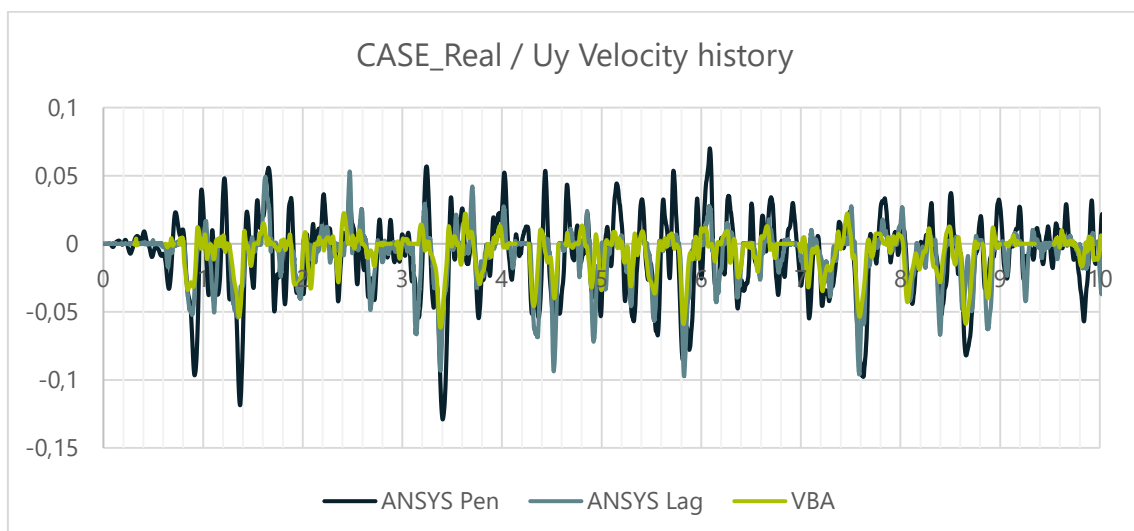


Figure 6.28 Case Real / Uy velocities comparison

These plots confirm the difference of variation in the displacements:

- ❖ VBA velocity is the lowest in both direction, and then the same problem already discussed in the previous character appears;
- ❖ Penalty velocity is the highest and so it leads to bigger displacement. Moreover, it presents some anomalies such as suddenly variation when the other methods calculate zero or slow speed;

Another interesting aspect comes out from the plot of the pressure on the contact elements. Below are present the images relative to the pressures calculated with the two ANSYS contact algorithm:

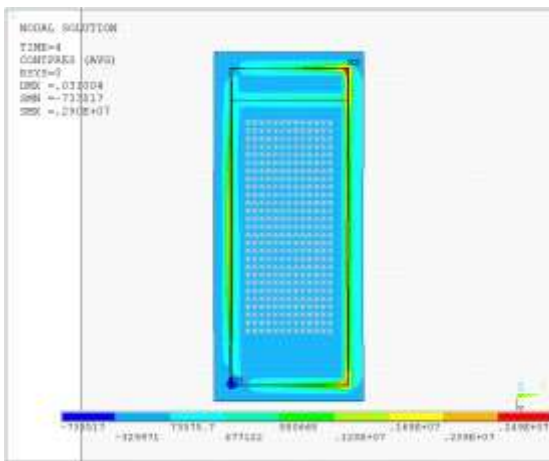


Figure 6.31 Contat pressure with ALM t = 4

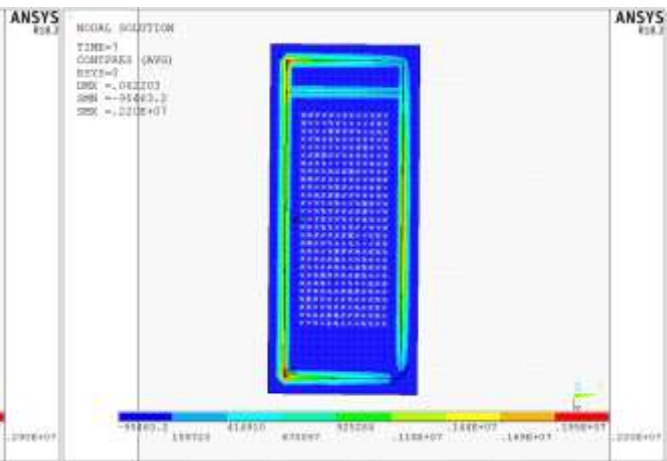


Figure 6.32 Contat pressure with ALM t = 7

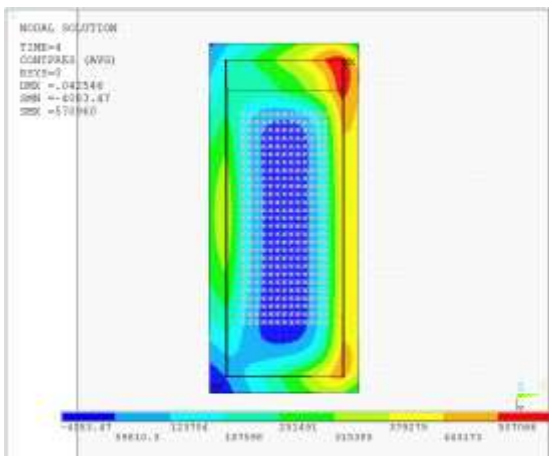


Figure 6.29 Contat pressure with PM t = 4

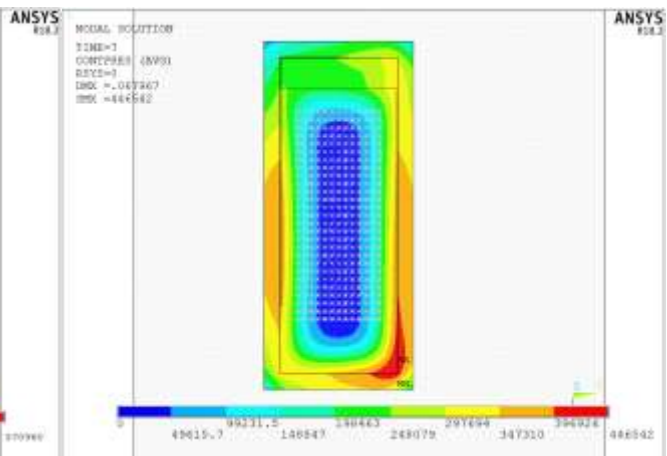


Figure 6.30 Contat pressure with PM t = 4

Between the two algorithms, there is a remarkable difference in the distribution of the pressure:

- ❖ With Lagrange algorithm all the pressure is concentrated under the wall, while the rest of the raft reacts with a negative pressure;
- ❖ Penalty method shows a more spread diffusion of the pressure, with only a small central area with negative or zero pressure.

Even if the second algorithm seems to have a better estimation of the pressure distribution, without a reference it is impossible to say which one is the most realistic.

6.3 Uplift evaluation

In this phase, the results relative to the uplifted area calculated with two methods will be compared: on one side there is the uplift calculated with the macro DECOLL, while on the other side the one calculated on ANSYS.

Before to execute the macro, some input data are needed: the geometric dimension of the raft and the torsors coming from a response spectrum analysis combined with the CQC rule.

In order to execute a proper comparison, the modal analysis has been done with the same spectrum from which the accelerograms have been obtained. Below are present all the modes with a frequency less than 33 Hz and the respective modal mass;

Mode	Freq [Hz]	Effective Mass		
		X	Y	Z
1	7.04	0.00%	51.11%	0.00%
2	9.87	0.00%	0.00%	2.24%
3	10.59	0.00%	0.00%	24.75%
4	12.00	0.15%	0.00%	0.01%
5	12.87	0.06%	0.00%	0.01%
6	14.91	0.00%	4.51%	0.00%
7	15.19	59.92%	0.00%	0.00%
8	15.54	0.01%	0.00%	2.02%
9	15.76	0.00%	5.23%	0.00%
10	17.11	0.00%	0.00%	2.08%
11	20.49	0.27%	0.00%	0.00%
12	23.32	0.00%	0.00%	0.00%
13	24.15	0.00%	3.06%	0.00%
14	25.59	0.00%	0.54%	0.00%
15	25.93	0.00%	0.38%	0.00%
16	26.45	0.00%	0.00%	1.91%
17	26.88	0.00%	0.50%	0.00%
18	28.62	0.00%	0.01%	0.00%
19	29.36	0.01%	0.00%	0.04%
20	29.83	0.00%	0.12%	0.00%
21	31.24	0.02%	0.00%	1.29%
22	31.37	0.00%	0.08%	0.00%
TOT		60.45%	65.54%	34.35%

Table 6.1 Modal frequencies and masses

6. Case Study 3

It is possible to notice that most of the modes have no modal mass, while for those who have a higher percentage it does not exceed 60 %. This means that this structure should not be analysed with a response spectrum analysis, but applying the pseudo mode method, this limitation can be overpassed. Below it is possible to see the images relative to the modes with more than 5 % of modal mass:

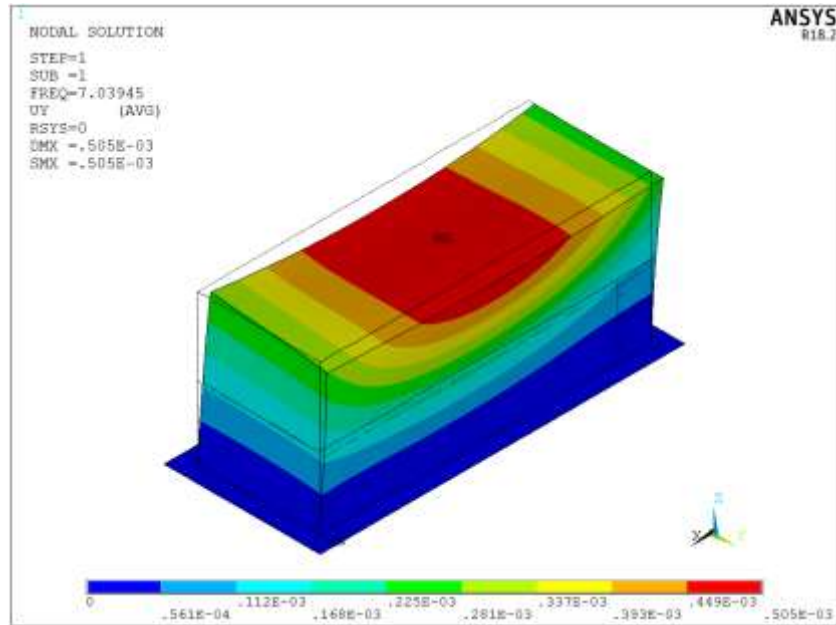


Figure 6.33 Deformed shape Mode 1

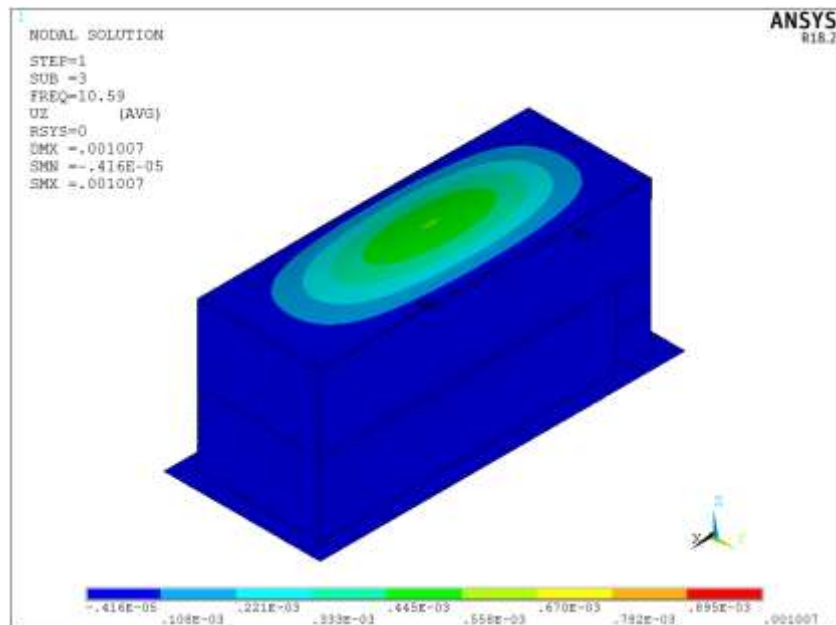


Figure 6.34 Deformed shape Mode 3

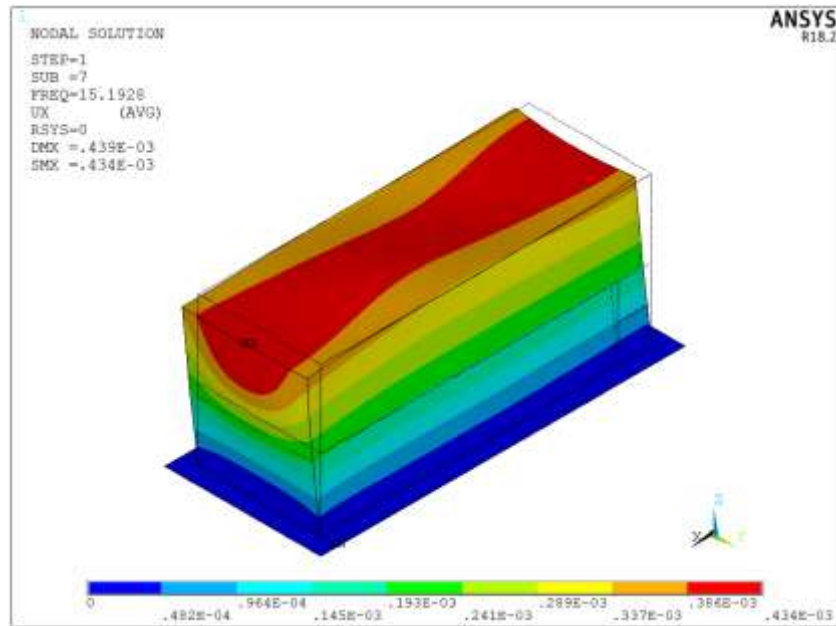


Figure 6.35 Deformed shape Mode 7

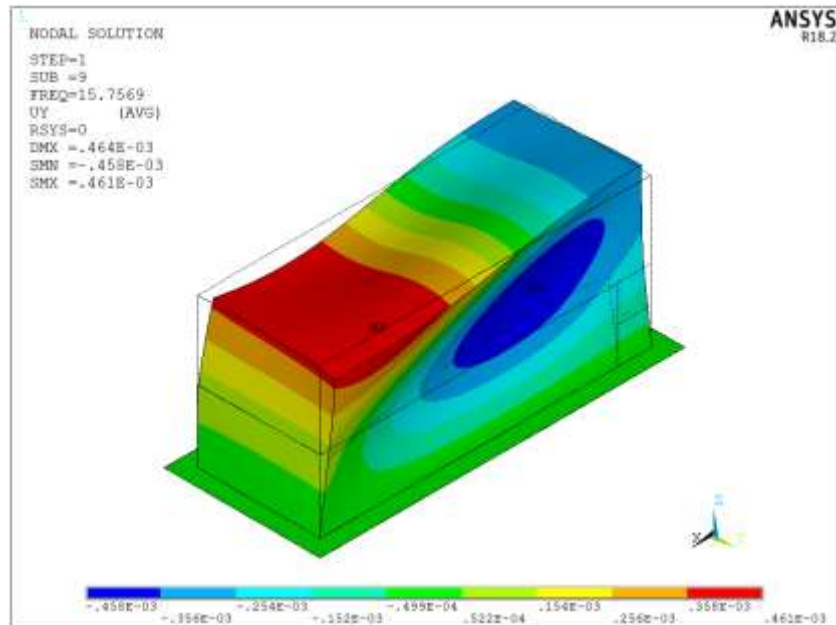


Figure 6.36 Deformed shape Mode 9

Subsequently, spectral analysis has been executed in order to calculate the static equivalent forces for each mode and then, these last have been combined with the CQC rule. Below are listed the torsors on the raft foundation for the combination in each direction:

	Fx [N]	Fy [N]	Fz [N]	Mx [Nm]	My [Nm]	Mz [Nm]
CQC x	0.564E+08	0.165E+02	0.142E+06	-0.825E+02	0.8399E+09	-0.200E+03
CQC y	1.658E+01	5.197E+07	2.945E+01	-7.545E+08	5.975E+02	-7.764E+07
CQC z	-9.491E+04	1.962E+01	2.790E+07	3.166E+02	1.875E+07	1.135E+02

Table 6.2 Torsors at the gravity centre of the raft

Then, these torsors have been superimposed in order to take into account the simultaneous presence of the seismic effort from more direction. This has been done following the Newmark combination:

$$1.0 \times G_C \pm 1.0 \times E_x \pm 0.4 \times E_y \pm 0.4 \times E_z$$

$$1.0 \times G_C \pm 0.4 \times E_x \pm 1.0 \times E_y \pm 0.4 \times E_z$$

$$1.0 \times G_C \pm 0.4 \times E_x \pm 0.4 \times E_y \pm 1.0 \times E_z$$

From these, 24 combinations come out, that leads to the following torsors:

Combo	Fz [N]	Mx [Nm]	My [Nm]
1	-1.54E+08	-3.02E+08	8.00E+08
2	-1.76E+08	-3.02E+08	7.85E+08
3	-1.54E+08	3.02E+08	8.00E+08
4	-1.76E+08	3.02E+08	7.85E+08
5	-1.54E+08	-3.02E+08	-8.79E+08
6	-1.77E+08	-3.02E+08	-8.94E+08
7	-1.54E+08	3.02E+08	-8.79E+08
8	-1.77E+08	3.02E+08	-8.94E+08
9	-1.54E+08	-7.55E+08	2.96E+08
10	-1.77E+08	-7.55E+08	2.81E+08
11	-1.54E+08	7.55E+08	2.96E+08
12	-1.77E+08	7.55E+08	2.81E+08
13	-1.54E+08	-7.55E+08	-3.75E+08
14	-1.77E+08	-7.55E+08	-3.90E+08
15	-1.54E+08	7.55E+08	-3.75E+08
16	-1.77E+08	7.55E+08	-3.90E+08
17	-1.37E+08	-3.02E+08	3.08E+08
18	-1.93E+08	-3.02E+08	2.70E+08
19	-1.37E+08	3.02E+08	3.08E+08
20	-1.93E+08	3.02E+08	2.70E+08
21	-1.38E+08	-3.02E+08	-3.64E+08
22	-1.93E+08	-3.02E+08	-4.02E+08
23	-1.38E+08	3.02E+08	-3.64E+08
24	-1.93E+08	3.02E+08	-4.02E+08

Table 6.3 Newmark's combinations of Fz, Mx, My

Once the total torsors have been obtained, these have been inserted in the input file for the uplift analysis with DECOL. Below are present the results relative to it:

Combo	UPLIFT %	
	ME	EE
1	2.88	2.67
2	0.60	0.59
3	2.88	2.67
4	0.60	0.59
5	4.14	3.74
6	1.47	1.41
7	4.14	3.74
8	1.47	1.41
9	25.13	18.58
10	15.28	12.32
11	25.13	18.58
12	15.28	12.32
13	25.63	18.69
14	15.88	12.45
15	25.63	18.69
16	15.88	12.45
17	0.00	0.00
18	0.00	0.00
19	0.00	0.00
20	0.00	0.00
21	0.02	0.02
22	0.00	0.00
23	0.02	0.02
24	0.00	0.00

Table 6.4 Uplift area percentage from DECOL

The table shows that the percentage of uplift calculated with the moment equivalence method is always higher than those calculated with the energetic equivalence method. Being a non – linear method, this last is less conservative than the first and so it leads to less uplift.

Then, for cases where is present the full component along Z the uplift is very small, while for cases where the z – component has been reduced the uplift reach value up to 25 %. Below is shown the picture with the neutral axis calculated with both

methods:

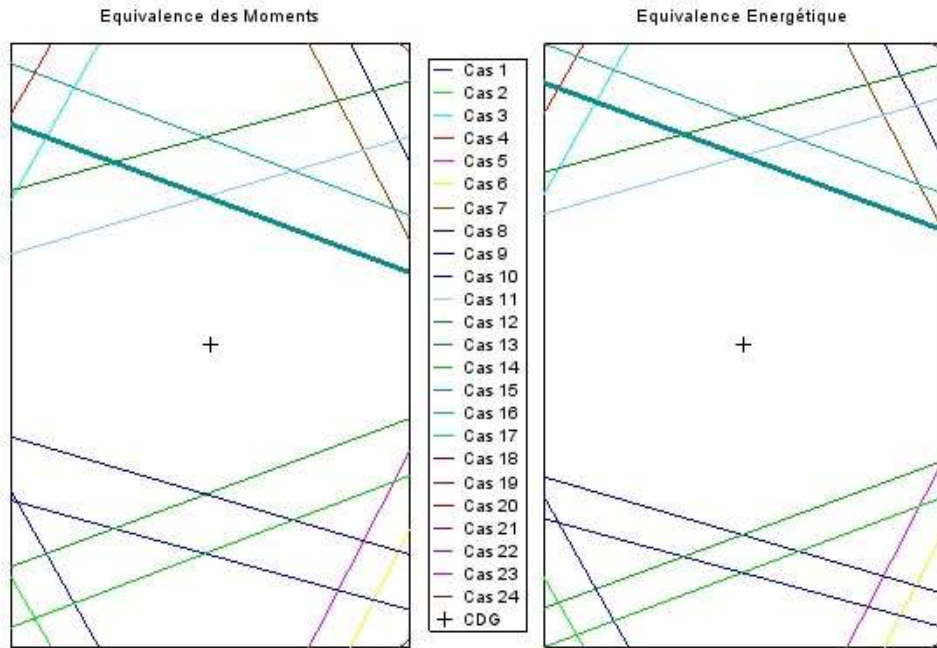


Figure 6.37 Neutral axis from DECOL

Now, these results have to be compared with those obtained from a transient analysis conducted with the two contacts algorithm:

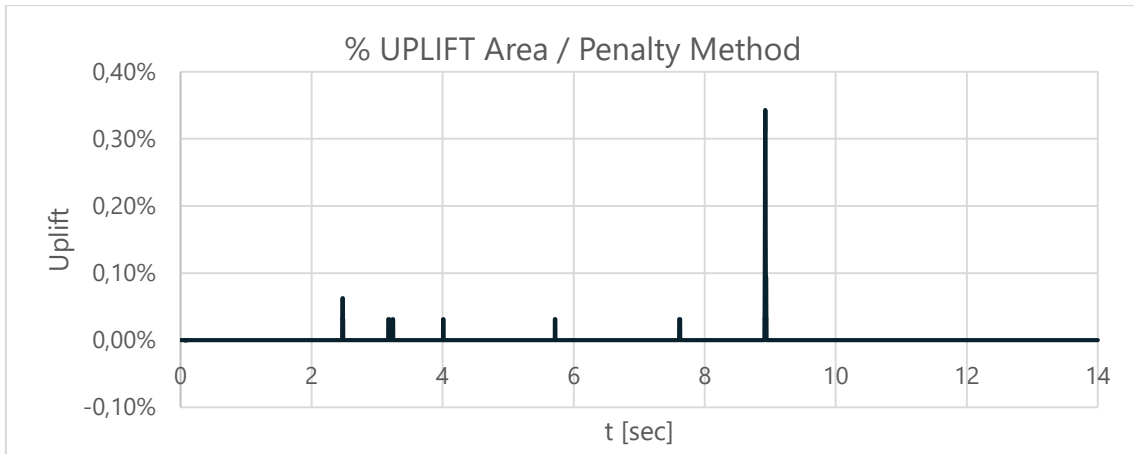


Figure 6.38 Time history of the uplifted area percentage / ALM

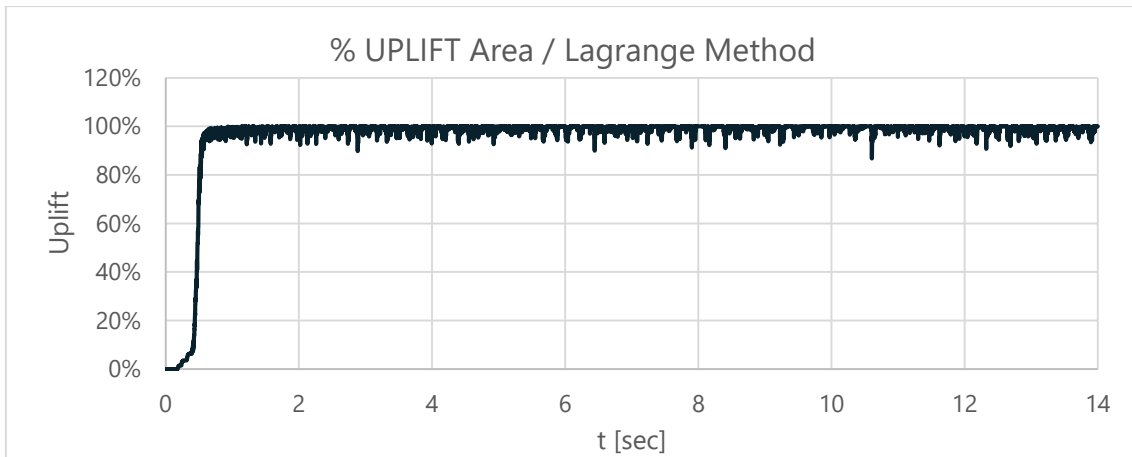


Figure 6.39 Time history of the uplifted area percentage / LM

The first graph (Penalty method) shows that the uplift is practically zero during all the analysis time. Some peaks are present and their values do not exceed 0,4%. These results are comparable with the one of DECOL which are, for some combination, around 1 – 2 %

The second graph (Lagrange method) shows a totally different situation: for the first instants the uplift is zero, but then it suddenly it jumps to 100% and remains steady constant for all the rest of the analysis. Of course, this is not a realistic situation, the building results to be uplifted even when the lateral seismic actions are zero.

Probably this is due to the erroneous distribution of the pressure already discussed in the previous graph.

7 Conclusions and future developments

Starting from an accurate analysis of the problem and a study of the theory behind of it, a methodology to calculate the displacements of a structure under a seismic event has been developed by means of the FEM software ANSYS. In the literature, there are not so many theories that allow doing that, so the Newmark – Elms method has been the reference for the entire project.

The principal element of the study is the modelling of the interface between the base of the structure in contact with the ground and the sliding surface. In ANSYS this is possible thanks to two families of elements, called Contact and Target. The computational methods behind them and the numerous options available allow to study various problems, but at the same time, they make the set-up of these elements very complex.

First of all, a reproduction of the NE method has been done in order to understand which parameters are well suited for this problem and to make a comparison between the two methodologies.

The first model under examination was composed of a unitary volume element (3D). The results not only were not so accurate but also shown a strong dependency by the parameter FKN and the sub-step time. Moreover, some base hypothesis of the NE methods were not respected: the pressure at the soil-structure interface was not constants and large rotation of the model arises. These incongruities were caused by the eccentricity of the external loads respect to the sliding surface.

Since the problems that came out in the previous model were caused by the 3rd dimension, the new model had only two dimensions and was composed by a unitary shell element and two rigid links that linked the corner of the model eliminating any possible deformation. Moreover, to be even more coherent with the NE hypothesis, all the mass was concentrated in the centre of gravity of the model by means of a mass element. This time the results were much more accurate and all the previous problems were not present.

Then, thanks to the previous positive results, the methodology was ready to be applied to a real structure. The more complex model needed a new modelization of the forces and the definition of different local coordinate systems. During the first part, the analysis was conducted without considering the uplift and utilizing both the contact resolution algorithms: Penalty solver showed good accuracy for some cases test but

also a breaking effect due to prevented uplift, while Lagrange solver does not worked because of an ill-conditioning of the stiffness matrix. Surprisingly, It only worked with the real accelerogram, giving results comparable to those of NE method.

The second and last part was conducted considering the uplift: unlike the other phase, the breaking effect disappeared and the displacements histories followed perfectly those of reference.

In the end, the comparison of the displacements on the real accelerogram showed that the model two follow almost perfectly those of the NE method, while the model three showed a slight difference in Y-direction. Apparently, the dimensions of the raft and the deformation of the structure influence the results, giving a better estimation of the real response of the building under a seismic event.

To sum up, the second model successfully reproduced the NE methodology confirming its reliability and the validity of the ANSYS solver. But, the VBA macro still has a big advantage: the computational time that is about ten-time faster.

Things are different if we decide to model a real structure: the complexity of the ANSYS environment allows to take into consideration several aspects of the problem like rocking, rotations and deformation of the elements. Furthermore, it is possible to extrapolate the displacements of every node of the structure, the pressure distribution under the foundation, the uplifted area, the opening gap and the history of the torsors at the base.

However, the vastness of the subject leaves opened the way to further improvement of this methodology. For future developments, the ground of the structure could be modelled by means of springs or volume elements, as well as the ground surrounding the structure. Indeed, we could even utilize non-linear and bi-phasic materials to simulate the soil behaviour in order to create a more realistic simulation. This would allow to do a more complete evaluation of the parameters that fall inside the global stability analysis like the effort inside the soil, the horizontal pressure of the ground against the vertical wall, the over-pressure of the water etc. Then, can be included also the dumping of the structure which should further decrease the displacements of the structure because of the higher dissipated energy. The work could be completed considering a complete load case as prescribed by the code in order to assess the whole combination and to have a complete evaluation in every condition.

On the other and, ther is to say that every refinement of the model augments its complexity, and consequently the computational time. The risk is to pass from analysis that runs in five hours (like the most complex done in this project) to those which could

take up to 1 month. There are solutions able to overcome this problem like the use of HPC (High Performance Computing) server, but usually they are not so cheap and not every company can afford it. To conclude, it is always necessary to find a good compromise between the complexity of the problem and the accuracy of the results.

Bibliografy

ANSYS Inc. (2017). ANSYS Mechanical 18.2 Product Help.

Bathe, K. J. (1996). *Finite element procedure*. Prentice Hall.

Elms, D. G. (2000). *Refinements to the Newmark Sliding Block Model*. WCEE 2000: 12th World Conference on Earthquake Engineering.

EN 1997-1 Eurocode 7: *Geotechnical design*. (2004).

ETC-C code description. (2019, July). Retrieved from www.afcen.com/en/about/our-codes

UK EPR reactor description. (2019, July). Retrieved from www.epr-reactor.co.uk

Wriggers, P. (2006). *Computational Contact Mechanics*. Springer.

Yastrebov, V. (2011). *Computational contact mechanics: geometry, detection and numerical techniques*. Paris: École Nationale Supérieure des Mines de Paris.

Yastrebov, V. (2013). *Numerical Methods in Contact Mechanics*. ISTE/Wiley.